



UNIVERSIDAD NACIONAL DE COLOMBIA

FIRST WEEK OF OIL WEATHERING OF COLOMBIAN CRUDE OIL IN THE COLOMBIAN CARIBBEAN SEA

Juan Guillermo Ramírez Hernández

Universidad Nacional de Colombia, Sede Medellín

Facultad de Minas

Medellín, Colombia

2014

FIRST WEEK OF OIL WEATHERING OF COLOMBIAN CRUDE OIL IN THE COLOMBIAN CARIBBEAN SEA

Juan Guillermo Ramírez Hernández

Thesis presented as a partial requirement to obtain the degree of:

M.Sc. in Chemical Engineering

Supervisor:

Alejandro Molina

Research group:

Bioprocesos y Flujos Reactivos

Universidad Nacional de Colombia, Sede Medellín

Facultad de Minas

Medelln, Colombia

2014

ABSTRACT

A module, MEUN (Módulo de Envejecimiento Universidad Nacional), that describes the processes that occur due to the interaction, also known as weathering, of the crude in an oil spill with the atmosphere and the ocean, was developed. This module, couples individual sub-models available in the literature used to describe the evaporation, emulsification, dispersion and spreading processes that characterize the first week after an ocean oil spill. MEUN predicts as well the variation in density and viscosity over time as a result of the weathering processes. All sub-model constants were adapted to the specific requirements of Colombian crudes, particularly to Cusiana ($^{\circ}\text{API}$ 43.2) and Vasconia ($^{\circ}\text{API}$ 20.7). While the first one represents light crudes, the second one is an example of heavier oils. These two crudes have high production and require marine transport. To evaluate MEUN predictions, experiments were carried out for evaporation and emulsification processes at conditions similar to those observed during an oil spill in the Colombian Caribbean Sea. In the case of the evaporation experiments, a wind tunnel of 3.0 m and a circular cross section of 30 cm in diameter was adapted to measure the weight loss of crude oil while varying the wind velocity between 3 m/s and 8 m/s. The emulsification process was simulated using the rotating-cylinder method, a standard in the weathering community. The emulsification experiments evaluated the effect of temperature (ranging from 22°C to 30°C) as well as the degree of evaporation of the crude oil in the rate and extent of emulsification. Variations in density and viscosity as a result of evaporation and emulsification were also measured. The evaporation results showed a strong dependence of evaporation rate with wind velocity, particularly for Cusiana. This behavior is not predicted by the state-of-the-art models used by the oil spill community. MEUN included a new correlation for the mass transfer coefficient that correctly predicts the evaporation process of Cusiana. Furthermore, the experiments revealed that Cusiana increases the pour point because of evaporation from 0°C for fresh oil up to 30°C when the evaporated fraction is 48 %. When the oil temperature is below the pour point, something rather possible even at the relative high temperatures of the Colombian Caribbean Sea given the significant increase in pour point because of evaporation, the evaporation rate significantly decreases to virtually zero. This effect was included in MEUN. Vasconia presents the typical behavior for oil emulsification described in the literature as

it forms an emulsion with a water content of 70-90% that becomes more stable as the evaporated fraction increases and the temperature decreases. Contrary, Cusiana only forms an emulsion when the temperature is below the pour point. The final version of MEUN reproduces these emulsification behaviors for Cusiana and Vasconia. When compared to well-established weathering software, such as ADIOS, MEUN gives predictions that are closer to the experimental behavior, particularly for Cusiana, as it considers the effect of pour point and predicts a combination of evaporation and dispersion considerably higher than that predicted by MEUN (100% vs 50% of the spilled amount, respectively, 30 hours after the spill).

Keywords: oil weathering, oil spill modeling, oil evaporation, water-in-oil emulsions, pollution modeling.

RESUMEN

Se desarrolló un módulo, MEUN (Módulo de Envejecimiento Universidad Nacional) que describe los procesos que ocurren debido a la interacción, del crudo en un derrame con la atmósfera y el océano también conocido como envejecimiento. Este modelo acopla sub-modelos disponibles en la literatura para describir los procesos de evaporación, emulsificación, dispersión y esparcimiento que caracterizan la primera semana después de un derrame de crudo en el océano. MEUN predice también la variación en la densidad y la viscosidad a través del tiempo como resultado de los procesos de envejecimiento. Las constantes de los sub-modelos fueron adaptadas a los requerimientos específicos de crudos Colombianos, particularmente para Cusiana ($^{\circ}\text{API}$ 43.2) y Vasconia ($^{\circ}\text{API}$ 20.7). Mientras que el primero representa los crudos livianos, el segundo es un ejemplo de un crudo más pesado. Estos dos crudos tienen alta producción y requieren transporte marítimo. Para evaluar la predicción de MEUN, se desarrollaron experimentos para los procesos de evaporación y emulsificación en condiciones similares a las observadas en un derrame de crudo en el mar Caribe Colombiano. En el caso de los experimentos de evaporación, un túnel de viento de 3.0 m de largo y una sección transversal circular de 30 cm de diámetro fue adaptado para medir la pérdida de peso de crudo mientras se varía la velocidad del viento entre 3 m/s y 8m/s. El proceso de emulsificación fue simulado usando el método de cilindro rotatorio, un método estándar en la comunidad del envejecimiento de crudos. Los experimentos de emulsificación evaluaron el efecto de la temperatura (variando de 22°C a 30°C) y el del grado de evaporación del crudo en la velocidad y el grado de emulsificación. Las variaciones en la densidad y la viscosidad como resultado de la evaporación y la emulsificación fueron también medidas. Los resultados de evaporación mostraron una fuerte dependencia de la velocidad de evaporación con la velocidad del viento, particularmente para Cusiana. Este comportamiento no es predicho por los modelos del estado del arte usados por la comunidad de derrames de hidrocarburos. Por esto, MEUN incluye una nueva correlación para el coeficiente de transferencia de masa que predice correctamente el proceso de evaporación para Cusiana. Más aun, los experimentos revelaron que el punto de fluidez del crudo Cusiana se incrementa debido a la evaporación desde 0°C para el crudo original hasta 30°C cuando la fracción evaporada es 48 %. Cuando la temperatura del crudo está por debajo del punto de

fluidez, algo que es posible incluso con las relativamente altas temperaturas del mar caribe Colombiano debido al incremento significativo del pour point con la evaporación, la velocidad de evaporación disminuye significativamente hasta alcanzar el valor de cero. Este efecto fue incluido en MEUN. Vasconia presenta el típico comportamiento de emulsificación de crudos descrito en la literatura ya que forma una emulsión con un contenido de agua de 70-90% que se convierte más estable a medida que la fracción evaporada aumenta y la temperatura disminuye. Contrariamente, Cusiana solo forma una emulsión cuando la temperatura este por debajo del punto de fluidez. La versión final de MEUN reproduce estos comportamientos de emulsificación de Cusiana y Vasconia. Al ser comparado con software de envejecimiento reconocidos como ADIOS, las predicciones de MEUN son más cercanas al comportamiento experimental, particularmente para Cusiana, ya que considera el efecto del punto de fluidez y predice una combinación de evaporación y dispersión considerablemente mayor que la predicha por MEUN (100% vs 50% de la cantidad derramada, respectivamente, 30 horas después del derrame).

Palabras claves: envejecimiento, modelamiento de derrames, evaporación de crudo, emulsiones water-in-oil, modelamiento de contaminación.

Acknowledgements

I am specially grateful to Professor Alejandro Molina, it was a pleasure to work with him and his good advice helped me to overcome the problems encountered in this work.

I would like to express my gratitude to Universidad Nacional de Colombia for the Facultad de Minas scholarship and to the Colombian oil company Ecopetrol-ICP for the partial funding of my master's program under the "Acuerdo de Cooperación Tecnológica No. 001 derivado del Convenio Marco ICP No. 5211385".

To COLCIENCIAS for the financial support with the scholarship "Colciencias, Jóvenes Investigadores 2013".

To my colleagues and friends from the research group "Bioprocesos y Flujos reactivos" for their help and time, especially to Aura Merlano and Juan Lacayo for their continuous support.

Last but not least to my parents Bertha and Argiro and my sisters Erica and Astrid for an entire life of company and support, to my girlfriend Vanessa for always being there in the most stressful moments, to my friends Montes, Ricardo, Juanes, Santiago, Ana Maria, Claudia, Jennifer, Alexander, Gabriel, Pablo... they, through the years, have earned all my gratitude.

Contents

ABSTRACT	III
RESUMEN	V
Acknowledgements	VII
List of Figures	XIV
List of Tables	XV
Physical constants	XVI
Symbols	XVII
1. Introduction	2
1.1. Motivation	2
1.2. Research objectives	3
1.2.1. Objective	3
1.2.2. Specific objectives	3
1.3. Description of the thesis	3
2. General concepts	5
2.1. Oil spill weathering	5
2.2. Colombian Caribbean Sea	7
2.3. Introduction to the behavior of waxy crude oils	8
3. Development of the weathering module MEUN	10
3.1. Evaporation	10
3.1.1. Evaporation models	10
3.1.2. Evaporation model implemented in the weathering module MEUN	14

3.1.3. Changes in density and viscosity	16
3.2. Emulsification	17
3.2.1. Emulsification models	18
3.2.2. Emulsification model implemented in the weathering module MEUN	21
3.3. Dispersion	21
3.3.1. Dispersion models	22
3.3.2. Dispersion model implemented in the weathering module MEUN	23
3.4. Spreading	23
4. Experimental Methodology	25
4.1. Test oils	25
4.1.1. True boiling point	25
4.1.2. SARA	26
4.1.3. Pour point	26
4.2. Evaporation	27
4.2.1. Wind tunnel	27
4.2.2. Wind velocity	28
4.2.3. Initial oil film thickness	32
4.3. Emulsification	34
4.3.1. Experimental setup	34
4.3.2. Experimental conditions	36
5. Results	38
5.1. Evaporation	38
5.1.1. Effect of wind velocity and crude oil type on evaporation rate	39
5.1.2. Effect of pour point on evaporation rate	49
5.1.3. Physicochemical properties	54
5.2. Emulsification	58
5.2.1. Pour point effect	59
5.2.2. Rate of formation of the emulsion	61
5.2.3. Effect of evaporation and temperature on the stability of the emulsion	62
5.2.4. Physicochemical properties	64
5.3. MEUN application to a spill incident in the Colombian Caribbean Sea	66
Conclusions	74

Appendix A	76
Appendix B	77
Appendix C	80
Appendix D	81
Appendix E	83
References	92

List of Figures

2.1. Weathering processes. a. schematic diagram, adapted from ITOPF [1]. b. relative importance over time, adapted from SINTEF [2], processes marked with blue are studied in this thesis.	5
2.2. Relative location of Colombian Caribbean Sea. a. With respect to South America. b. With respect to Colombia. The figure shows the port where hydrocarbons are exported.	7
2.3. Evolution of pour point with evaporated fraction for the waxy crude oil Grosbeak [3].	9
3.1. Evaluation of the evaporated fraction of Statfjord crude oil at 15°C and 15 km/h of wind velocity using the three evaporation models discussed in Section 3.1.1. Model results are compared with experimental data reported in Sebastião and Soares [4].	15
4.1. TBP curves for Colombian crude oils. Provided by the Colombian oil company Ecopetrol.	26
4.2. Pour point variation with evaporated fraction for Colombian crude oils. a. Cusiana. (measured in this research) b. Vasconia. (taken from reference [5]).	27
4.3. Scheme of the experimental setup designed to validate the model of crude oil evaporation.	28
4.4. Position of the velocity profiles evaluated along the wind tunnel in the CFD simulation.	29
4.5. Velocity profiles along the wind tunnel obtained with CFD simulation. a. Before Blockage 1, b. After Blockage 1. (Legends make reference to Figure 4.4).	30
4.6. Experimental velocity profiles in the wind tunnel at different blower rotational speed and comparison with CFD simulation a. Horizontal profiles and b. Vertical profile. . .	31
4.7. Experimental behavior of water evaporation. a. Evolution of evaporated fraction with time at 2, 3, 5 and 8 m/s. b. Effect of wind velocity in evaporation rate, experimental values are compared with a power law dependence with wind velocity.	32
4.8. Effect of initial oil thickness in the behavior of the evaporated fraction for Cusiana crude oil at a wind velocity of 5 m/s. a) Experimental data, b) MEUN predictions. . .	33
4.9. Effect of initial oil thickness in the behavior of the time-derivative of the evaporated fraction for Cusiana crude oil at 5 m/s. a) Experimental data, b) MEUN predictions .	34

4.10. Scheme of the experimental setup adapted from reference [6] to study the emulsification model.	35
4.11. Schematic representation of different of the emulsification experiment. a. Initial condition (before mixing). b. At time t of mixing. c. After 24 h mixing and 24 h settling. . .	35
4.12. Experimental conditions to study emulsification behavior of Cusiana crude oil.	37
5.1. Effect of the wind velocity on the evaporated fraction of a. Cusiana. b. Vasconia. Note the differences in the scale of both, vertical and horizontal, axes.	39
5.2. Effect of wind velocity in the behavior of the evaporated fraction for Cusiana crude oil. a. Experimental data. b. MEUN predictions.	40
5.3. Effect of the wind velocity on the behavior of the evaporated fraction for Vasconia crude oil. a. Experimental data. b. MEUN predictions.	41
5.4. Predicted versus experimental evaporated fraction. Predicted values based on state-of-art models. a. Cusiana. b. Vasconia.	42
5.5. Schematic example of the optimization made to find optimal value of mass transfer coefficient. a. Before optimization. b. After optimization.	43
5.6. Predicted versus experimental evaporated fraction. Predicted values using the mass transfer coefficient found with the optimization procedure. a. Cusiana. b. Vasconia. . .	44
5.7. Effect of wind velocity in the behavior of the mass transfer coefficient. Comparison between calculated values with the optimization procedure and with the state-of-the-art correlation. a. Linear scale. b. Logarithmic scale.	45
5.8. Effect of wind velocity in the behavior of the mass transfer coefficient. Comparison between calculated values with the optimization procedure and with the proposed correlation. a. Linear scale. b. Logarithmic scale.	47
5.9. Predicted versus experimental evaporated fraction. Predicted values computes mass transfer coefficient with the correlation in Equation 5.7. a. Cusiana. b. Vasconia. . . .	48
5.10. Graphical representation of the effect of the pour point on the evaporation rate of Cusiana. a. Evaporated fraction and temperature. b. Evaporation rate (expressed as the time-derivative of the evaporated fraction). c. Pour point curve. Check the text for an explanation of the different legends in these figures.	50
5.11. Comparison of the experimental evaporated fraction with MEUN predictions for Cusiana when the wind velocity was 5 m/s and the temperature was, at least for some periods of time, below that of the pour point. a. Variation of evaporated fraction with time b. Parity plot considering as well experiments at 3, 5 and 8 m/s.	51

5.12. Position of important parameters relative to the pour point curve to explain how MEUN models the pour point effect on the evaporation rate.	53
5.13. Comparison of the experimental evaporated fraction with MEUN predictions. a. Variation of the evaporation rate with time for a wind velocity of 5 m/s. b. Parity plot for all the experimental data.	54
5.14. Ratio between evaporated and fresh crude oil density as function of the evaporated fraction. Experimental results (points) are presented for Cusiana and Vasconia as well as predictions by the state-of-the-art correlation [7] (dashed line) and by the best regression (continuous lines) for Cusiana and Vasconia.	55
5.15. Ratio between evaporated and fresh crude oil viscosity as function of the evaporated fraction at 28°C. Experimental results are presented for Cusiana and Vasconia as well as recommended prediction according to Lehr et al. [8].	56
5.16. Variation of the viscosity of the slick with temperature with the evaporated fraction as parameter. Comparisons of experimental data (symbols) with model results (bold lines). a. Cusiana. b. Vasconia.	57
5.17. Experimental behavior in the rotating cylinder of Vasconia crude oil with the evaporated fraction as parameter. a. Mixing. b. Settling. The experiments were carried out at a temperature that varied between 23 and 25°C.	59
5.18. Experimental emulsification results for Cusiana crude oil. a. Behavior with respect to pour point curve. b. Evolution of water content with time for experiments above and below the pour point curve.	60
5.19. Evolution of water content with time for Cusiana 48 % evaporated and Vasconia 15.5 % evaporated. a. experimental behavior adjusted with a first order kinetic. b. extrapolated behavior to field conditions and compared with Mackay and coworkers' model [8].	61
5.20. Variation of the emulsion stability parameter $R_{2/1}$ for: a. Cusiana in terms of temperature value of pour point. b. Vasconia as function of evaporated fraction with temperature as parameter.	63
5.21. Comparison of the experimental and MEUN predictions for density of emulsions formed with Cusiana and Vasconia.	64
5.22. Variation of the viscosity ratio between emulsified and water-free crude oil as function of evaporated fraction. a. Cusiana, b. Vasconia. At temperature of 25°C	65
5.23. Prediction of oil spill budget for Cusiana crude oil in Case I (see Table 5.3). a. MEUN b. ADIOS.	68

5.24. Prediction of oil spill budget for Cusiana crude oil in Case II (see Table 5.3). a. MEUN b. ADIOS.	69
5.25. Comparison of the variation of viscosity with time as predicted with the module MEUN and the model ADIOS. a. Case I. b. Case II.	69
5.26. Temperature of test cases I and II with respect to pour point curve of Cusiana crude oil.	70
5.27. Prediction of oil spill budget for Vasconia crude oil in Case III (see Table 5.3). a. MEUN b. ADIOS.	72
5.28. Comparison between MEUN and ADIOS predictions for Vasconia crude oil in Case III (see Table 5.3). a. Water content b. Viscosity.	72
5.29. Comparison of evaporated fraction of Vasconia crude oil predicted with the module MEUN and the model ADIOS. a. Case III. b. Case IV.	73
5.30. Mesh and boundary conditions of the wind tunnel simulated.	81
5.31. Comparison between the evaporated fraction of Vasconia predicted with the optimized parameters (θ_{opt}) and with the parameters diverted from their optimized values (θ).	84
5.32. Effect of the uncertainties of the optimized parameters a , b and c (expressed in terms of the resulting mass transfer coefficient computed with Equation E-38) in the percentage error of the evaporated fraction predicted. a. Cusiana b. Vasconia.	85
5.33. Percentage error of the evaporated fraction with respect to deviations in the optimized parameters of Equation E-38. a. parameter a . b. Parameter b . c. parameter c	85

List of Tables

3.1. Viscosity increases from starting oil and typical water content of four possible kind of emulsions according to Fingas [9].	19
4.1. SARA composition of Colombian crude oils.	26
4.2. Experimental conditions to study the emulsification behavior of Vasconia crude oil. . .	36
4.3. Experimental conditions to study emulsification behavior of Cusiana crude oil.	37
5.1. Experimental viscosity of Cusiana and Vasconia crude oils as function of evaporated fraction and temperature.	56
5.2. Half-life time of the emulsification process for Vasconia as function of temperature and evaporated fraction.	62
5.3. General conditions to test MEUN predictions	67

Physical constants

Gravity

$$g = 9.81 \text{ m s}^{-2}$$

Gas constant

$$R = 8.314 \text{ m}^3 \text{ Pa K}^{-1} \text{ mol}^{-1}$$

Symbols

a, b	empirical constants ($a = 6.3$, $b = 10.3$, Stiver and Mackay [10])	
A	spill area	m^2
A_0	oil spill area after the first stage of spreading	m^2
c_{eva1}	empirical constant ($c_{eva1} = 10$ for crude oils, Mackay et al. [8])	
c_{eva2}	empirical constant ($c_{eva2} = 0.18$ for crude oils, Lehr et al. [7])	
C_0	proportionality constant which depends of oil type and weathered state	
d	oil particle diameter	m
D_d	dissipated breaking wave energy per unit surface area	Jm^{-2}
Δd	oil particle diameter interval	m
$\Delta\rho$	relative difference between water and crude oil density	
F	fraction of sea surface hit by breaking waves (“white-caps”) per unit time	s^{-1}
F_{eva}	Evaporated fraction	
K_{emu}	constant for the emulsification process	
k_1, k_2	empirical constants (1.14 and 1.45 respectively, Fay [11])	
K_{spre}	spreading constant with default value of 150	s^{-1}
k_w	mass transfer coefficient	ms^{-1}
k_{wi}	mass transfer coefficient for pseudocomponent i	ms^{-1}
μ	crude oil viscosity	cP
μ_0	viscosity of parent oil	cP
μ_{eva}	viscosity of evaporated oil	cP
μ_{ref}	crude oil viscosity at reference temperature	cP
μ_T	viscosity at temperature T	cP

MW_i	molecular weight of pseudocomponent i	$kg\ mol^{-1}$
ν_w	water kinematic viscosity	m^2/s
P_i^{sat}	vapor pressure of pseudocomponent i	Pa
ρ_{ref}	crude oil density at a reference temperature	kg/m^3
ρ_o	initial crude oil density	kg/m^3
ρ_w	water density	kg/m^3
S	fraction of sea surface covered by oil ($0 \leq S \leq 1$)	
Sc	Schmidt number	
S_i	specific gravity of pseudocomponent i	
s_t	oil-water interfacial tension	$dyn\ cm^{-1}$
T	temperature	K
$t_{1/2}$	half-life of emulsification process	s
T_{b_i}	boiling point temperature of pseudocomponent i	K
T_0	initial boiling point of oil	K
T_G	gradient of the oil distillation curve	K
U_w	wind velocity	$m\ s^{-1}$
$V_{disp}(d)$	volume of crude oil dispersed in the water column as oil droplet with droplet size in a interval Δd around d	
V_0	initial oil spill volume	m^3
v_i	molar volume of pseudocomponent i	$m^3\ mol^{-1}$
X	equivalent diameter of the oil spill	m
x_i	mole fraction of pseudocomponent i	
Y_{max}	maximum fractional water content in emulsion	

Chapter 1

Introduction

1.1. Motivation

In Colombia, two very important processes in oil industry have a potential risk of an ocean oil spill in case of accident: offshore hydrocarbon extraction and crude oil transportation, mainly, through the Colombian Caribbean Sea. Given the numerous environmental and economical hazards associated to an ocean oil spill, it is of paramount importance to characterize the behavior of the crude oil after an oil spill. This characterization can be done through simulations that predict the relative motion of the oil slick with respect to the point of the accident. By knowing the path of the spill it is possible to define populations or areas affected. At the same time an oil spill model must simulate oil weathering, or the physicochemical changes that occur to the spilled oil because of its interactions with the atmosphere and ocean.

Weathering modeling is useful in both, short (days to weeks) and long time scales (months to years). In the short time scales the change in physicochemical properties, particularly an increase in viscosity, has a great influence in the feasibility of various oil spills countermeasure techniques such as chemical treatment (dispersants), burning or mechanical recovery [12]. Oil weathering modeling also helps to estimate the distribution of the oil in surface, water column and air.

A crude oil weathering model must integrate different submodels that represent the set of possible physicochemical processes. In the reviewed literature there are different approaches that describe how to model each individual phenomenon responsible for oil weathering, i.e. evaporation, emulsification, dispersion and spreading. As existing models are of empirical character they demand adjustment to new environmental conditions. Furthermore, in the refereed literature the author did not find a cri-

tical evaluation of the performance of these models when modeling an oil spill of a Colombian crude oil.

Recognizing this, the present research has as objective the development of a weathering model for an oil spill of Colombian crude oils under metaocean conditions of the Caribbean Sea.

1.2. Research objectives

1.2.1. Objective

To model oil weathering of Colombian crude oil in the Colombian Caribbean Sea.

1.2.2. Specific objectives

- To define and model the different processes responsible of oil weathering in an ocean-atmospheric environment in the first week after an oil spill.
- To develop and calibrate a model that integrates submodels of physicochemical processes for the weathering of Colombian crude oils in the Colombian Caribbean Sea.

1.3. Description of the thesis

This thesis begins with a chapter defining some general concepts: an introduction to the concept of oil weathering after an oil spill, a description of the Colombian Caribbean Sea, region of study of this research and an introduction to the behavior of waxy crude oils that helps to describe the weathering behavior of one of the Colombian crude oils studied in this thesis.

The third chapter presents a discussion of the state-of-art in modeling strategies of weathering after ocean oil spills. Based on this discussion, the model with the best applicability to the Colombian oil and Caribbean Sea conditions was selected and implemented into MEUN.

Chapter four describes the experimental methodology to evaluate the main features of the evaporation and emulsification processes in order to obtain data to compare with MEUN predictions. In the case of evaporation this chapter describes a custom designed experimental setup; for emulsification the rotating-cylinder method, a standard in the weathering community for emulsification tests.

Chapter five compares the predictions by MEUN with the data collected from the experiments. This comparison is followed by the adjustment of the model to minimize differences between experiments and predictions. The final result of this chapter is a version of MEUN adjusted to the behavior of Colombian crudes. Chapter five ends evaluating the performance of MEUN in a set of weathering test cases under typical metaocean conditions of the Colombian Caribbean Sea.

Chapter 2

General concepts

2.1. Oil spill weathering

Immediately after a marine oil spill, the oil begins to suffer physicochemical interactions with the atmosphere and the water column. The whole set of processes is called oil weathering and most of them are represented schematically in Figure 2.1a. An important feature of these interactions is that each process has a time scale of relevance in the behavior or characteristics of the spill as seen in Figure 2.1b.

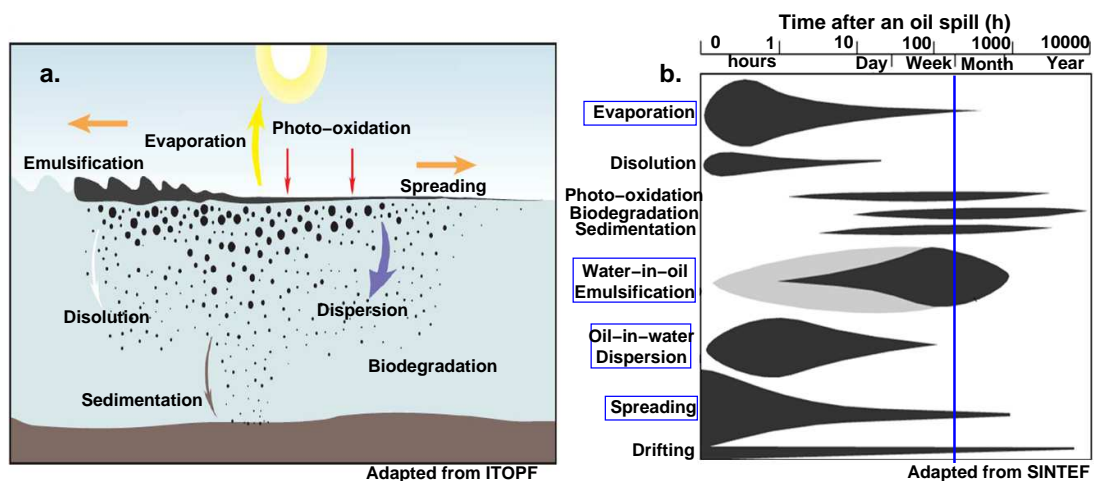


Figure 2.1: Weathering processes. a. schematic diagram, adapted from ITOPF [1]. b. relative importance over time, adapted from SINTEF [2], processes marked with blue are studied in this thesis.

The impact magnitude of each weathering process is relative to the oil spill aspect to evaluate. For example evaporation is an important process in order to define the overall impact of an accident,

removing up to 75 % of the spilled amount from oil spills with light crude oils [13]. However, for toxicological studies in the water column, dissolution plays an important role despite its small contribution to weathering (about 1 % of the spilled amount [14]) because the most soluble oil components are usually the most toxic and even low concentrations of those compounds may produce a serious effect on biological systems [15].

One of the most important processes in the short-time scale is emulsification. In this process, because of the mix of oil and ocean and the surfactant/stabilizing effect of certain compounds in the crude oil (mainly resins, asphaltenes and waxes) water-in-oil-emulsions are produced and they can reach up to 80-90 % of water content. This translates, in practical terms, in a four to five fold increase in the amount of the oil slick to be cleaned. Moreover, stable emulsions present a non-Newtonian behavior with a typical viscosity increase of up to 3 orders of magnitude [13]. This increase in viscosity can limit the effectiveness of mitigation strategies such as the use of dispersants or pumping with skimmers [16, 17].

Natural dispersion is another significant process in the first week after an oil spill. This process deals with the amount of crude oil that migrates to the water column as small droplets because of turbulence, particularly that produced by breaking waves. This process can have a significant effect on light crude oils under high turbulence. One anecdotic example is the oil spill of the Gullfaks crude oil. In this incident the low viscosity of the spilled oil and the high turbulence level during the accident produced the dispersion of almost all the 85000 spilled tons [18].

In addition to the challenge of dealing with a complex mixture like crude oil, there is a strong interaction between the weathering processes that must be considered in oil spill modeling. For example, as evaporation advances, some water-in-oil emulsions become more stable. This combination of evaporation and emulsification produces a significant viscosity increase, which in turn affects both natural and chemical dispersion in the water column.

The first week after an oil spill is responsible for the most significant changes in crude oil properties particularly in viscosity. Furthermore this time scale defines the “window of opportunity” for some countemesure techniques such as the use of chemical dispersants. During the first week, the weathering processes that are more important are evaporation, emulsification, dispersion and spreading, those marked with blue in Figure 2.1b. Although dissolution is active during the first week, its magnitude is low and relevant only to address the importance of toxicological effects.

2.2. Colombian Caribbean Sea

The Colombian Caribbean sea is situated in the northwestern corner of South America as shown in Figure 2.2a. The area located between latitudes 8-13°N and longitudes 79-71°W is of particular importance when studying oil weathering as it includes Colombia's main port dedicated to the transport of hydrocarbons marked as "Marine oil terminal Coveñas" in Figure 2.2b. Through this port the crude oils Cusiana and Vasconia, studied in this research and described below in Section 4.1, are exported.

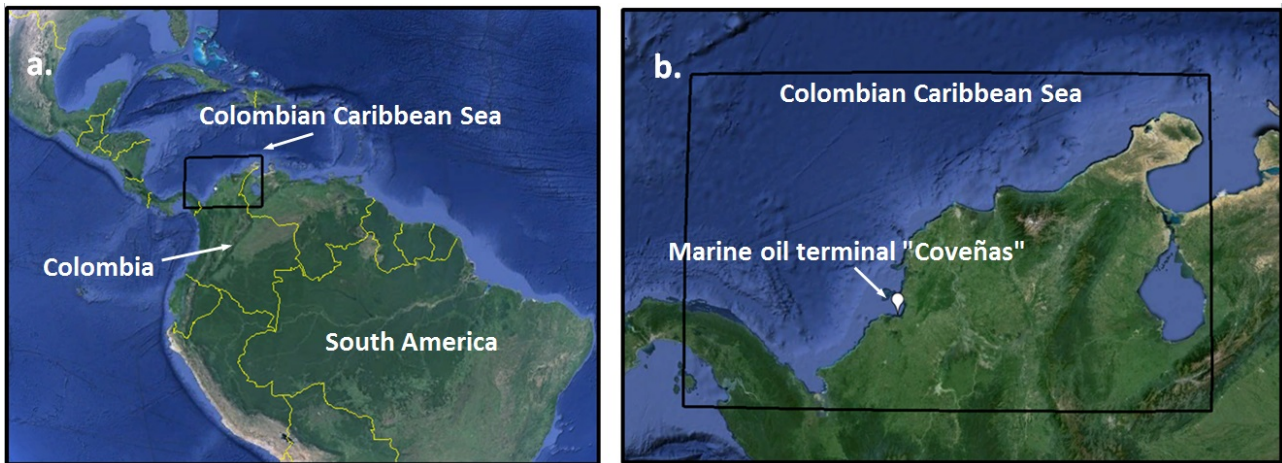


Figure 2.2: Relative location of Colombian Caribbean Sea. a. With respect to South America. b. With respect to Colombia. The figure shows the port where hydrocarbons are exported.

The metocean variables of interest for weathering are Sea Surface Temperature (SST) and the magnitude of wind velocity. With respect to SST, Bernal et al. [19] studied the space-time variability of the sea surface temperature for the Colombian Caribbean Sea from the database COADS (Comprehensive Ocean-Atmosphere Data Set). Their analysis included average and lower and upper limits for the SST during the year. Although the analysis was based on different quadrants in the Colombian Caribbean region, for the scope of this research it is enough to say that the average temperature in all quadrants varied mostly in the range 27-28°C, with maximum and minimum temperatures of 30°C and 24.5°C respectively, which suggests a typical annual interval of 4-5°C.

With respect to the magnitude of the wind velocity, Ruiz and Bernal [20] analyzed almost 60 years of monthly records of wind magnitude in the Caribbean Sea. According to them, depending on the region, the average wind velocity varies between 4.6 ± 1.6 - 8.2 ± 1.7 m/s.

2.3. Introduction to the behavior of waxy crude oils

Crude oil is a mixture of different types of compounds: saturates, aromatics, resins, asphaltenes and waxes. Waxes are paraffinic molecules of high molecular weight which are dissolved in the crude oil. If a crude oil contains high proportion of those paraffinic compounds is known as a waxy crude oil.

All crude oils have a wax solubility limit, known as Wax Appearance Temperature (WAT) or cloud point. At this temperature the waxes in the crude oil start to precipitate. As the crude oil temperature decreases below the cloud point, precipitation increases. This precipitation has consequences that are well known by the oil industry as in crude oil transportation precipitated waxes may deposit on the walls of a pipe and form a network of solid wax cristal that restricts oil flow and may stop production [21]. Under static conditions, the onset of gelation of crude oil is determined with the pour point and is measured according to the standard ASTM D97-12 [22].

An important issue when modeling the weathering behavior of crude oils after an oil spill is the impossibility to talk about a single pour point value because waxes as high-molecular weight molecules of low volatility, register an increase in concentration because of evaporation which in turn increases the cloud and the pour points. To illustrate this, Figure 2.3 shows the behavior of the pour point as the evaporated fraction for Grosbeak crude oil increases [3]. The figure shows that before evaporation the pour point is 0°C. However, when the evaporated fraction is 49 %, the pour point increases to 30°C. This means that the instant just after an oil spill in the Caribbean Sea, where temperatures are above 25°C, wax precipitation is negligible. However, as the oil slick evaporates the pour point increases and gets closer to the sea temperature, making the analysis of waxy behavior of some oils relevant.

Venkatesan et al. [23] have explained that the pour point does not serve as good reference for wax deposition under flow conditions, rather it should be referenced with respect to a gelation temperature which depend of crude oil properties and also of flow conditions. Those studies suggests that under flow conditions, wax precipitation occurs below the pour point, how far below the pour point is significantly determined by factors such as shear rate.

Contrary, in weathering community, waxy crude oil behavior is always referenced with respect to the pour point, but it is also accepted that the effects of wax precipitation rarely coincide exactly with the pour point curve and the crude oil temperature has to be certain degrees celsius below that of the

pour point to detect any particular effect [1, 24, 25].

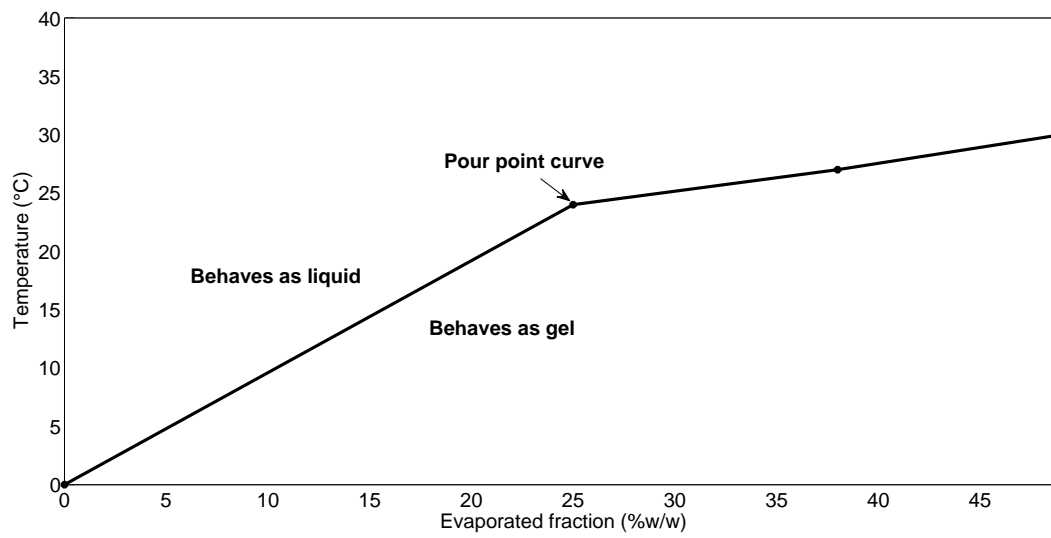


Figure 2.3: Evolution of pour point with evaporated fraction for the waxy crude oil Grosbeak [3].

Chapter 3

Development of the weathering module MEUN

As it was discussed above, based on their relative importance, the weathering processes to study in this research are evaporation, emulsification, dispersion and spreading, as well as the changes in density and viscosity of the oil slick. For each one of those processes, this chapter describes different modeling strategies reported in the state of the art and discusses the selection of those with better performance to be implemented in the weathering module MEUN.

3.1. Evaporation

When crude oil is spilled at sea, evaporation is one of the most important processes to understand and predict because in most of cases the evaporation of the volatile fractions of crude oil is the most important route that remove oil after a spill. As a rule of thumb in the first few days after an oil spill, the light, medium, and heavy crude oils can evaporate respectively up to 75 %, 40 % and 10 % of its original mass [15]. Furthermore, evaporation causes a significant change in some oil properties such as density, viscosity and pour point [26]. Some researchers consider evaporation so important that it is the only weathering process considered by some oil spill prediction models [13].

3.1.1. Evaporation models

In evaporation modeling, one of the main challenges is to handle the complex crude oil composition, with an initial high evaporation rate -exponential with time- of the lighter components leaving a residual part each time more resistant to evaporate, producing a logarithmic behavior of the overall evaporated fraction with time [15]. Another important challenge is the significant influence of other

variables such as oil spill thickness and area, oil temperature and wind velocity [4].

To overcome these challenges, since the early 60's different modeling strategies were developed as described in several reviews [4, 15, 26, 27] that agree in the existence of three main methodologies for modeling evaporation as briefly discussed below.

3.1.1.1. Evaporative exposure or analytical model

This model considers the crude oil as a single component that changes its thermodynamic properties with the progress of evaporation. This approach attempts to reproduce the fact that at the beginning of the evaporation, the light compounds are quickly evaporated leaving heavy compounds with virtually zero evaporation rate. This formulation has been widely used because of its simplicity that makes its solution simple. This model considers that the evaporation rate is proportional to a mass transfer coefficient k_w and to a driving force that is the difference between the vapor oil concentration at the interface (immediately above the oil slick) and that in the bulk fluid (in this case air), assumed to be zero. An important assumption of this model is that the distillation curve of the crude can be represented as a straight line so that the vapor oil concentration at the surface can be expressed in terms of the initial point and the slope of the distillation curve, T_0 and T_G respectively, as well as in terms of the empirical constants a and b with suggested values of 6.3 and 10.3 respectively.

This model, originally proposed by Stiver and Mackay [10], computes the evaporated fraction by the solution of Equation 3.1.

$$\frac{dF_{eva}}{dt} = e^{a - \frac{b(T_0 + T_G F_{eva})}{T}} \frac{k_w A}{V_0} \quad (3.1)$$

where A is the area of the oil slick (m^2) and V_0 the initial oil spill volume (m^3). An important thing in this equation is that it reflects how the evaporation rate decreases as the evaporated fraction F_{eva} increases and how evaporation rate increases as the temperature T increases.

3.1.1.2. Pseudocomponent model

A more complete model, proposed by Payne et al. [28] considers the use of pseudocomponents to more adequately represent the complex thermodynamic behavior of a heterogeneous mixture such as crude oil. Crude oil is approximated as a group of pseudocomponents, each one with different thermodynamic properties and different evaporation rates. Similar to the evaporative exposure model discussed above, this model considers the evaporation rate -in this case of each pseudocomponent i -

as a combination of the mass transfer coefficient k_{w_i} and a concentration difference as driving force, assuming that the concentration in air is equal to zero. In this model, the concentration of each pseudocomponent at the surface of the oil slick is related to its partial pressure which in turn is estimated with Raoult's law assuming ideal gas and ideal solution. Equation 3.2 shows the final result expressing the evaporation rate of the pseudocomponent i in terms of its vapor pressure P_i^{sat} , mole fraction x_i and molar volume v_i .

$$\frac{dV_i}{dt} = -\frac{k_{w_i} A x_i P_i^{sat} v_i}{RT} \quad (3.2)$$

where R is the gas constant and V_i the volume of the pseudocomponent i (m^3). To calculate the thermodynamic properties of each pseudocomponent required to solve Equation 3.2 a common approach is to use the expressions recommended by the API [29] showed in detail in Appendix A. These expressions require the specific gravity S_i and the normal boiling point T_{b_i} for each pseudocomponent.

Some similarities between the first two evaporation models discussed above are:

- Both models consider the oil slick as an homogeneous mixture, i.e. there is no vertical gradients of any component along the oil thickness, neglecting any possible diffusion resistance. In the weathering community this is called “the well-mixed oil slick” assumption.
- The driving force for evaporation is the effective vapor pressure of the crude oil and the limiting factor will be the ability of the wind to remove the oil vapor from the surface boundary layer [30], otherwise, the assumption made by both models of a concentration equal to zero in the air would be not that valid. The effect of wind speed is included in the mass transfer coefficient k_w of equations 3.1 and 3.2. Some existing correlations to calculate k_w are discussed below.

One of the correlations most used in literature [31–34], was developed by Mackay and Matsugu [13] who, from experiments carried out with water, cumene and gasoline, determined dependencies of the mass transfer coefficient with respect to wind speed and an effect, referred to as “pool size effect”, that considers that the air downstream of the mass transfer area has a certain concentration of volatile compounds, decreasing the effective mass transfer rate, represented in Equation 3.3 with the negative sign of the exponent of the scale factor X .

$$k_{w_i} = 0.0048 U_w^{0.78} X^{-0.11} S_{C_i}^{-0.67} \quad (3.3)$$

where U_w is the wind velocity (m/s), X is defined as the equivalent diameter of the oil spill (m) and Sc is the schmidt number defined as the ratio of kinematic viscosity and diffusivity.

In 1977, Yang and Wang [35] proposed a similar expression (Equation 3.4), this time using three different crude oils with relative gravities varying between 0.84 and 0.88 and the “pool size effect” expressed in terms of the mass transfer area A .

$$k_{w_i} = 69A^{-0.055}e^{0.42U_w} \quad (3.4)$$

Riazi et al. [36] proposed a correlation fitting experimental data with crude oils with relative densities varying between 0.71 and 0.93. This correlation adds the dependency on the molecular weight of each pseudocomponent i , as expressed in Equation 3.5.

$$k_{w_i} = 1.5 \times 10^{-5} (U_w)^{0.8} (T/MW_i)^2 \quad (3.5)$$

To take into account the effect that differences in crude oils can have in mass transfer coefficient, Hamoda et al. [37] proposed an expression (Equation 3.6) that considers the API gravity of the crude oil.

$$k_{w_i} = 1.68 \times 10^{-5} (API)^{1.253} (T)^{1.80} (e)^{-0.1441} \quad (3.6)$$

The limitation of some of the correlations discussed above and others available in the literature and reviewed by Fingas [13] is that they have been forced-fit to the experimental results leaving the doubt of its applicability to other conditions (type of crude oil, wind velocity, temperature).

3.1.1.3. Fingas model

Based on a large series of experiments, this model suggests that the evaporation rate is not strictly controlled by mass transfer in the air/slick interface, therefore the process can be represented with a simplistic evaporation equation that only considers the time and temperature as important factors and neglects aspects such as wind velocity, turbulence level, slick area, thickness, and scale size [38]. In his research, Fingas defines a particular empirical equation for over 120 crude oils including two Colombian crude oils as presented in equations 3.7 and 3.8.

- Cusiana

$$F_{eva}(t) = (3.39 + 0.0457T) \ln(t) \quad (3.7)$$

- Vasconia

$$F_{eva}(t) = (0.84 + 0.045T) \ln(t) \quad (3.8)$$

3.1.1.4. Evaporation model for waxy crude oil

In the case of waxy crude oils Mackay and McAuliffe [14] propose that a film may form at the evaporating surface which impedes evaporation from the bulk of the oil. In terms of modeling, in the revised literature two different approaches have been described to model evaporation as described below.

- The research by Yang and Wang [35], reports in the experiments a thin film formed on the surface which restricted the evaporation rate. This study did not indicate whether it was a waxy crude oil or not. To model this behavior, they proposed that the film was formed when the ratio between density at time t and the initial density was 1.0078, and thereafter evaporation rate would be reduced by 80 %. This approach is very empirical as it defines the threshold to decrease evaporation in terms of a ratio of densities and not to the gelation effect per se.
- In the work developed by Buist et al. [24] it was an explicit interest in characterize waxy crude oils behavior, they suggest that in case of waxy oils a waxy “crust” may be formed offering resistance to diffusion. To model this, they propose a system of two mass transfer resistances in series, the regular boundary layer resistance and other resistance for the crust. Although the formulation is logical, they do not propose a way to calculate that new mass transfer resistance, they just give a specific value obtained from fitting experimental data for a specific crude oil.

As described in the first paragraph of this chapter, the approach followed to develop MEUN was to first describe, as already carried out for evaporation in Section 3.1.1, the state of the art of the models involved in each process and then to select those that performed the best for MEUN. Section 3.1.2 and similar below, describe how to model for each individual process was developed in MEUN.

3.1.2. Evaporation model implemented in the weathering module MEUN

In order to select the best approach to represent the evaporation of crude oil after the spill, simulations with the three models described above were carried out and compared to the experimental data for the evaporation of Statfjord crude oil at 15°C and at 15 km/h of wind velocity reported in Sebastião and Soares [4]. Equation 3.9 presents the empirical expression for Statfjord crude oil according to Fingas [38].

$$F_{eva}(t) = (2.67 + 0.06T) \ln(t) \quad (3.9)$$

The thermodynamic parameters needed to solve the evaporative exposure model (Equation 3.1) were taken from Sebastião and Soares [4]. The methodology of the pseudocomponent model explained in Section 3.1.1.2 only requires the TBP curve of the crude oil of interest; for Statfjord it was taken from the crude oil database of the simulation program ASPEN [39].

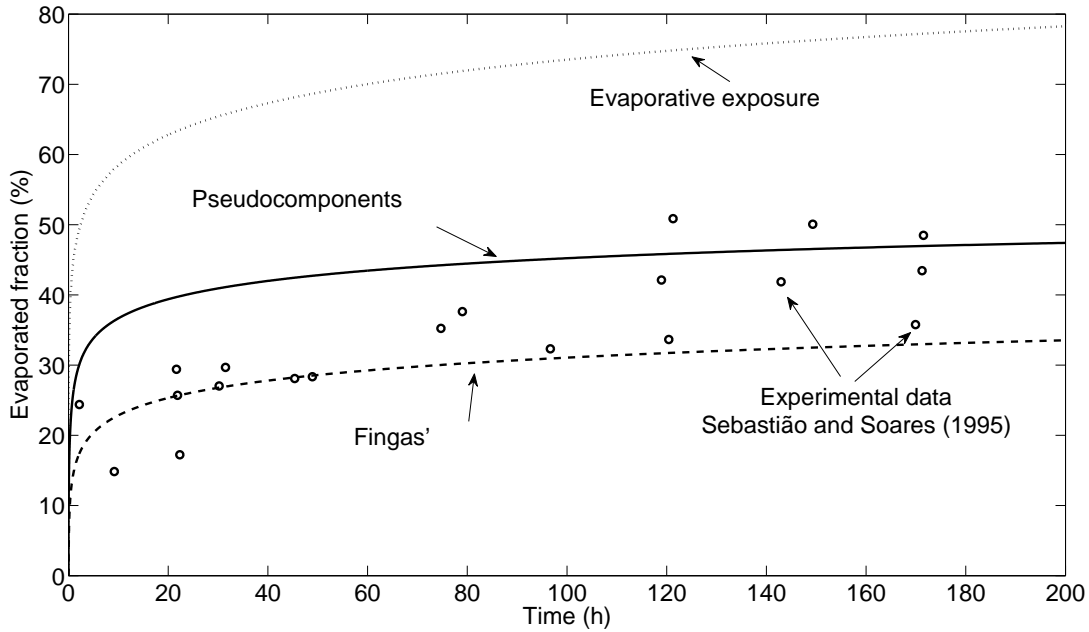


Figure 3.1: Evaluation of the evaporated fraction of Statfjord crude oil at 15°C and 15 km/h of wind velocity using the three evaporation models discussed in Section 3.1.1. Model results are compared with experimental data reported in Sebastião and Soares [4].

Figure 3.1 shows that the evaporative exposure model overestimates the evaporated amount of crude oil. Furthermore, the assumption that the distillation curve is a straight line seems far-fetched as most distillation curves of Colombian crudes exhibit a marked non-linear behavior as shown in Figure 4.1. The results of both, the pseudocomponent and Fingas' models are closer to the experimental data of the evaporated fraction. Because the Pseudocomponents model has more details in its formulation than the Fingas' model as it includes a term for the effect of wind velocity, that model was selected to compute the evaporation rate in MEUN. The final equation for this model, Equation 3.10, can be derived from the definition of the evaporated fraction and Equation 3.2.

$$F_{eva}(t) = 1 - \frac{1}{V_o} \sum_{i=1}^{n_{pc}} V_i \quad \text{with} \quad \frac{dV_i}{dt} = -\frac{k_w A x_i P_i^{sat} v_i}{RT} \quad (3.10)$$

where the summation is made over the number of pseudocomponents n_{pc} .

3.1.3. Changes in density and viscosity

As discussed in Section 3.1.1, there are different approaches in the state of the art to evaluate the evaporated fraction of crude oil. Contrary to estimate the increase in density and viscosity due to evaporation, only equations 3.11 and 3.12, originally proposed by Mackay et al. [8] were found in the refereed literature. These are the two equations used by MEUN.

$$\mu_{eva} = \mu_{ref} e^{c_{eva1} F_{eva}} \quad (3.11)$$

$$\rho_{eva} = \rho_{ref} (1 + c_{eva2} F_{eva}) \quad (3.12)$$

where:

μ_{eva} , ρ_{eva} : crude oil viscosity (cP) and density (g/ml) after evaporation, respectively

μ_{ref} , ρ_{ref} : fresh crude oil viscosity (cP) and density (g/ml), respectively

c_{eva1} , c_{eva2} : empirical constants ($c_{eva1} = 10$ for crude oils according to Mackay et al. [8], $c_{eva2} = 0.18$ according to Lehr et al. [7])

To evaluate the change in viscosity with temperature, the exponential form in Equation 3.13 is widely used.

$$\mu_T = \mu_{T_{ref}} \exp \left[c_{vT} \left(\frac{1}{T} - \frac{1}{T_{ref}} \right) \right] \quad (3.13)$$

where:

$\mu_{T_{ref}}$: crude oil viscosity (cP) at a reference temperature T_{ref} (K)

μ_T : crude oil viscosity (cP) at temperature T (K)

c_{vT} : adjustment constant ($c_{vT} = 5000$ K according to NOAA [40] or 9000 K according to Payne et al. [28])

In the oil industry the empirical constant c_{vT} is expressed as Ea/RT , where the activation energy is the crude oil-dependent parameter to adjust. The weathering module takes the recommended value $c_{vT} = 5000$ K corresponding to an activation energy of 41570 J/mol. It is important to note that empirical

constants c_{eva1} and c_{vT} do not represent the solid-like behavior of waxy crude oils at temperatures below the pour point.

3.2. Emulsification

A submodel for the process of emulsification predicts the evolution of the water content of the oil slick with time, also called emulsification rate, and the changes in the viscosity of the slick as the water content increases. The water uptake of the oil slick continues until it reaches the maximum water content that is possible to stabilize with the amount of surfactant compounds in the crude oil. Based on the the features of this process, the author proposes some aspects that should be considered by an appropriate emulsification approach:

- Crude oil-dependent maximum water content and emulsification rate. Experimental studies carried out by Daling et al. [41] suggest that the maximum water content and water uptake rate have significant variations from one crude oil to another. Moreover Daling et al. recommend that these parameters should be determined experimentally for every crude oil and to be considered as an intrinsic characteristic that serves as input in a weathering model.
- Emulsion stability effect on viscosity predictions. The stability is a measure of the decrease in the water content of an emulsion kept in stagnant conditions. Only stable emulsions have an increase of almost three orders of magnitude in the viscosity of the slick. For unstable emulsions the viscosity increase is almost never more than an order of magnitude [26].
- Weathering effect on emulsification behavior. One of the particular characteristics in oil weathering is that even a crude oil that at the initial time of the spill does not form any kind of emulsion, can form very stable emulsions after weathering, particularly as a result of evaporation and photo-oxidation [12, 42]. With evaporation there is a reduction in the concentration of aromatic compounds that solubilize asphaltenes and polar molecules. Once those compounds leave the oil phase they are available to stabilize water droplets in the oil mass, preventing droplet coalescence and increasing the amount of water in the slick [12, 43].

Three different emulsification approaches widely referenced by the oil spill community are presented below.

3.2.1. Emulsification models

3.2.1.1. Mackay and coworkers' model [8]

This model assumes that the rate of water uptake by the oil slick follows a first order kinetics with respect to the ratio of the current and the maximum water content. This rate law involves variables as wind speed, the fraction of water in the crude and the maximum water content that can support and stabilize the oil slick.

The model of Mackay et al. solves equations 3.14 and 3.15 to calculate the water content and change in viscosity of the oil slick, respectively.

$$\frac{dY}{dt} = K_{emu} (1 + U_w)^2 \left(1 - \frac{Y}{Y_{max}}\right) \quad (3.14)$$

$$\mu = \mu_0 e^{\frac{aY(t)}{1-bY(t)}} \quad (3.15)$$

where a and b are empirical constants (2.5 and 0.654 respectively), Y is the fractional water content in volume, Y_{max} is the fractional maximum water content in volume (≈ 0.7 for crude oils and heavy crude oils and 0.25 for home heating oil) and K_{emu} is an emulsification rate constant ($2.0 \times 10^{-6} s/m^2$).

Equation 3.14 shows that Mackay and coworkers' model predicts the emulsification process according to a first order kinetics with values of kinetic constant and maximum water content that do not depend on the type of crude oil. The increase in viscosity solely depends on water content but is independent of emulsion stability. Despite its empirical nature, this model has been widely used in the literature of spill simulation [33, 44, 45], obtaining acceptable predictions of water content and viscosity even when compared to field data with different crude oils [46].

3.2.1.2. Fingas model [9]

This model proposes general empirical rules of emulsification through a comprehensive experimental work with more than 400 crude oils. This model considers that, depending on SARA composition, density and viscosity of the crude oil, four different types of emulsions are formed: stable, meso-stable, entrained water and unstable. Table 3.1 as discussed below, describes the ratio of change in viscosity and the typical water content of these types of emulsions.

The stable emulsion persists for several months once formed, has a typical value of 75% water content and generates a viscosity increase close to three orders of magnitude with respect to the non-

emulsified crude oil. Meso-stable emulsions has characteristics between those of stable and unstable emulsions. Although meso-stable emulsions may initially have a water content close to 65 %, this type of emulsion does not have the right concentration of resins and asphaltenes to stabilize the water droplets and most of this water content is lost in hours or days. This lack of stability is reflected in the fact that typically the viscosity of meso-stable emulsions is only 7 to 11 times the viscosity of the initial crude oil. Entrained water emulsions are formed by viscous oils (typically ≥ 1000 mPa.s) and the water retention mechanism is not stabilized by surfactant action. Instead, oil viscosity alone may be a partial barrier to the recoalescence of the water droplets. This type of emulsion has in average 44 % of water content and its viscosity increase averages a multiple of two. Unstable emulsions are characterized by the fact that the oil does not hold significant amounts of water.

The Fingas model defines at any time after an oil spill the kind of emulsion formed and the water content and viscosity increase according the Table 3.1.

Table 3.1: Viscosity increases from starting oil and typical water content of four possible kind of emulsions according to Fingas [9].

Emulsion Type	Viscosity increase on		Typical water content	
	First day	Week	First day	Week
Stable	405	1054	81	78
Meso-stable	7.2	11	64.3	30
Entrained	1.9	1.9	44.5	27.5
Unstable	0.99	1.00	6.1	6

In publications that extend this model, Fingas [9, 27] and Fingas and Fielhouse [42, 47] showed an extensive amount of experimental data for a significant number of commercially-relevant crude oils, that included the type of emulsion formed and the changes in the nature of the emulsion with changes in the evaporated fraction.

According to Fingas and Fielhouse [42], a possible way to simulate emulsification is coupling this experimental data with an evaporation model, so that at any time t , it would be possible to know the evaporated fraction, with this value and the knowledge of the nature of crude oil of interest the experimental data in references [9, 42] gives the type of emulsion formed, and then using Table 3.1 the weathering model would predict the average water content and the viscosity increase of the emulsion. This approach presents two main limitations:

- It only predicts final values of water content and viscosity without discussing the evolution of those properties with time.
- The database should include experimental data for the crude oil of interest.

3.2.1.3. SINTEF's oil weathering model (OWM) [48]

This model fulfills the three desired characteristics in an emulsification model mentioned at the beginning of Section 3.2. However, as was the case with Fingas' model, the predictions depend on experimental data obtained for a specific crude, limiting its application to crude oils in SINTEF's databases.

The OWM model computes the evolution of water content with time using Equation 3.16:

$$Y(t + \Delta t) = Y_{max}(t) - [Y_{max}(t) - Y(t)] 0.5^{\frac{\Delta t}{t_{1/2}}} \quad (3.16)$$

Equation 3.17 presents the differential form of Equation 3.16 (for deduction see Appendix B).

$$\frac{dY}{dt} = \frac{Y_{max}(t) \ln(2)}{t_{1/2} (U_w)} \left(1 - \frac{Y}{Y_{max}(t)} \right) \quad (3.17)$$

Comparing Equations 3.17 and 3.14 it is possible to see some similarities. Both equations are based on first-order kinetics for the water uptake rate, but only the equation of OWM has a parameter, the half-life $t_{1/2}$ that depends on the crude oil of interest. Using expressions explained in more detail in Appendix B, it is possible to relate the half-life under field conditions $t_{1/2}$ with the half-life of a laboratory scale experiment $t_{1/2|lab}$ explained in detail in reference [6]. Equation 3.18 shows the final expression to calculate the water uptake rate.

$$\frac{dY}{dt} = \frac{Y_{max}(t) \ln(2)}{605 t_{1/2|lab}} (1 + U_w)^2 \left(1 - \frac{Y}{Y_{max}(t)} \right) \quad (3.18)$$

The OWM model also includes Equation 3.15 to calculate the changes in viscosity but instead of fixed values for a and b , these constants are adjusted to fit experimental data, with a varying between -10 and 5 and b between -2 and 0.9.

The last two models highlight the importance of experimental work in the prediction of the emulsification behavior of crude oils as already described in reference [32]. An empirical approach that considers oil-specific properties such as the emulsification rate and the stability of the emulsion seems mandatory.

3.2.2. Emulsification model implemented in the weathering module MEUN

Comparing SINTEF's and Mackay and coworkers' models for the water uptake rate (equations 3.18 and 3.14 respectively) it is evident that Equation 3.14 is a particular case of Equation 3.18 when $Y_{max}(t) = Y_{max} = 70\%$ and $t_{1/2|cyl} = 400.8\text{ s}$. MEUN considers Equation 3.18 having as inputs the maximum water content and half-life time for a particular oil determined with the experimental methodology initially proposed in reference [6] and described in Section 4.3.

With respect to the viscosity increase, MEUN uses the experimental methodology described in Section 4.3 to define the stability of the emulsions formed after evaporation, i.e. at different times after the oil spill and Table 3.1 to define the viscosity of the resulting emulsion.

Equation 3.19 presents how MEUN computes the variation of the density due to emulsification by the mixing rule widely used in previous researches [4, 7, 34, 46].

$$\rho_{emu}(t) = \rho_{wf}(1 - Y) + \rho_w Y \quad (3.19)$$

where:

ρ_{emu} : density of emulsion (g/ml)

ρ_{wf} : density of water-free oil (g/ml)

ρ_w : density of water (g/ml)

3.3. Dispersion

Dispersion can be defined as the breakdown of the oil slick on the surface due to the turbulence that exists in the sea that generates small oil droplets that migrate to the water column. After evaporation, dispersion is the process with the most significant impact on the extent of time that the oil slick remains on the surface. Dispersion, however, does not produce changes in the physicochemical properties of the spill, since oil droplets migrating to the water column have the same chemical composition as the surface oil.

3.3.1. Dispersion models

3.3.1.1. Mackay and coworkers' model [8]

This approach considers that the dispersion rate follows a first order kinetic with respect to the crude oil volume remaining at surface as it is evident in Equation 3.20.

$$\frac{dV_{disp}}{dt} = \left(\frac{0.11 (U_w + 1)^2}{1 + 50 \mu^{1/2} \delta s_t} \right) V \quad (3.20)$$

where:

V_{disp} : volume of crude oil dispersed in the water column (m^3)

V : volume of crude oil remaining on surface (m^3)

μ : crude oil viscosity (cP)

δ : oil slick thickness (cm)

s_t : oil-water interfacial tension ($dyn\ cm^{-1}$)

3.3.1.2. Delvigne and Sweeney's model [49]

In this empirical model, the authors consider the dissipated breaking wave energy per unit area as the parameter with the most significant effect in dispersion. The authors carried out experiments in 15-m and 200-m flumes and related the turbulent energy released by a breaking wave with the dispersion rate and the droplet size distribution in the water column according to Equation 3.21:

$$\frac{dV_{disp}(d)}{dt} = \frac{C_0 D_d^{0.57} S F d_0^{0.7} \Delta d A}{\rho} \quad (3.21)$$

where:

$V_{disp}(d)$: volume of crude oil dispersed in the water column as oil droplets with droplet size in an interval Δd around d_0 (m^3)

C_0 : proportionality constant that depends on oil type and weathered state

D_d : dissipated breaking wave energy per unit surface area

F : fraction of sea surface hit by breaking waves ("white-caps") per unit time

S : fraction of sea surface covered by oil ($0 \leq S \leq 1$)

d : oil particle diameter (m)

Δd : oil particle diameter interval (m)

Appendix C has the empirical expressions required to estimate all terms of Equation 3.21. The

link between dispersion and the rest of weathering processes is partially simulated with the proportionality constant C_0 , as described in Appendix C, C_0 decreases with an increase in oil slick viscosity caused by evaporation and emulsification.

3.3.2. Dispersion model implemented in the weathering module MEUN

Because the Delvigne and Sweeney model considers crude oil properties (density and viscosity), wave characteristics (significant wave height and period) and the size distribution of the droplets migrating to the water column, while the one by Mackay and coworkers does not, the former was implemented in MEUN.

3.4. Spreading

Once crude oils is spilled at sea, the oil slick is subjected to mechanical forces producing oil spill spreading. In this process there are two main forces in favor of spreading, gravity and surface tension and two against, inertial and viscous forces [50]. Therefore, oil slick spreading occurs even in the absence of currents or deformations caused by wind.

Most of spreading models found in the reviewed literature are based on the research made by Fay [50], who suggested that oil slick spreading after an oil spill can be divided into three stages or phases, where in each stage predominates a force in favor and another force against spreading. The first stage called “gravity - inertia” involves the first few minutes after an accident and, because of its short duration, it is usual in weathering modeling [4, 34, 45], to assume that it occurs at a very fast rate so that there is no need to model the spreading rate. The typical approach is, therefore, to estimate the slick area after this phase as described in Equation 3.22.

$$A_0 = \pi \frac{k_2^4}{k_1^2} \frac{(V_0^5 g \Delta\rho)^{1/6}}{\nu_w^2} \quad \text{with} \quad \Delta\rho = \frac{\rho_w - \rho_o}{\rho_o} \quad (3.22)$$

where:

A_0 : oil spill area after the first stage of spreading (m^2)

k_1, k_2 : empirical constants (1.14 and 1.45 respectively according to Fay [11])

V_0 : initial oil spill volume (m^3)

$\Delta\rho$: relative difference between water and crude oil density

ρ_w : water density (kg/m^3)

ρ_o : initial crude oil density (kg/m^3)

ν_w : water kinematic viscosity (m^2/s)

The third stage referred, as “tension-viscous”, is usually not modeled either because it occurs at a long-time scale when the slick may be dispersed or broken in separate oil slicks [4]. Most of spreading models are concentrated with the second stage called “gravity-viscous”. The highly-referenced model by Mackay et al. [8] represents several properties that determine oil spreading with an empirical constant and the spreading rate is only function of the current oil slick area A and the oil spill volume remaining on the surface, as shown in Equation 3.23.

$$\frac{dA}{dt} = K_{spre} A^{1/3} \frac{V^{4/3}}{A} \quad (3.23)$$

where:

K_{spre} : Constant with default value of 150 s^{-1}

Spreading is also affected by the precipitation of waxes in oil spills in seas with temperature lower than of the pour point. According to Sebastião and Soares [4] a requirement for normal spreading is an ambient temperature above the pour point. Buist et al. [24], through a series of spreading experiments with different waxy crude oils, showed that spreading when the sea temperature is below that of the pour point is possible but with an equilibrium thickness higher than of normal spreading. Unfortunately, none of these researches proposed a clear equation to represent this process and, therefore, was not considered this effect in MEUN.

Chapter 4

Experimental Methodology

4.1. Test oils

Colombian crude oils Cusiana (43.2 °API) and Vasconia (20.3 °API) were selected for this research because they have been during some periods of time the two crudes most exported by the oil Colombian company [51]. Another important reason for choosing them is the significant difference in physicochemical properties which challenge the predictive ability of the weathering module. These significant differences are explained below.

4.1.1. True boiling point

According to their API gravities, Cusiana is a representative of light crude oils while Vasconia is closer to the range of heavy crude oils (8 - 20 °API). The difference in the nature of both crudes has an important effect on the different weathering processes. For instance during evaporation Figure 4.1, that shows the TBP curves of both crude oils, indicates that at any given temperature, the difference in the distillate volume is almost 30 %.

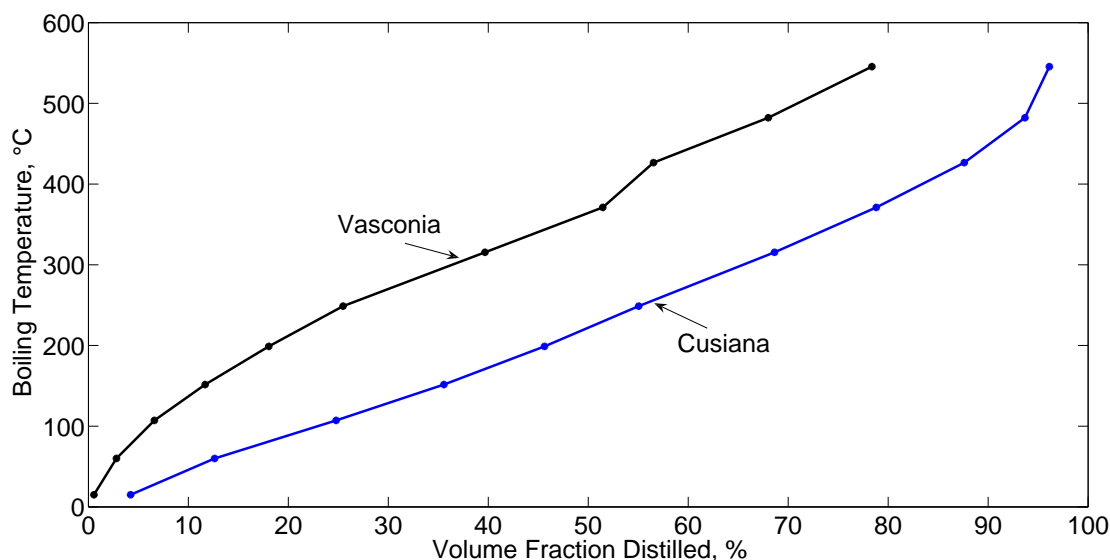


Figure 4.1: TBP curves for Colombian crude oils. Provided by the Colombian oil company Ecopetrol.

4.1.2. SARA

Table 4.1 shows the SARA (saturates, aromatics, resins and asphaltenes) and wax content of both crude oils. As expected the lighter oil, Cusiana, has a higher content of saturates and aromatics. However, more interesting because of its impact in the emulsification and the general weathering behavior, it is important to highlight the difference in the content of resins and asphaltenes. While the concentration of asphaltenes is twenty times higher for Vasconia, Cusiana has almost twice the amount of waxes than Vasconia.

Table 4.1: SARA composition of Colombian crude oils.

	°API	Saturates ₁	Aromatics ₁	Resins ₁	Asphaltenes ₁	Waxes ₁	Viscosity(cP) ₂	
		(% w/w)	(% w/w)	(% w/w)	(% w/w)	(% w/w)	25°C	35°C
Cusiana	43.2	74.3	23.0	2.3	0.3	10.0	1.96	1.84
Vasconia	20.3	40.7	38.2	14.7	6.4	4.5	64	48

1. Provided by the Colombian oil company Ecopetrol.

2. Provided by the Colombian oil company Ecopetrol. Measured at a shear rate of 100 s^{-1} using an AR 1500 EX rheometer.

4.1.3. Pour point

The pour point is defined as the temperature below which a sample of crude oil will not flow as explained in detail in ASTM D97-12 [22]. The pour point increases as the crude evaporates. Figures 4.2a

and 4.2b show the variation in pour point with the evaporated fraction for Cusiana and Vasconia, respectively. To measure this behavior, the ASTM D97 test was carried out with crude oil samples with different evaporated fraction obtained with the wind tunnel, as explained in Section 4.2.1. Figures 4.2a and 4.2b show how both crude oils have a similar pour point (0°C Cusiana - 6°C Vasconia). However, with evaporation the difference in the pour points of both crude oils increases. According to Figure 4.2a, once Cusiana reaches 35% of evaporated fraction the pour point is about 25°C , which is in the range of temperatures registered for the Colombian Caribbean Sea. Contrary, the pour point for Vasconia does not exceed 21°C . This particular behavior for Cusiana is due to its paraffinic nature with relative high wax content of 10.0% for fresh crude. (Table 4.1).

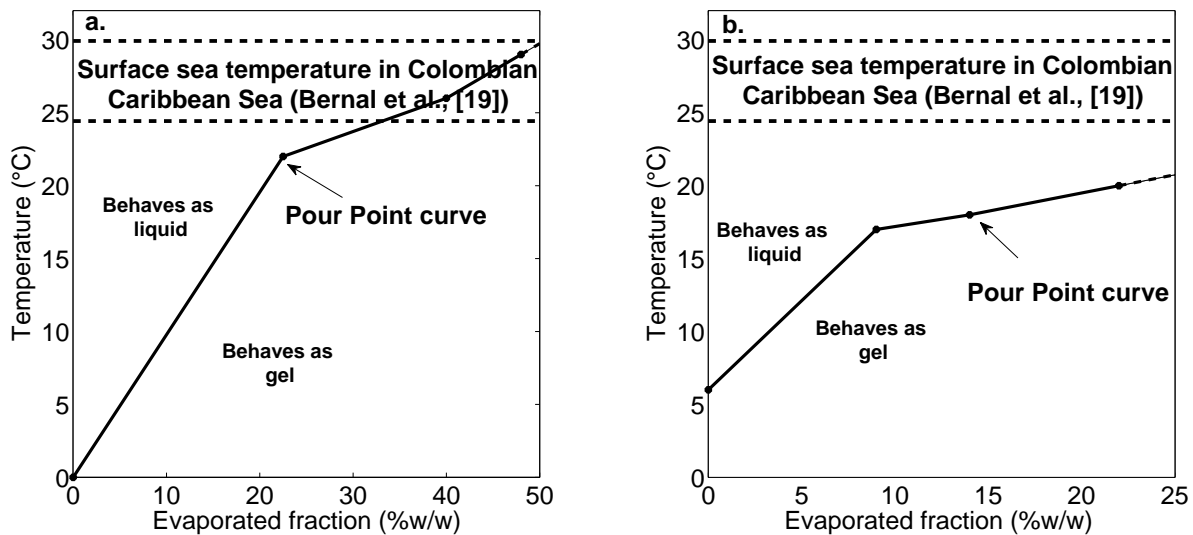


Figure 4.2: Pour point variation with evaporated fraction for Colombian crude oils. a. Cusiana. (measured in this research) b. Vasconia. (taken from reference [5]).

4.2. Evaporation

4.2.1. Wind tunnel

A wind tunnel was adapted to evaluate the evaporation rate of Colombian crude oils. Figure 4.3 shows a schematic description of the experimental setup. The total length of the tunnel is 3.0 m with a circular cross section of 30 cm of diameter. Two blockages were included at the interior of the tunnel to avoid alterations caused by the wind in the balance scale measurements. The crude oil was deposited in a stainless steel tray of rectangular cross section of $40\text{ cm} \times 20\text{ cm}$ and a height of 1.5 cm. An OHAUS balance scale measured the weight loss due to evaporation with 1 g of sensibility and

5 seconds of temporal resolution. An interface connected the scale to a computer allowing an online evaluation of the evaporation rate. To isolate the evaporation from the effect of temperature, given that the experimental setup does not control temperature, only the experiments carried out when temperature varied between 21 and 25°C were considered. The exception to this rule was when the effect of the pour point was studied.

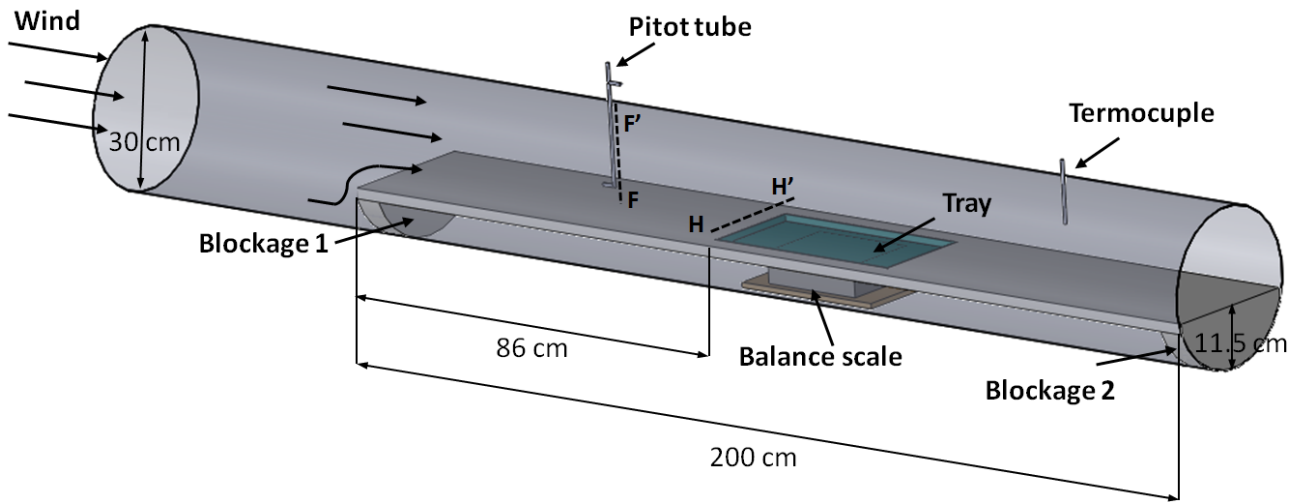


Figure 4.3: Scheme of the experimental setup designed to validate the model of crude oil evaporation.

4.2.2. Wind velocity

The wind velocity was measured with a conventional pitot tube coupled to an electronic manometer which displays the wind velocity with a sensibility of 0.01 m/s. A thermocouple type “J” measured the air temperature each 5 seconds aided by a DAQ device and the Labview software. Figure 4.3 shows the location of the pitot tube and the thermocouple in the wind tunnel with respect to the evaporation tray. The tunnel has a radial blower, coupled with a variable-speed drive (VSD) device that guarantees different wind velocities, with good accuracy and reproducibility, keeping during all the experiments, the velocity at its nominal value ± 0.2 m/s.

An unconventional wind velocity profile in the measuring region of the balance scale was expected because of the combination of a tunnel with circular cross section and the blockage marked in Figure 4.3 as “Blockage 1”. To guarantee that the experiments would provide data that could be used in the model it was necessary to:

- 1) Guarantee that the distance between Blockage 1 and the evaporation tray, 86 cm in Figure 4.3,

allows a developed air velocity profile above the tray.

2) Evaluate the velocity gradients in the evaporation region and the value of the “effective” velocity that would be used as input to the evaporation model.

To respond to the first issue a Computational Fluid Dynamics (CFD) simulation using the commercial software ANSYS FLUENT 13.0 [52] was carried out to evaluate the hydrodynamic behavior along the wind tunnel, particularly the effect of Blockage 1 in the velocity profiles. The details of the CFD simulation are presented in Appendix D. The section presents the main simulation results.

The CFD results are presented along vertical lines crossing through the center of the wind tunnel (AA', BB', CC', DD', EE', FF' and GG' in Figure 4.4). FF' and GG' are of particular interest because they are located before and after the evaporation tray, respectively.

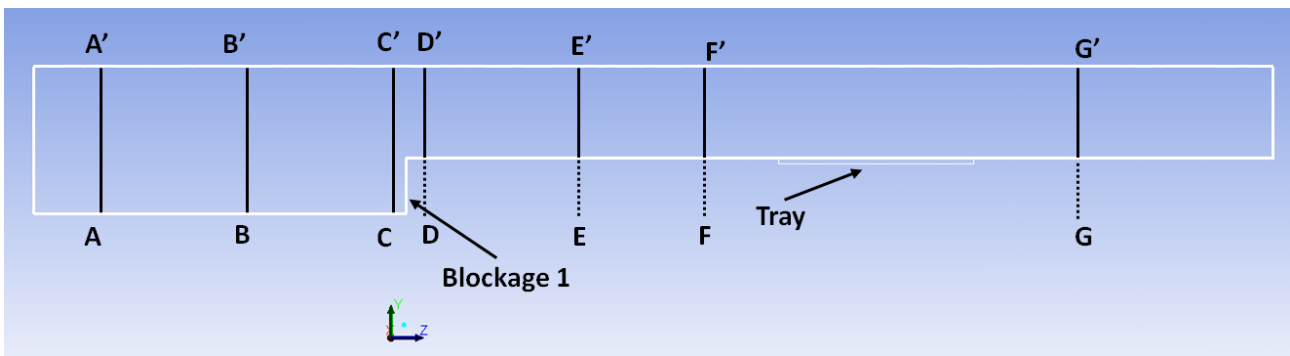


Figure 4.4: Position of the velocity profiles evaluated along the wind tunnel in the CFD simulation.

The results of the CFD simulation in Figure 4.5a show that for lines AA' and BB' the velocity profiles are typical of turbulent flows in tubes [53]. However, in profile CC' it is evident the effect of the obstruction in the flow that decreases the velocity at the bottom of the tunnel and increases the velocity at the top due to the reduction in the cross sectional area.

Figure 4.5b shows that profile DD' has significant differences with respect to the other three profiles because of its proximity to the change in the cross section. Profile EE' also presents differences with respect to the profiles downstream. However, and most important, there is almost no difference between the profiles FF' and GG'. This finding suggests that the velocity profile is “completely” developed before the evaporation tray. This implies that the experimental velocity profiles determined with the pitot tube shown in Figure 4.3 (which coincide with line FF') correspond to the developed flow.

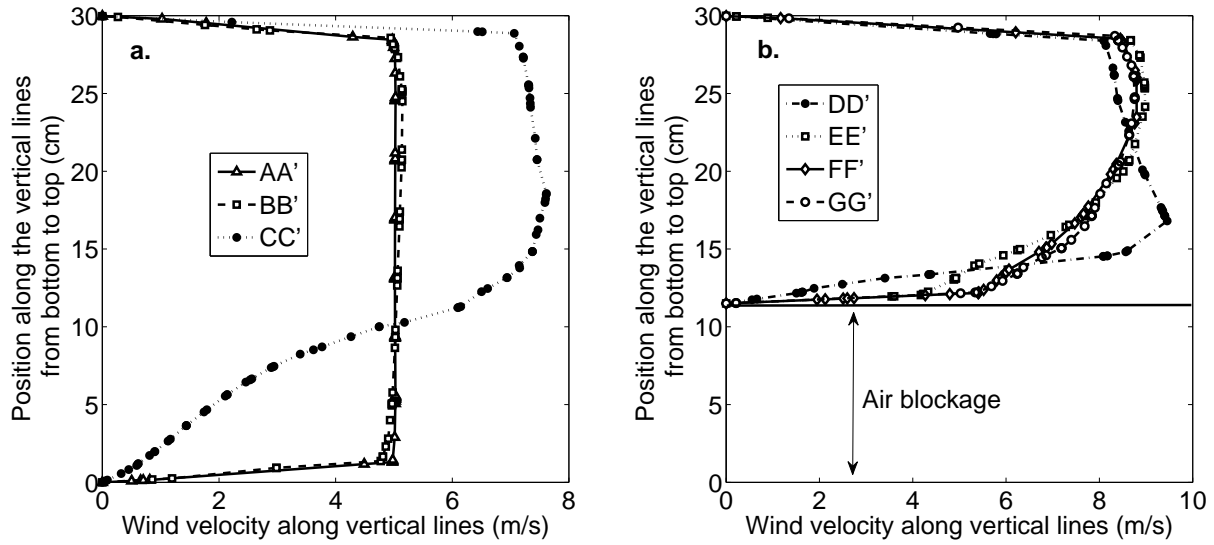


Figure 4.5: Velocity profiles along the wind tunnel obtained with CFD simulation. a. Before Blockage 1, b. After Blockage 1. (Legends make reference to Figure 4.4).

The experimental profiles of the horizontal (HH' in Figure 4.3) and vertical (FF' in Figure 4.3) wind velocity in Figure 4.6 were obtained at different rotational speeds of the wind tunnel blower (150, 250 and 400 rpm). Figure 4.6 includes as well the CFD simulation explained above.

The results of CFD simulation are, in general, in good agreement with the trend of the experimental profiles obtained with 250 and 400 rpm. The horizontal profiles are more uniform than vertical, for this reason, to obtain an “effective” velocity for each rotational speed of the blower this work proposes an average value along the vertical direction. Thus, the profiles shown in Figure 4.6b obtained with 150, 250 and 400 rpm correspond to average value of 3, 5 and 8 m/s respectively and from now on those values will be used in the validation discussion. To evaluate the uncertainties due to uncontrolled variations in the experimental setup, the standard deviation of two or three experiments for each wind velocity was evaluated.

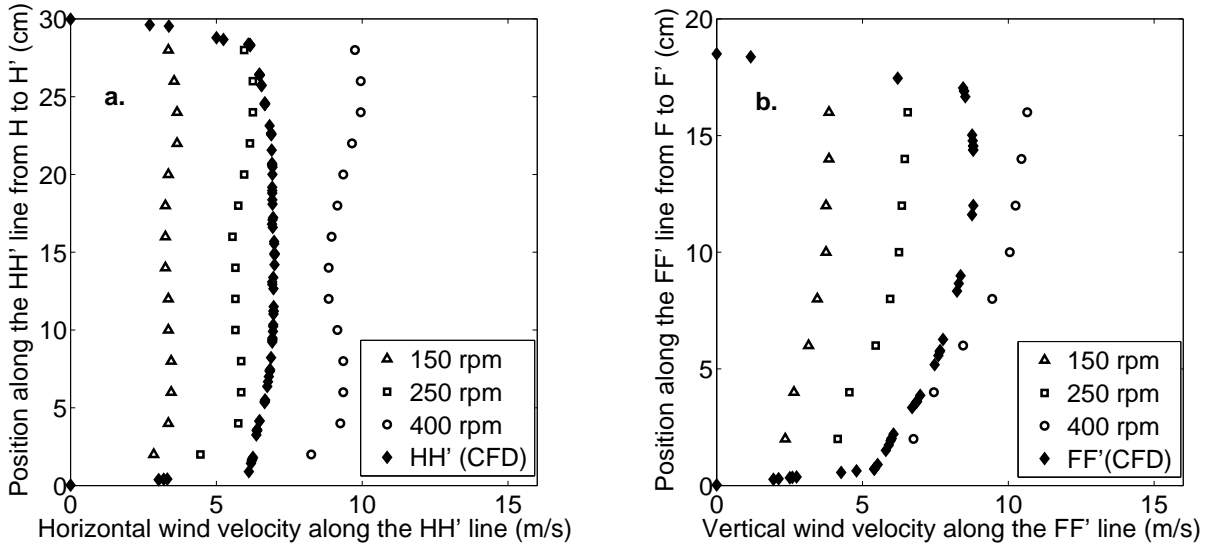


Figure 4.6: Experimental velocity profiles in the wind tunnel at different blower rotational speed and comparison with CFD simulation a. Horizontal profiles and b. Vertical profile.

To confirm the wind velocity characterization discussed above and to test the results obtained with the wind tunnel, this work studied the well-known process of water evaporation. Figure 4.7a presents the behavior of water evaporated fraction over time at different wind velocities (2, 3, 5 and 8 m/s). These experiments were conducted at similar conditions of temperature (23.5-25.5 °C) and relative humidity (62-66 % RH) to isolate the effect of wind speed on the evaporation rate. The experiment at 2 m/s lasted just over an hour because the wind tunnel cannot operate at this low speed for long periods of time. This time interval, however, was enough to calculate the evaporation rate. Figure 4.7b shows the experimental evaporation rate obtained for all the studied wind velocities. In this figure the solid line is the result of a fit to the experimental data when the dependence of the evaporation rate (E) with the wind speed (U_w) is forced to a power law expression ($E = aU_w^b$). The best estimate for b in Figure 4.7b is 0.8, very close to the value of 0.78 reported by Sutton [54], which gives confidence on the wind-tunnel experiments.

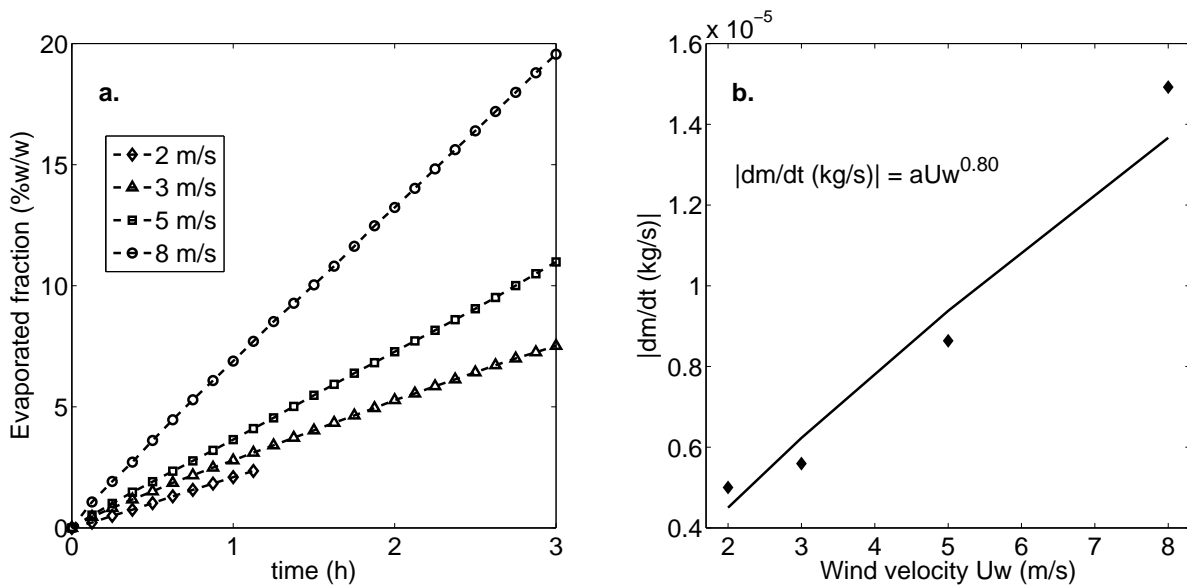


Figure 4.7: Experimental behavior of water evaporation. a. Evolution of evaporated fraction with time at 2, 3, 5 and 8 m/s. b. Effect of wind velocity in evaporation rate, experimental values are compared with a power law dependence with wind velocity.

4.2.3. Initial oil film thickness

The depth of the oil film in the tray, or oil film thickness, is an important variable in the experiments as it may affect the formation of the boundary layer. In this research, two values of the oil thickness were evaluated. Figure 4.8 presents the experimental results for Cusiana along with MEUN predictions when the slick thickness corresponds to that of the full (10-11 mm) and half-full (4.0-5.0 mm) tray and the velocity is 5 m/s. In Figure 4.8.a and 4.8.b, the evaporated fraction for both, the experimental and simulated values is for the same time, when the thickness is 4 - 5 mm. This difference is because the shallower oil film has a lower amount of initial crude oil but the same mass transfer area.

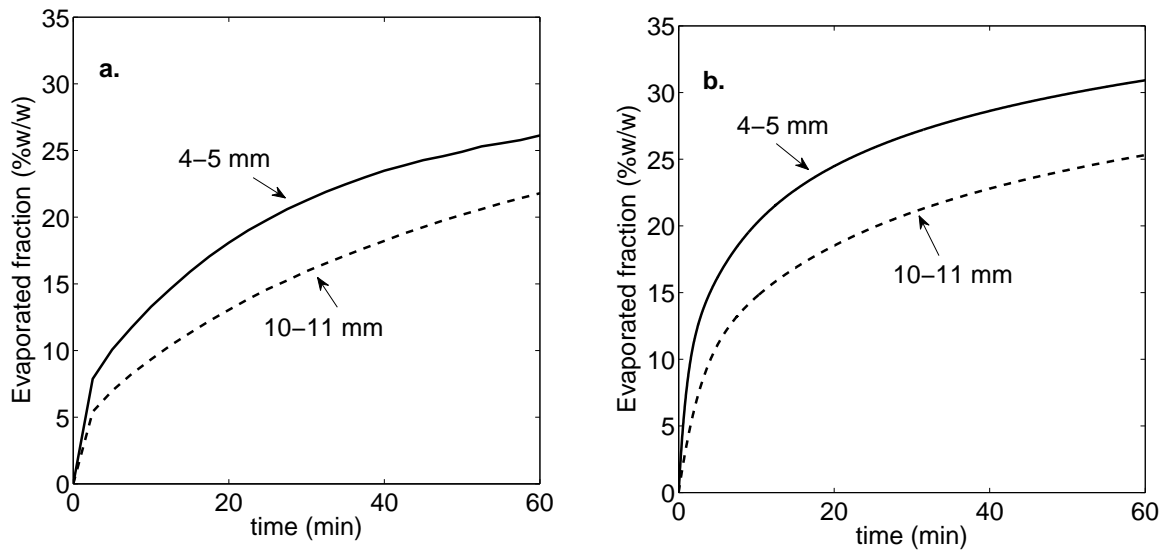


Figure 4.8: Effect of initial oil thickness in the behavior of the evaporated fraction for Cusiana crude oil at a wind velocity of 5 m/s. a) Experimental data, b) MEUN predictions.

In terms of evaporation rate, Figure 4.9 shows the time derivative of the evaporated fraction. Although not with the same values, Figure 4.9a (experimental data) and Figure 4.9b (MEUN predictions) show that the evolution of the evaporated fraction with time is higher for the shallower thickness at the beginning of the experiment but this difference is not considerable after 30 min. Considering that a similar behavior was obtained with Vasconia, the correspondence between model and experimental behavior suggests that any of both initial oil thickness could be selected. However, most experiments were conducted when the initial oil thickness was 10 to 11 mm, i.e. the tray was full as this minimizes the effect of the edges of the evaporation tray as well as the uncertainties in weight measures.

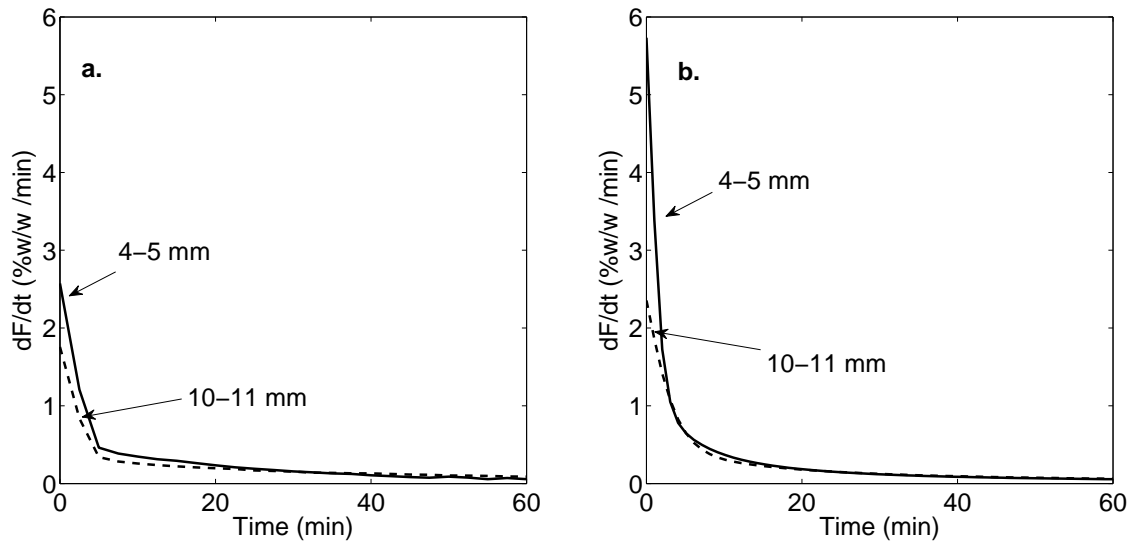


Figure 4.9: Effect of initial oil thickness in the behavior of the time-derivative of the evaporated fraction for Cusiana crude oil at 5 m/s. a) Experimental data, b) MEUN predictions

4.3. Emulsification

4.3.1. Experimental setup

For the experimental study of emulsification the setup used in the Norwegian research center SINTEF [6], was adapted as portrayed in Figure 4.10. In this experiment 300 ml of water with a typical salinity of the Colombian Caribbean Sea (35 g/ml) were mixed with 30 ml of crude oil in a 500-ml separation funnel placed in a rotary frame at 30 rpm. The water content in the emulsion was recorded at defined time intervals (5 min, 10 min, 15 min y 30 min, 1 h, 2 h, 4 h, 6 h, 8 h, 12 h and 24 h). The maximum water content was considered as that measured after 24 h. The way to determinate the water content at each time is schematically explained in Figure 4.11. Figure 4.11a presents the initial test condition when the oil film has a height h_0 . Once the experiment stops at any time t , the water-in-oil emulsion reaches a height $h(t)$ (h_{max} when t is 24 hours).

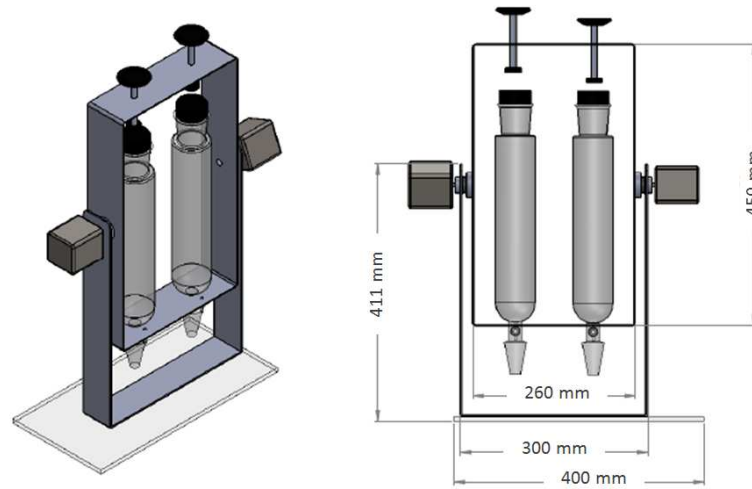


Figure 4.10: Scheme of the experimental setup adapted from reference [6] to study the emulsification model.

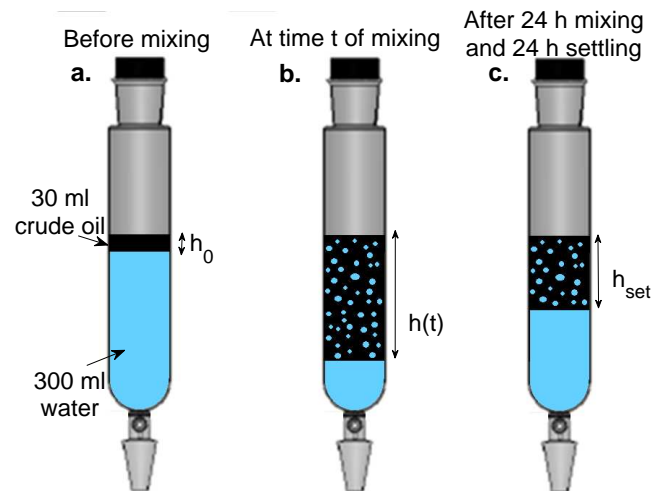


Figure 4.11: Schematic representation of different of the emulsification experiment. a. Initial condition (before mixing). b. At time t of mixing. c. After 24 h mixing and 24 h settling.

Because the funnel diameter is constant, the amount of water in the emulsion is proportional to the increase in height. The water content, in percentage, can be calculated with Equation 4.1.

$$Y(t) = \frac{h(t) - h_0}{h(t)} 100\% \quad (4.1)$$

The evaluation of the variation of the water content with time can be converted into a kinetic index that can be related to the emulsification rate. An example of such an index is that proposed by Daling et al. [41] who proposed a half-life index ($t_{1/2}$), defined as the mixing time elapsed when the water content is half of its maximum value.

Further understanding of the emulsification process requires the study of the stability of the emulsion. This can be obtained by a settling period of 24 h after h_{max} is reached as Figure 4.11c shows. Daling et al. [41] proposed to compare the water-to-oil ratio before and after the settling period through Equation 4.2 as a way to estimate emulsion stability.

$$R_{2/1} = \frac{R_2}{R_1} = \frac{\text{Water - to - oil ratio after settling period}}{\text{Water - to - oil ratio before settling period}} \quad (4.2)$$

Stable emulsions were assigned a value of $R_{2/1}$ equal or close to 1.0 while $R_{2/1}$ would be close to 0 for unstable emulsions.

4.3.2. Experimental conditions

As discussed in Section 3.2, one of the aspects with major influence in emulsification is the level of evaporation of the crude oil. This research carried out the emulsification experiments under the conditions discussed below to evaluate this effect.

Table 4.2 shows that the experimental conditions for Vasconia evaluates the fresh crude oil (0% of evaporated fraction) and two different levels of evaporation. According to Table 4.2, where the number of “x” represents the numbers of replications, this work also evaluates the effect of temperature. Although 19-20°C is below the expected temperature in the Colombian Caribbean Sea, these data help to understand the temperature effect on the process.

Table 4.2: Experimental conditions to study the emulsification behavior of Vasconia crude oil.

Temperature	Evaporated fraction		
	0 %	5 %	15.5 %
19-20°C	x	x	x
23-25°C	xx	x	x
29-31°C	x	x	xx

Table 4.3: Experimental conditions to study emulsification behavior of Cusiana crude oil.

Temperature	Evaporated fraction			
	0 %	22.5 %	40 %	48 %
21-23°C	xx	x	xx	xx
23-25°C	x	x	x	xx
29-31°C	-	-	x	x

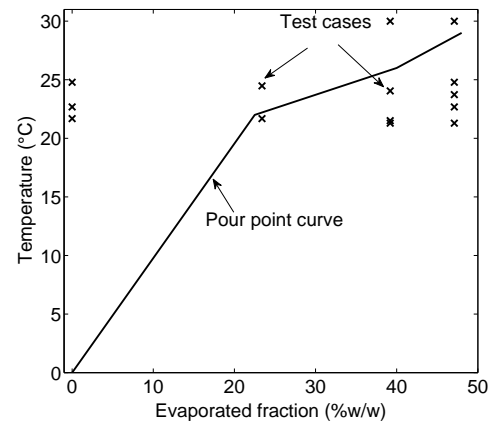


Figure 4.12: Experimental conditions to study emulsification behavior of Cusiana crude oil.

Chapter 5

Results

Chapter 3 described the development of the weathering module MEUN from state-of-art sub-models that predict change in the physicochemical behavior of crude oils after an oil spill. However, the objective of this work is to accurately predict the behavior of the Colombian crude oils Cusiana and Vasconia under typical conditions of the Colombian Caribbean Sea. This chapter describes first the evaporation and emulsification of Cusiana and Vasconia crude oils studied following the experimental methodology explained in Chapter 4. These experimental results are compared with the predictions of the weathering module that includes the original sub-models reported in the literature, as already described in Chapter 3. In case of significant differences between model predictions and experimental data, this section describes how the model was modified to obtain agreement with experiments. A third section evaluates the performance of MEUN in a set of cases under typical metaocean conditions of the Colombian Caribbean Sea. MEUN predictions are compared with the commercial software ADIOS.

5.1. Evaporation

The first part of this section evaluates the effect of wind velocity and type of crude oil on the evaporation rate. The second part describes the effect of the pour point in the evaporation rate. A third section shows how the model deals with changes in density and viscosity as the evaporation advances.

5.1.1. Effect of wind velocity and crude oil type on evaporation rate

5.1.1.1. Experimental results

Figures 5.1a and 5.1b show, respectively, for Cusiana and Vasconia the experimental behavior of the evaporated fraction at different wind velocities. For any of the three wind velocities, the evaporated fraction of Cusiana at the same time t , is higher than that of Vasconia, due to the greater amount of volatile compounds of Cusiana crude oil. Note the differences in the scale of both, vertical and horizontal, axes that result of the different physicochemical response of both crudes as explained above.

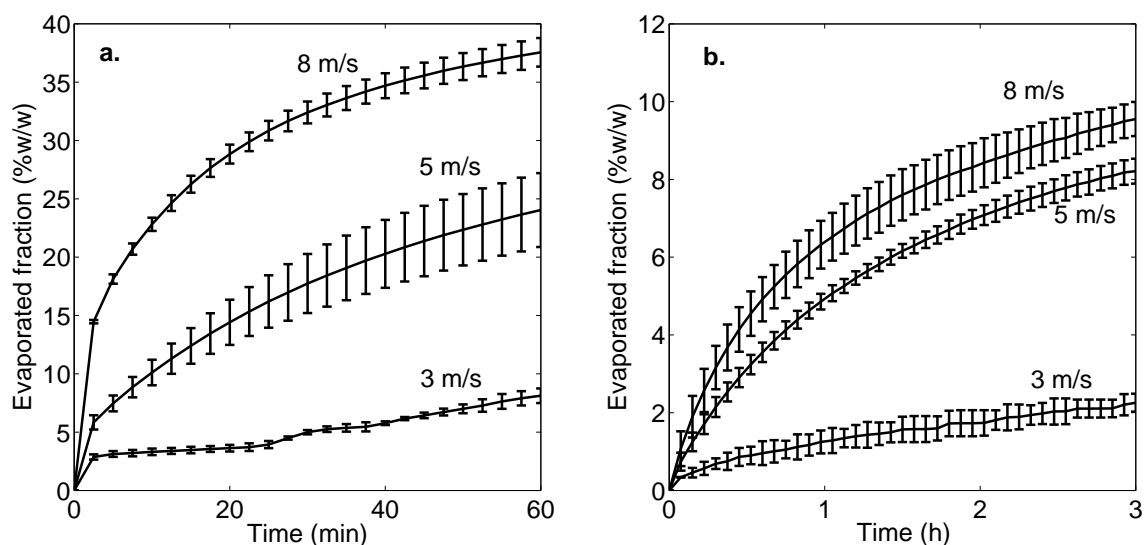


Figure 5.1: Effect of the wind velocity on the evaporated fraction of a. Cusiana. b. Vasconia. Note the differences in the scale of both, vertical and horizontal, axes.

With respect to error bars of Figure 5.1, the reason for the uncertainties may be the combined effect of temperature variations, small differences in the initial amount of crude oil and the mentioned above, wind velocity variation. However, as it is seen in Figures 5.1a and 5.1b, despite these uncertainties, the effect of wind velocity on evaporation rate is predominant and more significant than error bars for both, Cusiana and Vasconia crude oils.

Interestingly, the effect of wind velocity on the evaporation rate is different for both crude oils. In the case of Cusiana, in Figure 5.1a the increase in wind velocity causes a significant increase in the evaporation rate. Contrary, the change of the evaporation rate of Vasconia crude oil with wind velocity is less pronounced, particularly when the wind velocity changes from 5 m/s to 8 m/s. Considering an evaporation rate boundary-layer controlled, the wind removes oil vapor from the spill surface. In

Vasconia crude oil, due to the low amount of volatile compounds, a wind velocity of 5 m/s could to effectively remove any evaporated vapors remaining on the surface. An increase in wind velocity from 5 m/s to 8 m/s does not significantly affect the evaporation rate as the concentration of oil vapors above the boundary layer would remain close to zero. For Cusiana, a lighter oil with a higher content of volatile compounds, the results in Figure 5.1a tends to suggest that at 5 m/s, the wind velocity is still a limiting factor of evaporation and an increase to 8 m/s would decrease the concentration of volatile compounds in the boundary layer in a proportion enough to increase the evaporation rate.

5.1.1.2. Comparison of experimental data with MEUN predictions

Figure 5.2 shows for Cusiana crude oil, the comparison between experimental behavior and MEUN predictions of evaporated fraction at different wind velocities. Experimentally, as shown in Figure 5.2a, the dependence of the rate of evaporation on wind velocity is stronger than that predicted by the model (Figure 5.2b).

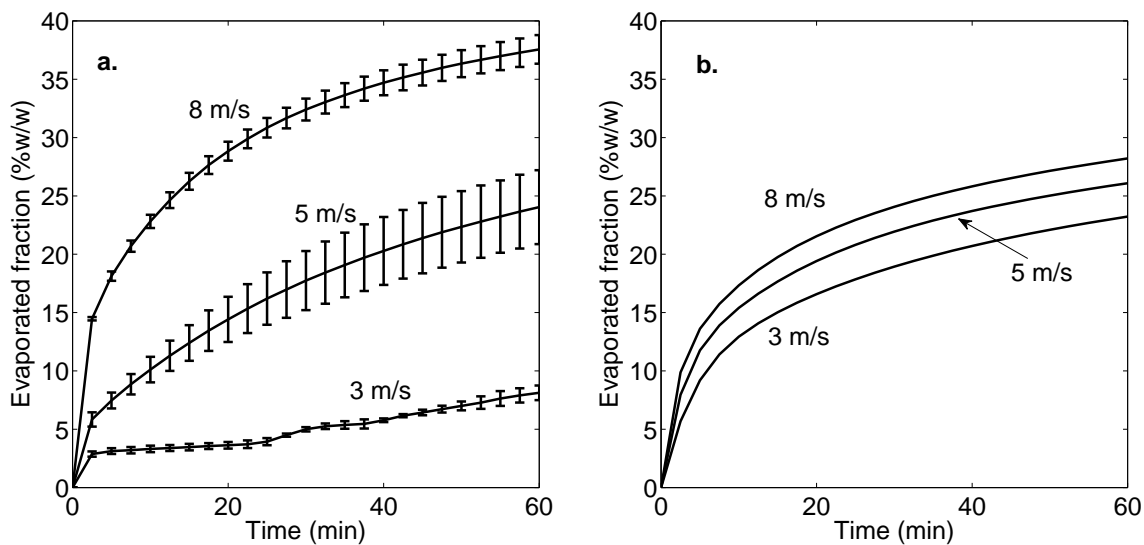


Figure 5.2: Effect of wind velocity in the behavior of the evaporated fraction for Cusiana crude oil. a. Experimental data. b. MEUN predictions.

In the case of Vasconia, the effect of wind velocity on the evaporated fraction, both in the experiments and as described by the model and presented in Figures 5.3a and 5.3b respectively, is similar when the wind velocities are 5 and 8 m/s. However, for a wind velocity of 3 m/s the measured rate of evaporation is much lower than the values predicted by the model.

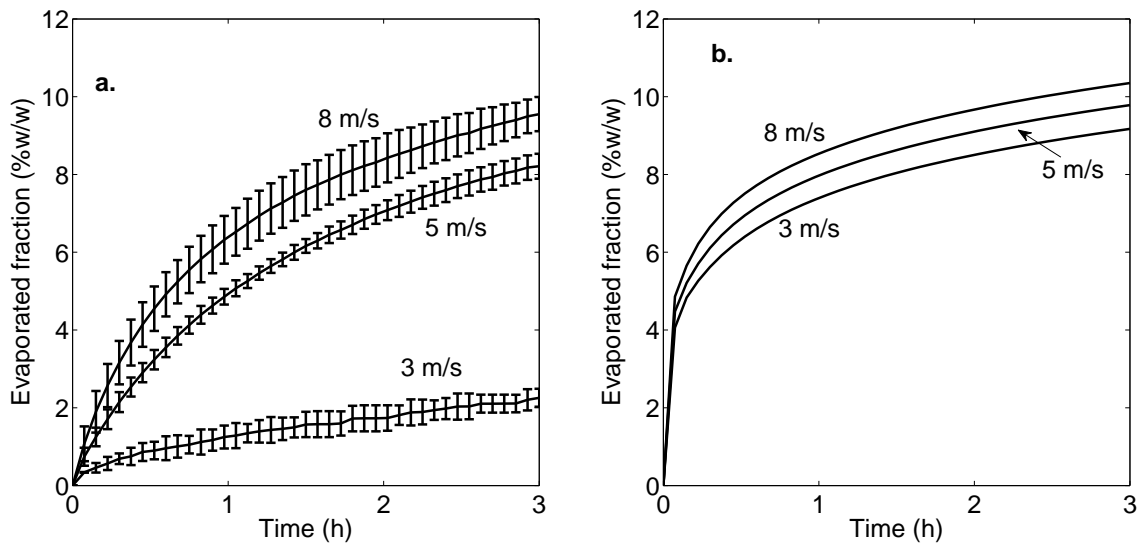


Figure 5.3: Effect of the wind velocity on the behavior of the evaporated fraction for Vasconia crude oil. a. Experimental data. b. MEUN predictions.

The parity plots in Figures 5.4a and 5.4b allows a better comparison between experiments and model predictions. In the case of Cusiana, Figure 5.4a shows an acceptable agreement between model prediction and experimental data at 5 m/s. At 3 m/s the model overestimates the evaporated fraction. Model predictions are lower than experimental data when the wind velocity is 8 m/s. For Vasconia, at 5 and 8 m/s the model overestimates the evaporated fraction at the initial stage of evaporation but, with time the difference between predictions and experimental data decreases. The major problem with Vasconia predictions is at lower velocities, at 3 m/s the model has a serious overestimation of the evaporated fraction and the tendency persists with the increase of the evaporated fraction.

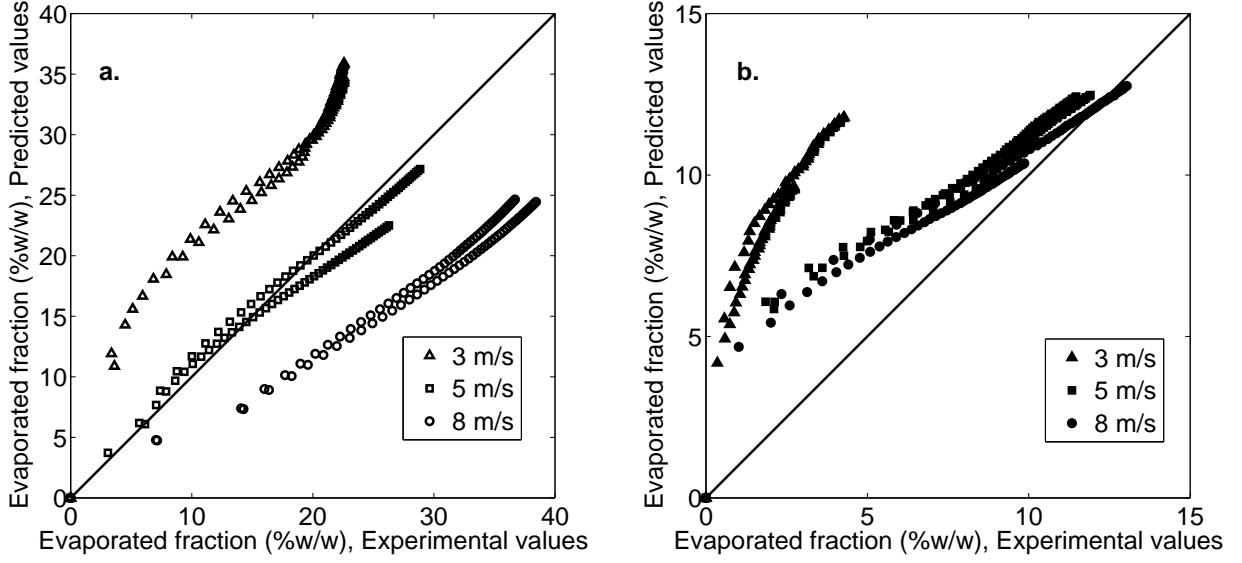


Figure 5.4: Predicted versus experimental evaporated fraction. Predicted values based on state-of-art models. a. Cusiana. b. Vasconia.

5.1.1.3. Evaporation model calibration

Equations 5.1 and 5.2 recall the evaporation model implemented in MEUN. These equations show that the effect of wind velocity U_w , on the evaporation rate is present in the mass transfer coefficient k_w . According to that and as solution to the problems with the model discussed above, this work proposed a calibration of the mass transfer coefficient for the behavior of Colombian crude oils.

$$\frac{dFme_{pred}}{dt} = 1 - \frac{1}{m_o} \sum_{i=1}^{n_{pc}} \frac{dm_i}{dt} \quad \text{with} \quad \frac{dm_i}{dt} = -\frac{k_w A x_i P_i^{sat} MW_i}{RT} \quad (5.1)$$

$$k_w = 0.0048 U_w^{0.78} X^{-0.11} Sc^{-0.67} \quad (5.2)$$

To perform the calibration, for each individual experiment the value of the mass transfer coefficient k_w that minimizes the difference between experimental and predicted values was calculated. Figure 5.5a shows the experimental results of evaporated fraction at 3 m/s for Cusiana and Vasconia as well as the respective MEUN predictions with the mass transfer coefficient calculated according to the state of the art (Equation 5.2). The objective of the optimization was to reduce the difference between each pair of experimental and predicted evaporated fraction ($Fme_{exp}(t_k)$, $Fme_{pred}(t_k; k_w)$), shown exquematically as vertical dotted lines in Figure 5.5a, based on the residual sum of squares in Equation 5.3.

$$F_c(k_w) = \frac{1}{2} \sum_{k=1}^{N_d} [Fme_{pred}(t_k; k_w) - Fme_{exp}(t_k)]^2 \quad (5.3)$$

At each time t_k , Fme_{exp} is the experimental evaporated fraction and Fme_{pred} is the predicted value calculated with Equation 5.1 after the solution of the ODEs system with the methodology discussed in Section 3.1.2.

Finally Figure 5.5b shows the same comparison between experimental values and MEUN predictions of Figure 5.5a but in this case the predicted values are obtained with the mass transfer coefficient calculated following the optimization procedure. Clearly the optimization procedure works and MEUN predictions are evidently improved.

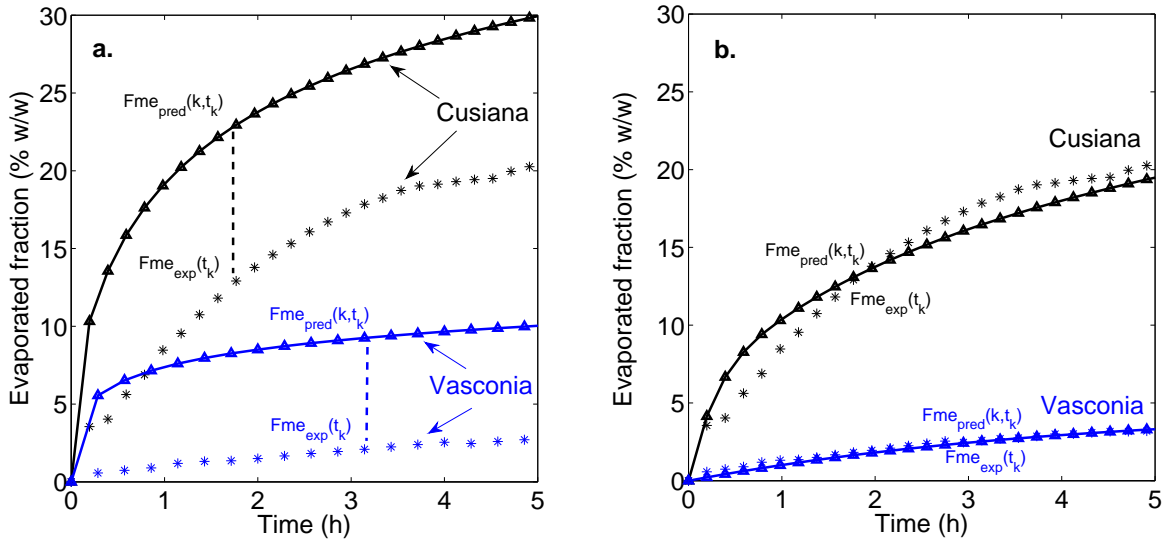


Figure 5.5: Schematic example of the optimization made to find optimal value of mass transfer coefficient. a. Before optimization. b. After optimization.

Following the same optimization procedure for the rest of experiments the results are the parity plots of Figures 5.6a and 5.6b. In the case of Cusiana, a comparison between Figures 5.4a and 5.6a shows that the predictions in the case of Cusiana are greatly enhanced for the three wind speeds considered. For Vasconia, the comparison between Figures 5.4b and 5.6b demonstrates a significant improvement in predictions at 3 m/s but the evaporated fraction is still overestimated at 5 and 8 m/s in the first stage of evaporation.

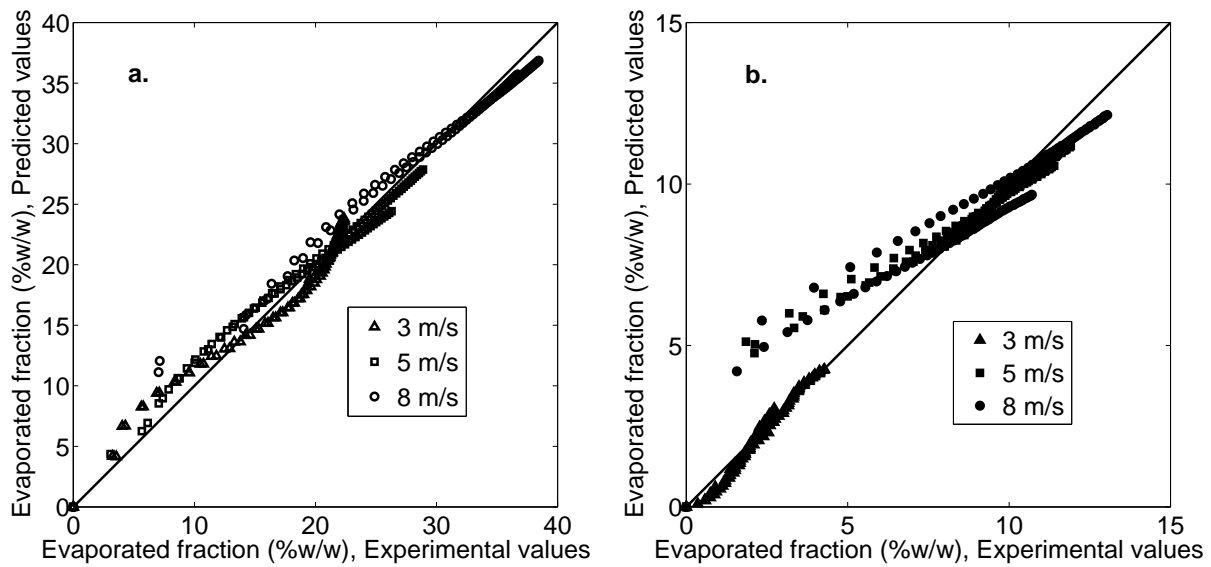


Figure 5.6: Predicted versus experimental evaporated fraction. Predicted values using the mass transfer coefficient found with the optimization procedure. a. Cusiana. b. Vasconia.

Figure 5.7a compares the optimized mass transfer coefficients for both crudes at the wind speeds selected with the mass transfer coefficients calculated with the state-of-the-art correlation used by MEUN until this point. Figure 5.7b has the same information but in logarithmic scale to present a detailed view at low values of mass transfer coefficients. In Figure 5.7a the effect of wind velocity on the mass transfer coefficient is significantly different for Cusiana and Vasconia. Cusiana has a greater increase in k_w with wind velocity. Actually the optimized mass transfer coefficient changes from overestimated at 3 m/s by the state-of-the-art correlation to underestimated at 8 m/s. Although the mass transfer coefficient also increases with wind velocity for Vasconia, the increase is not as strong as for Cusiana and the state-of-the-art correlation always overestimates the optimized value.

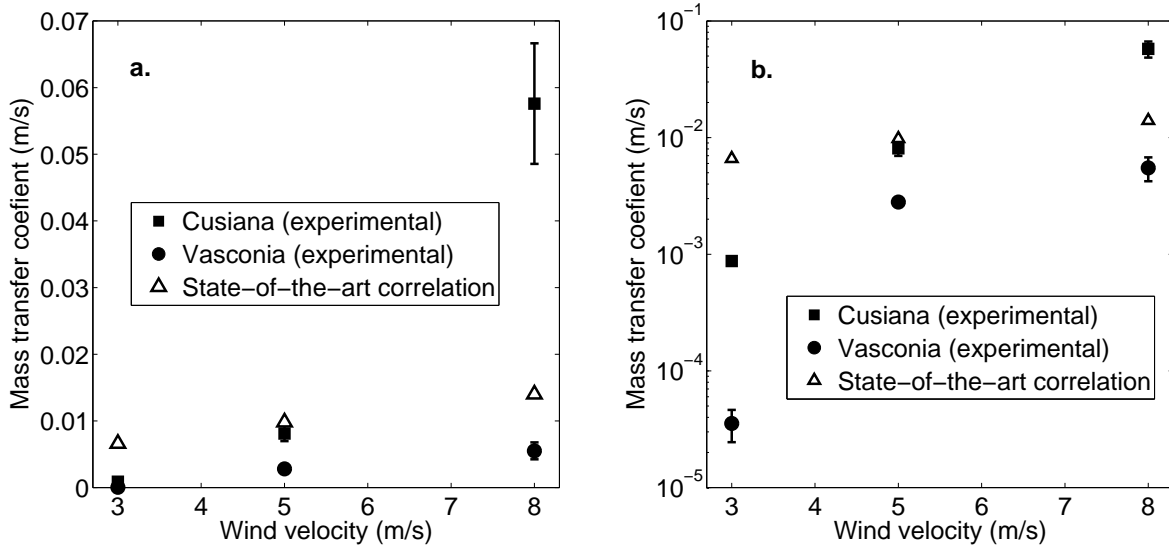


Figure 5.7: Effect of wind velocity in the behavior of the mass transfer coefficient. Comparison between calculated values with the optimization procedure and with the state-of-the-art correlation. a. Linear scale. b. Logarithmic scale.

According to Fingas [38] one of the main problems with the state-of-the-art mass transfer correlation with the function $U^{0.78}$ is that they are based on the studies of water evaporation developed by Sutton [54].

The discrepancy between experiments and the state-of-the-art correlations that is evident in Figure 5.7 compels the development of a new mass transfer correlation that considers two aspects:

- A dependence with crude oil type. As it is evident in Figure 5.7b, Cusiana's mass transfer coefficient is greater than Vasconia's for each one of the three wind velocities considered and at 3 m/s and 8 m/s the difference between crudes oil is almost one order of magnitude.
- An improved dependence of the mass transfer coefficient with wind velocity. Figure 5.7a shows that the state-of-the-art correlation does not follow the trend of neither of the two Colombian crude oils.

5.1.1.4. Adjusted correlation for the mass transfer coefficient

To satisfy the two conditions described above for the mass transfer coefficient and combining some aspects of the current understanding of the phenomenon of evaporation, as was described in Section 3.1.1, Equation 5.4 proposes a general form of the mass transfer coefficient correlation. The dependence of the mass transfer coefficient with respect to the type of crude discussed above is

presented with the first term of Equation 5.4. The second term is function of the wind velocity and aims to improve the deviation of the state-of-the-art prediction with respect to experimental data showed in Figure 5.7. The last term in Equation 5.4, is a dependence with respect to a scale factor -in this case the equivalent diameter-, this effect considers that the air downstream of the mass transfer area has a certain concentration of volatile compounds, decreasing the effective mass transfer rate. The larger the oil spill, the greater the decrease in evaporation rate.

$$k_w = a f(\text{type of crude}) f(U_w) f(X) \quad (5.4)$$

This experimental study did not consider different length scales of the spill, since all the experiment were made with the same evaporation tray with fixed geometrial dimensions. For this reason this thesis used the dependence with respect to the length scale of the slick proposed by Mackay and Matsugu [55] and widely used in previous works [31–34]. Equation 5.5 presents the new expression for k_w with $f(X)$ as $X^{-0.11}$.

$$k_w = a f(\text{type of crude}) f(U_w) X^{-0.11} \quad (5.5)$$

To take into account the type of crude oil, this study used the correlation proposed by Hamoda et al. [37] that uses the API gravity as correlation parameter. In the referred literature, another way to consider crude oil type is through a function in terms of the Schmidt number, however, due to the complexity of estimating diffusivity of a heterogeneous mixture such as crude oil, previous works have considered an average value of 2.7 for any crude [4, 31–33], making this second approach unfeasible. The effect of wind velocity was addressed with an exponential function as originally proposed by Yang and Wang [35], this exponential function was chosen because, as it is shown in Figures 5.7, there is a stronger dependence of mass transfer with wind velocity than that predicted by the state-of-the-art power law dependence.

$$k_w = a ({}^\circ API)^b e^{cU_w} X^{-0.11} \quad (5.6)$$

After a parameter optimization carried out following a methodology analogous to the one described above to calculate the mass transfer coefficient, the combination of parameters a , b and c that guaranteed the minimum difference between the mass transfer coefficient calculated with Equation 5.6 and the experimental mass transfer coefficients was found. Equation 5.7 shows the correlation with the optimized values of a , b and c .

It should be noticed that the expression for fuel dependency only considered two points (Cusiana or Vasconia) and, therefore, should be considered as a fitting exercise that is only valid for these two crudes under the limited range of wind velocities and temperature of this study. To compute the error produced in the predictions due to uncertainties in the optimized parameters a , b and c , this thesis presents in Appendix E a sensitivity analysis.

$$k_w = 3.04 \times 10^{-9} (API)^{3.06} e^{0.67U_w} X^{-0.11} \quad (5.7)$$

Figure 5.8a in linear and Figure 5.8b in logarithmic scale show the mass transfer coefficients calculated with Equation 5.7 for Cusiana and Vasconia for 3, 5 and 8 m/s as well as the mass transfer coefficients obtained using the experimental data marked as “experimental”. This figure shows that for Cusiana the values calculated with Equation 5.7 are in a good agreement with the individual “optimized” values in the entire velocity interval. In the case of Vasconia there is good agreement at 8 m/s but the correlation starts to fail as the wind velocity decreases.

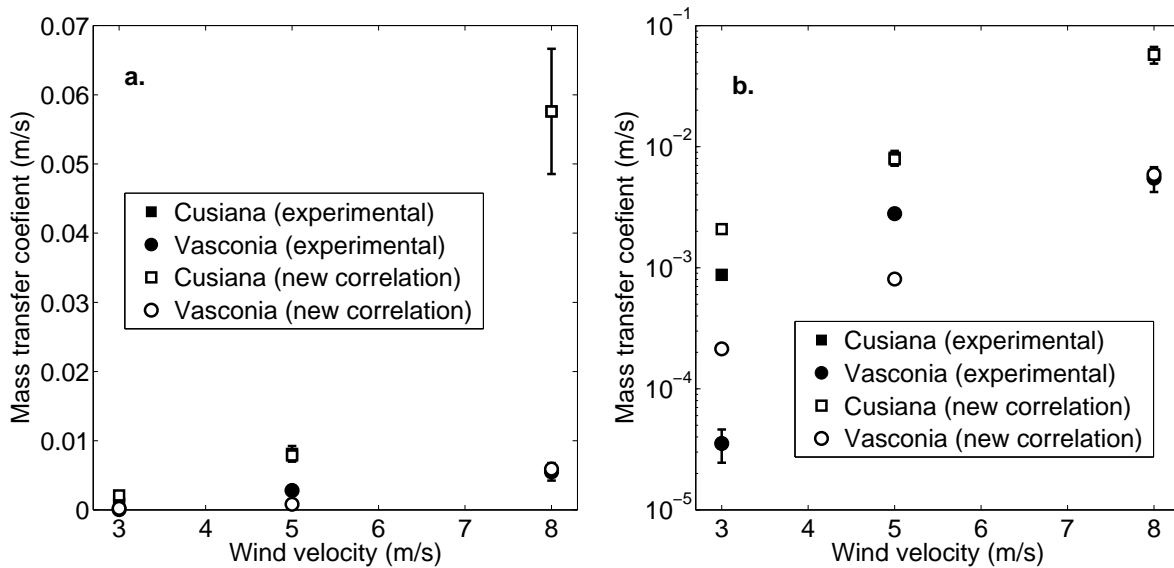


Figure 5.8: Effect of wind velocity in the behavior of the mass transfer coefficient. Comparison between calculated values with the optimization procedure and with the proposed correlation. a. Linear scale. b. Logarithmic scale.

To evaluate the calibration process described above, this research computes from the parity plots, an estimate of the error referred in this thesis as the overall error in the correlation (ϵ), and calculated with Equation 5.8.

$$\epsilon = \frac{1}{2} \sum_{k=1}^{N_p} [Fme_{pred}(k) - Fme_{exp}(k)]^2 \quad (5.8)$$

where the summation is made over the total number of points in the parity plot, N_p .

Figures 5.9a and 5.9b show, respectively, the parity plots for the evaporated fraction of Cusiana and Vasconia, when the values of the mass transfer coefficient are obtained using Equation 5.7. Figure 5.9a shows a good performance of the correlation proposed for the three velocities considered, particularly when compared with Figure 5.4a. In terms of the overall error in the correlation (Equation 5.8), the value decreases from 12630 considering Figure 5.4a to 1810 with the correlation proposed. In the case of Vasconia the parity plots show that at 8 m/s the correlation in Equation 5.7 correctly predicts the mass transfer coefficient. At lower velocities, however, the correlation does not do that well when predicting the mass transfer coefficient. Nevertheless, the correlation in Equation 5.7 represents an improvement with respect to the original parity plot shown in Figure 5.4b where, particularly, at 3 m/s, the differences between experimental data and those predicted by the correlation could be as high as 8%. Meanwhile with the correlation in Equation 5.7, the differences are never higher than 3%. This is confirmed evaluating the values of overall error in the correlation. With the state-of-the-art correlation (Figure 5.4b) this value was 2570 and with the proposed correlation the error decreases to 816.

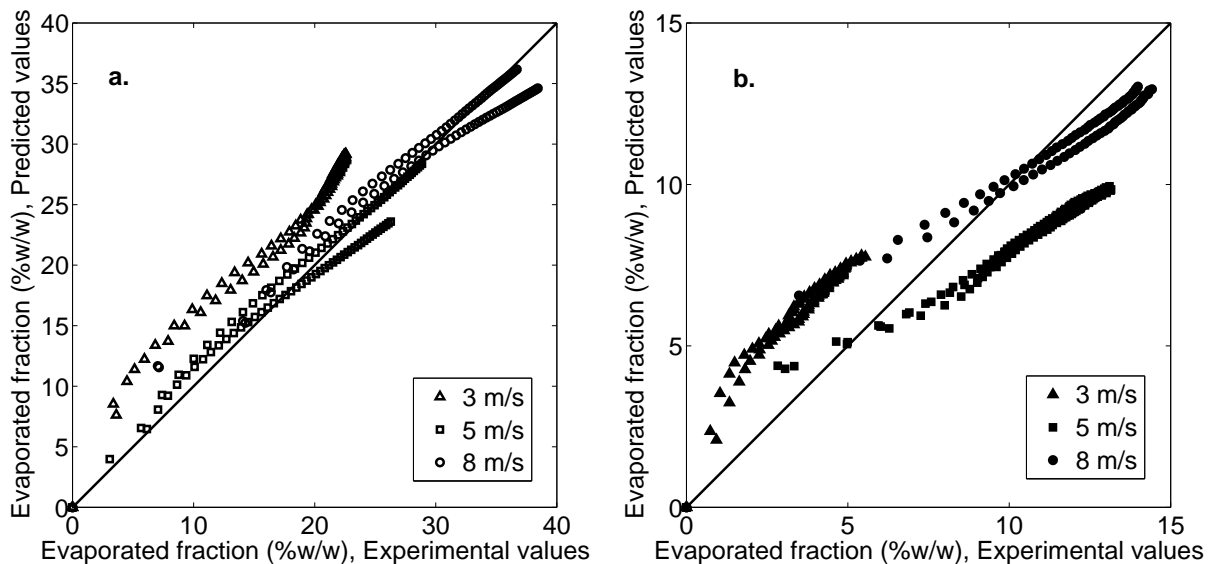


Figure 5.9: Predicted versus experimental evaporated fraction. Predicted values computes mass transfer coefficient with the correlation in Equation 5.7. a. Cusiana. b. Vasconia.

5.1.2. Effect of pour point on evaporation rate

As previously mentioned, experimental data obtained at temperatures below the pour point were not selected for the evaluation of the mass transfer coefficient because below the pour point the phenomena that control the evaporation rate changes. As the experimental temperature was always above the pour point for Vasconia, this section only considered the waxy crude oil Cusiana that according to Figure 4.2a, once submitted to some evaporation, presents a pour point of the order of the experimental temperatures.

5.1.2.1. Experimental results

Figure 5.10 presents the results of an experiment with Cusiana that illustrates how conducting experiments below the pour point affects the evaporation rate. Figure 5.10a shows the evolution of the evaporated fraction and the temperature with time when conducting an experiment as that described in Section 4.2. At any time t_k the values of the evaporated fraction $F_{eva}(t_k)$ and temperature $T(t_k)$ form the pair $(F_{eva}(t_k), T(t_k))$. Figure 5.10b shows the evolution with time of the evaporation rate (expressed as the time-derivative of the evaporated fraction). Figure 5.10c presents the variation of the pour point with the evaporated fraction for Cusiana already given in Figure 4.2. To this pour point figure, pairs of $(F_{eva}(t_k), T(t_k))$ from Figure 5.10a were added to form the line $\overline{0abc1}$.

In Figure 5.10a the initial part of the evaporated fraction curve ($\overline{0a}$), marked with a black solid line, the evaporated fraction has the expected increasing behavior with time that agrees with a positive value of the evaporation rate in Figure 5.10b. This section corresponds to an experiment carried out at a temperature above or fairly close to the pour point curve, as can be seen in Figure 5.10c. The line segment marked as \overline{ab} in Figure 5.10a shows a significant decrease in the evaporation rate that causes an almost asymptotic behavior in the evaporated fraction confirmed with the evaporation rate fairly close to zero shown in Figure 5.10b. Figure 5.10c shows that in this \overline{ab} segment the experiment was below the pour point. In Figures 5.10a and 5.10b the line segment \overline{bc} shows an increase in the evaporation rate. In Figure 5.10c, the line segment \overline{bc} corresponds to an experiment carried out at temperatures closer to the pour point curve than segment \overline{ab} . Finally, in line segment $\overline{c1}$ in Figures 5.10a and 5.10b, the evaporation rate drastically decreases again while the experiment is carried out at temperatures considerable below the pour point in Figure 5.10c. These experiments suggest the following conclusions:

- In regions where the crude oil is above, or fairly close to, the pour point curve (marked as “regular evaporation” in Figure 5.10) the oil slick undergoes a typical evaporation process as that described in Section 3.1.2.

- If the crude oil is well below the pour point, (marked as “gel behavior” in Figure 5.10) the evaporation rate drastically decreases as it is shown in Figure 5.10b and the evaporated fraction get an almost asymptotic value as it is evident in Figure 5.10a.

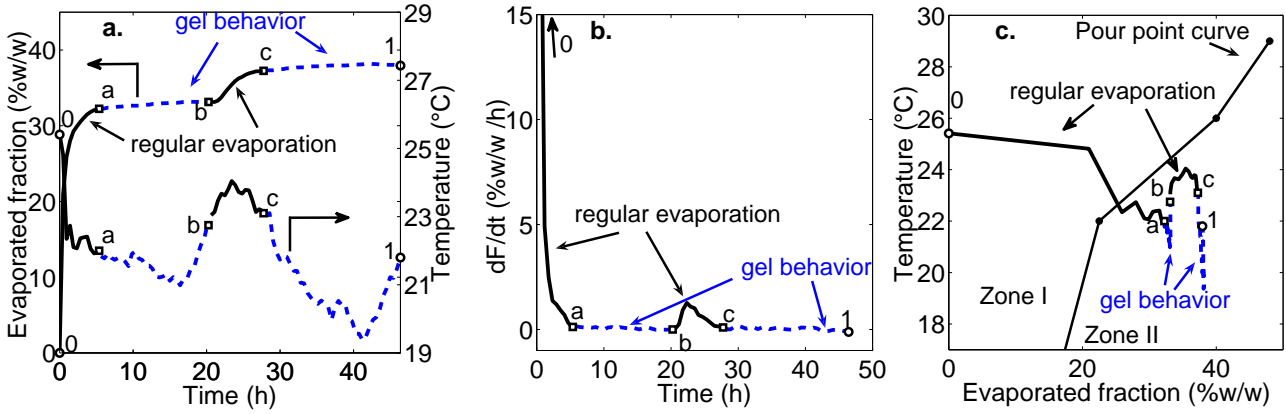


Figure 5.10: Graphical representation of the effect of the pour point on the evaporation rate of Cusiana. a. Evaporated fraction and temperature. b. Evaporation rate (expressed as the time-derivative of the evaporated fraction). c. Pour point curve. Check the text for an explanation of the different legends in these figures.

5.1.2.2. Comparison of experimental data with MEUN predictions

Figure 5.11a compares the experimental variation of the evaporated fraction with time with predictions obtained with MEUN for experiments that, at least during some periods of time, registered temperatures below the pour point. Zone I and Zone II correspond, respectively, to conditions above and below the pour point curve. In this figure, MEUN does not consider the decrease in the evaporation rate due to the pour point effect, and it computes the evaporated fraction during all the simulation with Equation 5.1. It is evident that a model that does not consider the pour point effect can significantly overestimate the evaporated fraction.

Figure 5.11b presents the same comparison as Figure 5.11a but in a partity plot format and considers the experiments for the three wind velocities used in this research. The agreement between model predictions and experiments, as evident in the black points that represent Zone I experiments (those conducted at temperatures above the pour point) was expected giving that these data correspond to

that obtained after the optimization described in Section 5.1.1.3. However, in Figure 5.11b the model overestimate the evaporated fraction for the experiments carried out at temperatures below the pour point, (blue points in Zone II). In fact, in the parity plot the blue dots form vertical lines because the experimental evaporated fraction reaches an asymptotic value while the model predicts a continuous increase in the evaporated fraction.

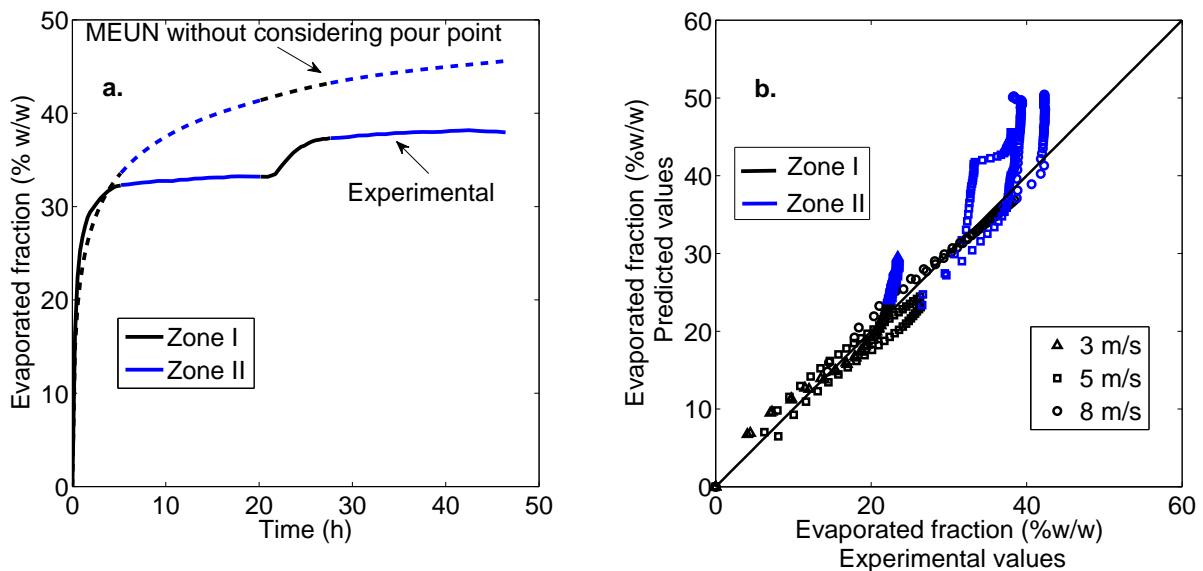


Figure 5.11: Comparison of the experimental evaporated fraction with MEUN predictions for Cusiana when the wind velocity was 5 m/s and the temperature was, at least for some periods of time, below that of the pour point. a. Variation of evaporated fraction with time b. Parity plot considering as well experiments at 3, 5 and 8 m/s.

5.1.2.3. Evaporation model calibration

The results in the previous section suggest that the model needs to take into account the effect of the pour point when representing the evaporation of Cusiana after an oil spill. This section describes how the model was modified to include such an effect.

Figure 5.12 reproduces the data in Figure 5.10c, but adds some data points obtained when the evaporation rate changed from significant to almost zero and a blue line 3°C below the pour point curve. As discussed above, when the temperature of the slick is above or fairly close to the pour point curve (as in point *e* of Figure 5.12) the slick follows what was described as regular evaporation process. The fact that all the data points in Figure 5.12 but one lie above the blue line in Figure 5.12 suggests that 3°C below the pour point, the evaporation had significantly decreased. To model this behavior, this thesis proposes that for a given evaporated fraction, e.g. EvF in Figure 5.12, when the experiment

temperature is 3° below the pour point, as in point f , the model considers an evaporation rate of zero. When the temperature lies in an intermediate point between the pour point curve and the blue line, as in point g , the evaporation rate is interpolated between that of point e , i.e. that at the pour point temperature, and zero.

In MEUN this is implemented with the factor f_{eva} that has a value that depends on the temperature and the evaporated fraction of the slick, and the pour point at that evaporated fraction. This factor directly affects the evaporation rate predicted by MEUN as shown in Equation 5.9.

$$\frac{dFme_{pred}}{dt} = -\frac{f_{eva}}{m_o} \sum_{i=1}^{n_{pc}} \frac{dm_i}{dt} \quad \text{with} \quad \frac{dm_i}{dt} = -\frac{k_w A x_i P_i^{sat} MW_i}{RT} \quad (5.9)$$

In other words, f_{eva} is defined as:

- Regular evaporation rate

$$\text{if } T(t_k) \geq PP(F_{eva}) \text{ then } f_{eva} = 1 \quad (5.10)$$

- Gel behavior

$$\text{if } T(t_k) \leq PP(F_{eva}) - 3^\circ C \text{ then } f_{eva} = 0 \quad (5.11)$$

- Transition region

$$\text{if } T(t_k) > PP(F_{eva}) - 3^\circ C \text{ and } T(t_k) < PP(F_{eva}) \text{ then } f_{eva} = \left(1 - \frac{Diff_to_PP(F_{eva})}{3}\right) \quad (5.12)$$

where:

$T(t_k)$ and $F_{eva}(t_k)$: temperature and evaporated fraction of the crude oil at any time t_k .

$PP(F_{eva})$: pour point of crude oil, function of the evaporated fraction and represented with a black line in Figure 5.12.

$Diff_to_PP(F_{eva})$: $(PP(F_{eva}) - T(t_k))$, is the difference between the pour point and the oil temperature.

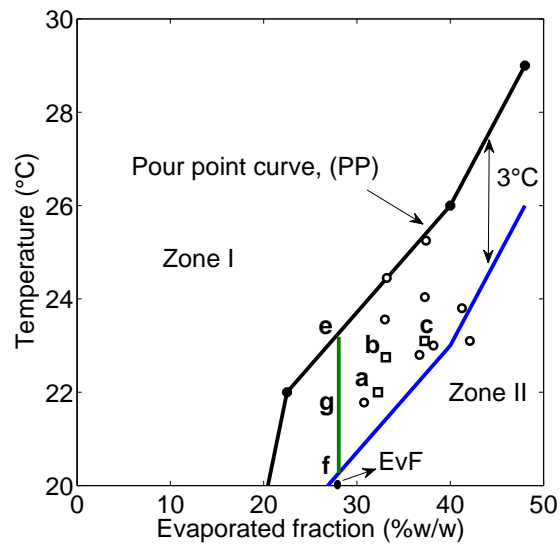


Figure 5.12: Position of important parameters relative to the pour point curve to explain how MEUN models the pour point effect on the evaporation rate.

Figure 5.13a present the comparison between predicted and experimental evaporated fraction in a modified version of MEUN that considers the pour point effect as described above. It is evident the improvement in MEUN predictions when compared with the original results in Figure 5.11.

It can be seen comparing Figures 5.11b and 5.13b that the conditional rules proposed to consider wax precipitation in evaporation rate improve MEUN predictions of experimental behavior obtained with different wind velocities.

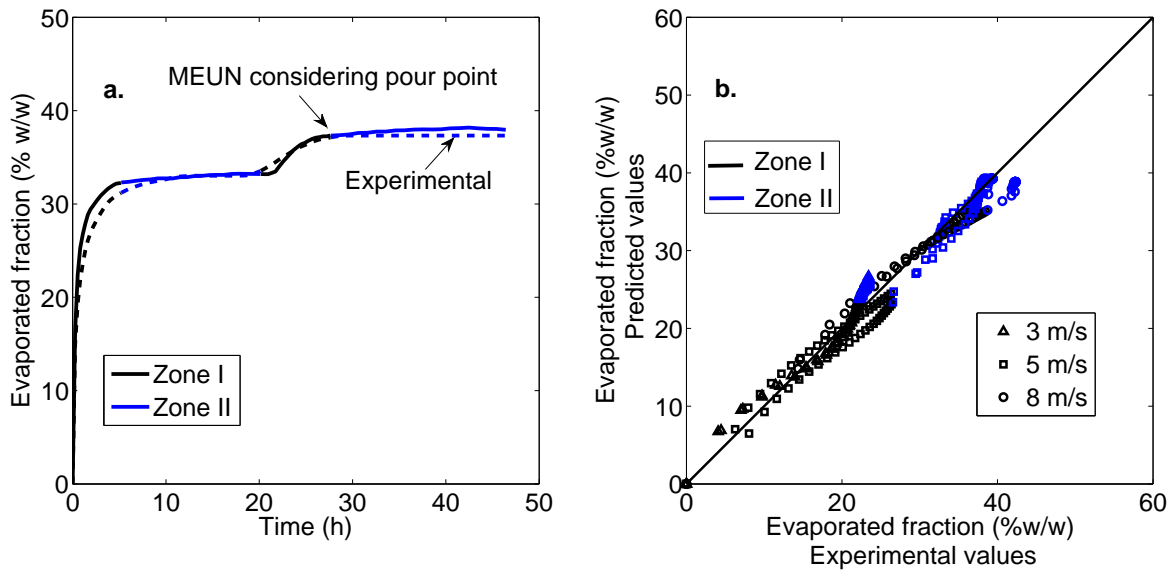


Figure 5.13: Comparison of the experimental evaporated fraction with MEUN predictions. a. Variation of the evaporation rate with time for a wind velocity of 5 m/s. b. Parity plot for all the experimental data.

5.1.3. Physicochemical properties

- Density

Figure 5.14 shows in the y axis the ratio between the evaporated and fresh crude oil density as function of the evaporated fraction. Experimental and predicted values are compared. As can be seen the default value for the empirical constant $Ceva_2$ of 0.18, recommended by Lehr et al. [7] and described in Section 3.1.3 allows a prediction of the change in density with evaporation that lies just between the trends observed for Cusiana and Vasconia independently. While the use of the original correlation would be acceptable when predicting changes in density with evaporation, for the application in MEUN the values obtained from the linear correlation in Figure 5.14 were ($Ceva_{2_{Cus}} = 0.16$, $Ceva_{2_{Vas}} = 0.22$).

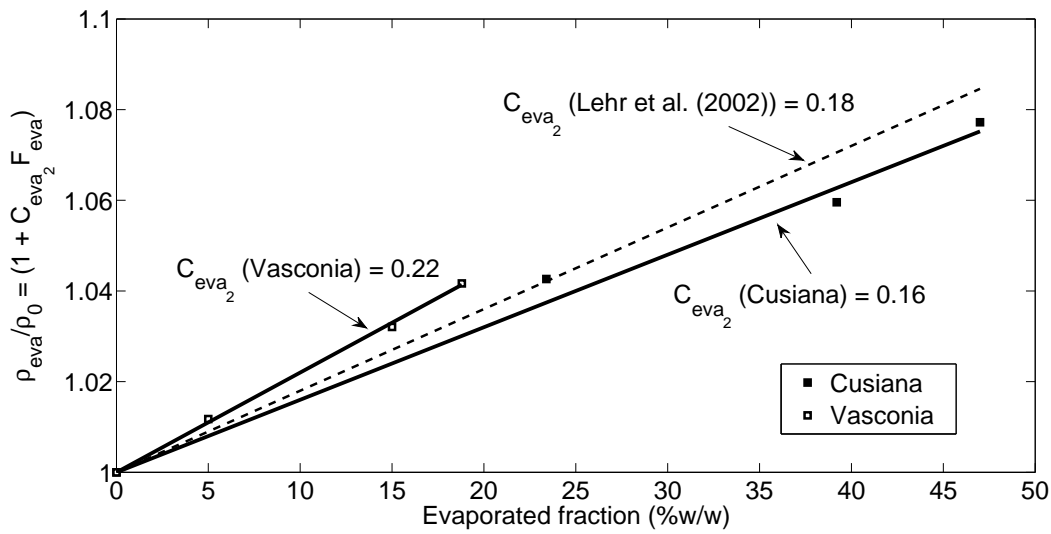


Figure 5.14: Ratio between evaporated and fresh crude oil density as function of the evaporated fraction. Experimental results (points) are presented for Cusiana and Vasconia as well as predictions by the state-of-the-art correlation [7] (dashed line) and by the best regression (continuous lines) for Cusiana and Vasconia.

- Viscosity

Table 5.1 shows, for Cusiana and Vasconia, the experimental behavior of crude oil viscosity as function of the evaporated fraction and temperature. The variation of viscosity with evaporation for both crude oils agrees with previous results that showed that viscosity increases with evaporation but decreases with temperature. As can be seen in Table 5.1, Cusiana presents multiple values of viscosity when the evaporated fraction is 44% at 25°C because at this point the crude oil is below its pour point and due to the non-Newtonian behavior the viscosity is shear-rate dependent. For Vasconia, according to Table 5.1, at any temperature, the viscosity increases almost an order of magnitude once it evaporates 15.5%. Viscosity dependence with evaporated fraction and temperature are both important when modeling weathering. A comparison of experimental data with current MEUN predictions and model calibration is given below.

Table 5.1: Experimental viscosity of Cusiana and Vasconia crude oils as function of evaporated fraction and temperature.

	Cusiana		Vasconia			
	Evaporated fraction		Evaporated fraction			
	0%	44%	0%	5%	15.5%	
Temperature	25°C	1.96	*	64	132	682
	28°C	1.91	9	55	111	533
	30°C	1.84	7	48	93	400

* non-Newtonian behavior (below pour point)

The first effect to evaluate is the increase in viscosity due to evaporation, Figure 5.15 shows the experimental values and MEUN predictions in terms of the empirical parameter C_{eva_1} at 28°C, A recommended value for C_{eva_1} is between 1 and 10 [8]. Despite the limited data, Figure 5.15 shows that $C_{eva_1} = 4$ and $C_{eva_1} = 15$ are the results of the regression for Cusiana and Vasconia respectively. Even though the value of C_{eva_1} for Vasconia is higher than the maximum ($C_{eva_1} = 10$) suggested in [8], Equation 3.13 is an empirical expression and it is expected that the behavior of all crudes oils are not described by a sole set of values of the adjustment parameter C_{eva_1} .

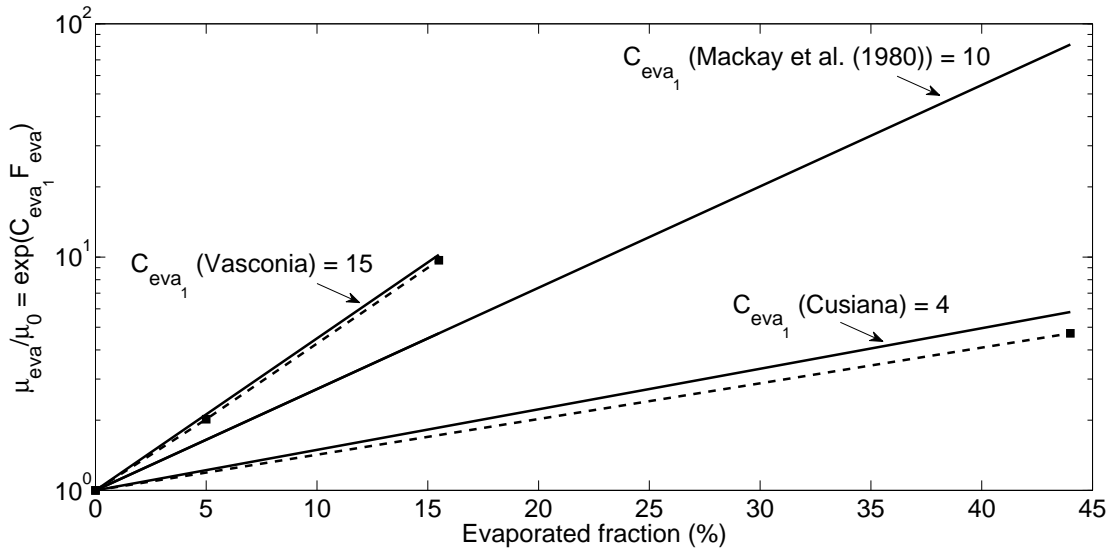


Figure 5.15: Ratio between evaporated and fresh crude oil viscosity as function of the evaporated fraction at 28°C. Experimental results are presented for Cusiana and Vasconia as well as recommended prediction according to Lehr et al. [8].

The other effect on crude oil viscosity is produced by temperature variations. To complement the

viscosity data in Table 5.1 for the crude oil Cusiana, the reported data in the crude oil database of Environment Canada [5] were selected. This database makes emphasis in crude oil properties with an expected effect on the weathering behavior after an oil spill and it has information for more than 450 oils.

Figure 5.16a and 5.16b show the variation of viscosity with temperature for Cusiana and Vasconia, respectively, at different evaporated fractions. The figure presents for Vasconia the experimental data from Table 5.1, for Cusiana the data taken from Environment Canada [5], the figure includes predictions with Equation 3.13. As mentioned in Section 3.1.3, the weathering literature recommends two values (41750 and 74826 J/mol) of activation energy to represent the effect of temperature on viscosity. While the behavior of Cusiana is described with $Ea_{Cus} = 41750$ J/mol, that of Vasconia responds to $Ea_{Vas} = 74826$ J/mol. The agreement between experiments and predictions, for both crudes, is remarkably good. In the case of Cusiana, however, Figure 5.16a shows that the predictions deviate from the experiments, when the evaporated fraction is 38%. This occurs because, for this evaporated fraction, the pour point is higher than the temperature of the experiments. The referred literature did not present an expression to predict the viscosity below the pour point and MEUN predictions are subject to that underestimation.

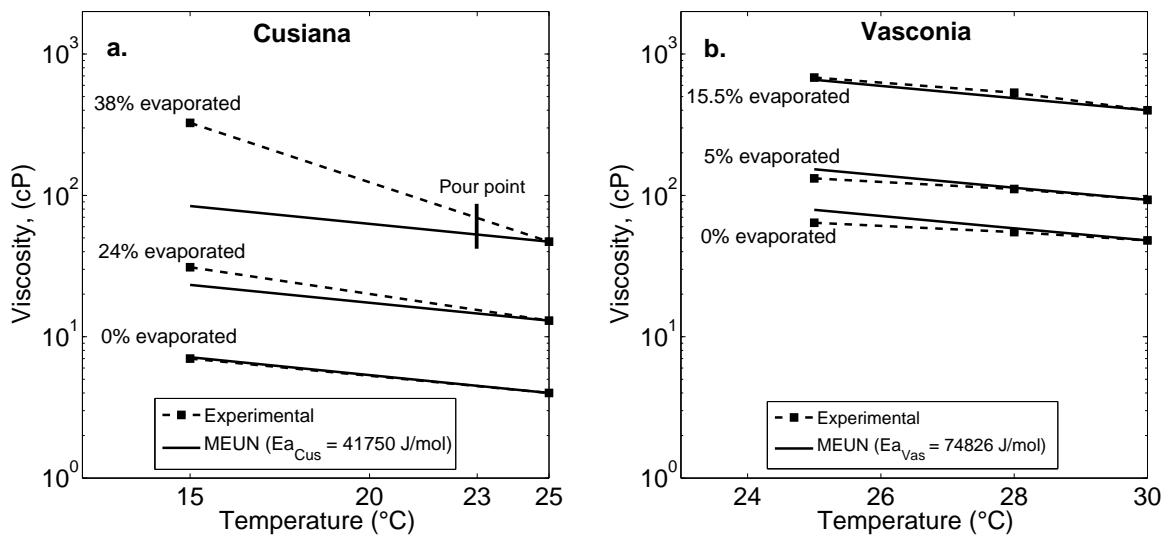


Figure 5.16: Variation of the viscosity of the slick with temperature with the evaporated fraction as parameter. Comparisons of experimental data (symbols) with model results (bold lines). a. Cusiana. b. Vasconia.

5.2. Emulsification

This section deals with emulsification of Cusiana and Vasconia when mixed with salted water. The first part illustrates the effect of the pour point in the emulsification of Cusiana. A second section explains the dynamics of emulsification after an oil spill. A final discussion describes the effect of weathering on emulsion stability and viscosity. After presenting experimental data related to each part, the discussion centers on how the empirical model is adjusted to represent the emulsification phenomenon.

Figure 5.17 presents typical experimental results obtained with the rotating cylindrical methodology explained in Section 4.3. In Figure 5.17a the increase of water content in the emulsion of a mixture of Vasconia crude oil with different evaporation levels and salted water submitted to mixing for 24 hours shows an asymptotic behavior in the water content also called maximum water content. Figure 5.17 also gives the information required to calculate the half-life time ($t_{1/2}$), the time required to obtain 50% of the maximum water content. Figure 5.17a shows that, as already reported in [41], both parameters, maximum water content and half-life time depend on the evaporated fraction. This dependence is explained below.

Figure 5.17b illustrates the typical behavior of the emulsion during the settling period, that gives information about emulsion stability and about how it is influenced by the extent of the evaporation of the oil. In this figure, while the emulsion formed with fresh oil (0% evaporated fraction) loses most of the water during the settling period, the emulsion with Vasconia when the evaporated fraction is 15.5% is stable.

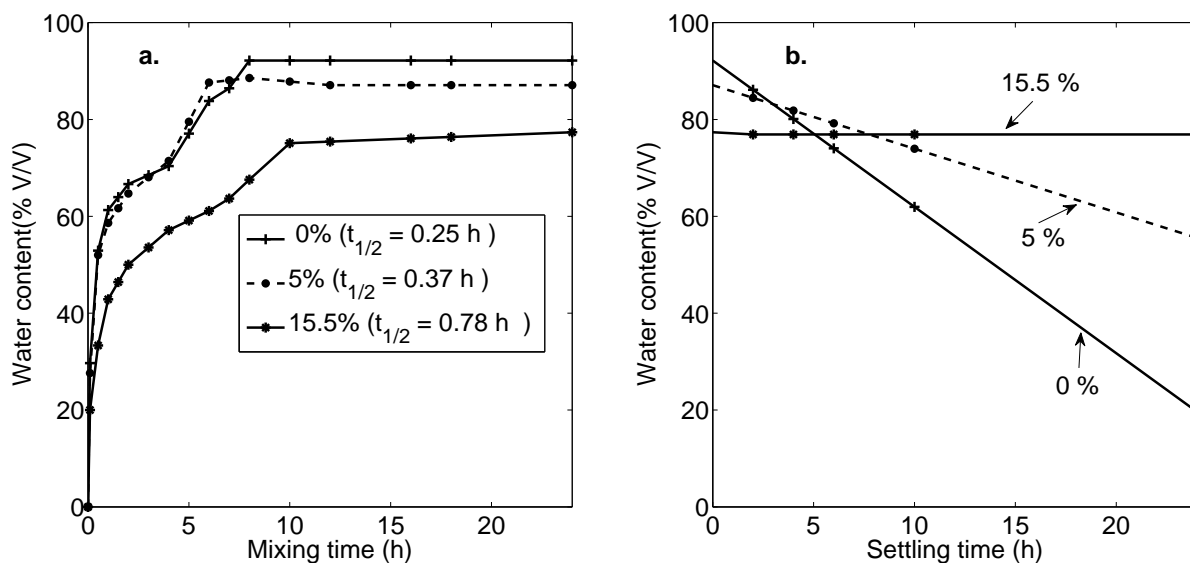


Figure 5.17: Experimental behavior in the rotating cylinder of Vasconia crude oil with the evaporated fraction as parameter. a. Mixing. b. Settling. The experiments were carried out at a temperature that varied between 23 and 25°C.

5.2.1. Pour point effect

Figure 5.17 shown how crude oil Vasconia forms a mesostable emulsion and that stability of the emulsion increases as the level of evaporation increases. This indicates that from the beginning of an eventual oil spill the water content of the slick would increase under mixing conditions. In the case of Cusiana the study of the emulsification process is more complex. Figure 5.18a shows the location with respect to the pour point curve of the experiments carried out to study the emulsification process of Cusiana. According to the figure, all the experiments carried out at temperatures above the pour point do not form emulsion. The reason for this is the absence of stabilizing compounds in Cusiana, a crude that has a low concentration of resins and asphaltenes (2.3 and 0.3% respectively). Even an increase in the concentration of this pseudocomponents, caused by evaporation, does not guarantee a stable emulsion. Stabilization of the emulsion only occurs when the temperature of the experiment is below the pour point as evident in Figure 5.18a where a high water content in the emulsion is only possible when the temperature is below the pour point. The effect of the temperature with respect to pour point is more important that the effect of evaporation as, the evaporation level of the experiments marked as IV and V are the same as in experiments III and VI, respectively, but only III and IV, those below the pour point curve, form an emulsion. The relative small temperature difference (5°C) between points V and VI is enough to cause wax precipitation, convert this light crude oil into a network of solid wax cristals that traps liquid oil [23] and water. This stabilization of water within waxy

crude oils has a great impact on the petroleum industry for flow assurance purposes [56]. In oil spill scenarios Strøm-Kristiansen et al. [57] studied the particular weathering behavior of waxy crude oils showing emulsions favored by wax precipitation in experiments carried out 12°C below the pour point.

Figure 5.18b complements the analysis of Figure 5.18a by showing the evolution of water content with time for emulsions formed in different regions of the pour point curve, i.e. the behavior of experiments marked as I,II,III and VI in Figure 5.18a, carried out at a similar temperature (24-26°C) but at different evaporated fractions. Figure 5.18b shows that in experiments I and II (conducted at temperatures above the pour point) the water content is very low ($\approx 13\%$) during all the mixing time. When the temperature gets closer to the pour point, as in experiment III, the water content does not reach an asymptotic value, as in the range of temperatures that the experiments were carried out (24-26°C) the sample was sometimes above and sometimes below the pour point. In experiment VI, conducted at a temperature several degrees below the pour point, the emulsion rapidly achieves a high water content and this value is stable during all mixing time.

The variation in the emulsion process with temperature was represented in MEUN using a conditional rule that declares the start of the emulsification process only when the predicted evaporated fraction combined with the oil temperature lies 3°C below the pour point. The analysis about the stability of this particular kind of emulsion and its respective viscosity increase is discussed below.

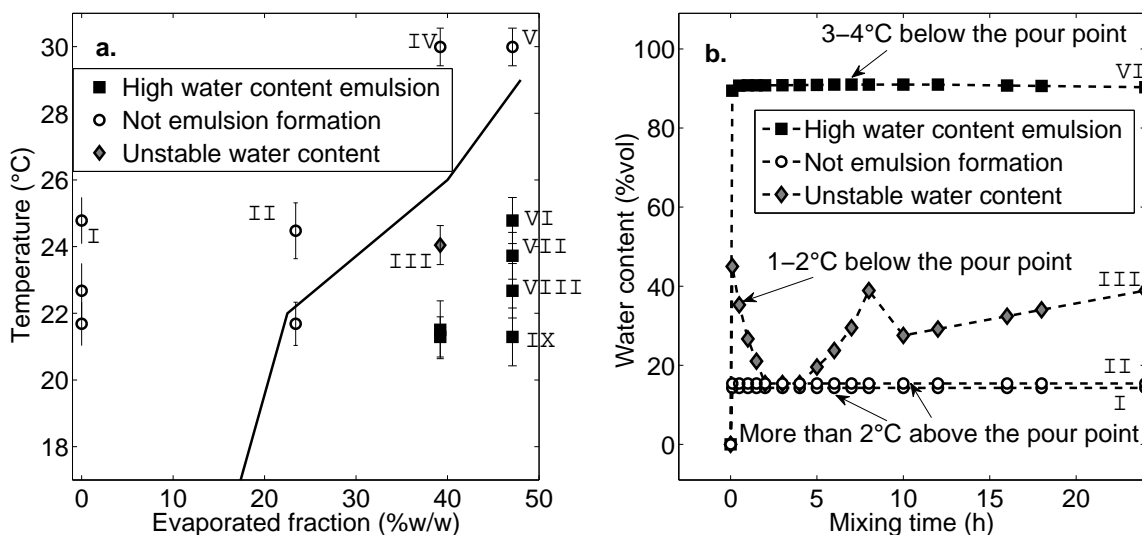


Figure 5.18: Experimental emulsification results for Cusiana crude oil. a. Behavior with respect to pour point curve. b. Evolution of water content with time for experiments above and below the pour point curve.

5.2.2. Rate of formation of the emulsion

Figure 5.19a shows the variation of water content with time in the rotating cylinder for a sample of Cusiana with an evaporated fraction of 48 % and Vasconia when the evaporation is 15.5 % Both crudes exhibit a different emulsification rate and, therefore, great variation in the values of half-life time (2.5 min Cusiana, 46.8 min Vasconia).

As mentioned in Section 3.2.2, MEUN estimates the emulsification rate under field conditions based on the half-life time evaluated in the rotating cylinder experiments. In Appendix B it is discussed that one of the main assumption of the emulsification model implemented in MEUN and first proposed by Hokstad et al. [6] is that the water uptake rate in the rotating cylinder at 30 rpm is approximately 4-6 (5 selected for this work) times faster than that observed in the field with a wind velocity of 10 m/s. Using this water-uptake relation, Figure 5.19b extrapolates to field conditions the results in Figure 5.19a with a half-life time five times higher. Figure 5.19b also presents the predictions obtained with the model proposed by Mackay and coworkers [8], explained in Section 3.2.1.1 and widely used in the weathering community. Recalling that Mackay and coworkers' model considers a typical value of maximum water content (70 %) and a unique kinetic constant to generalize any crude oil behavior, is evident from this figure, than both parameters are crude-oil dependent and this has to be taken into account by an emulsification model as MEUN does.

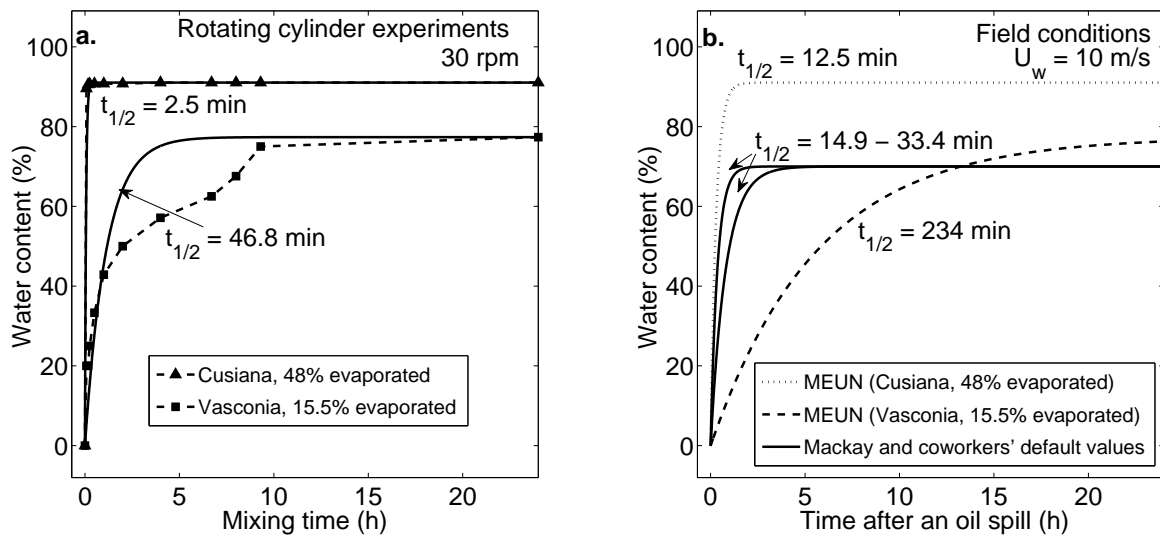


Figure 5.19: Evolution of water content with time for Cusiana 48 % evaporated and Vasconia 15.5 % evaporated. a. experimental behavior adjusted with a first order kinetic. b. extrapolated behavior to field conditions and compared with Mackay and coworkers' model [8].

For Cusiana crude oil and particularly for those experiments carried out below the pour point, the half-life time value was always close to 2.5 min in any of the conditions shown in Figure 5.18. For Vasconia, Table 5.2 shows the effect of temperature and evaporated fraction in the half-life time. Although there is not a clear trend of half-life time with respect to temperature, Table 5.2 shows that in the three ranges of temperature, the half-life time increases with the level of evaporation. In Section 3.2.2 it was shown that the emulsification model implemented in MEUN uses a single value of half-life time during all the simulation and this work considers as representative the average between the values obtained with the three levels of evaporation at the temperature of interest.

Table 5.2: Half-life time of the emulsification process for Vasconia as function of temperature and evaporated fraction.

half-life time (min)			
Evaporated fraction			
Temperature	0 %	5 %	15.5 %
19-20°C	15.0	16.2	94.8
23-25°C	20.4	21.6	46.8
29-31°C	13.8	15.0	26.4

5.2.3. Effect of evaporation and temperature on the stability of the emulsion

The effect of evaporation and temperature on emulsion stability is presented in Figures 5.20a and 5.20b for Cusiana and Vasconia, respectively. Stability of the emulsion is measured is made in terms of $R_{2/1}$, introduced in methodology section as a parameter that measures the amount of water lost from the emulsion in a settling period of 24 hours. $R_{2/1}$ values close or equal to 1.0 reflects a stable emulsion without considerable water loss and $R_{2/1}$ values close to 0.0 represent an unstable emulsion that does not retain water.

As explained above, while Vasconia presents the typical emulsion stabilization mechanism by emulsifying agents such as resins and asphaltenes, Cusiana's emulsions are only possible by the interaction with waxy crystals precipitated below the pour point. Therefore, the analysis of emulsion stabilization for both crudes, presented in Figure 5.20, is different.

For Cusiana the emulsion stability analysis in Figure 5.20a considers the variation of $R_{2/1}$ with temperature. The figure also includes the value of pour point to give an idea of what experiments

were conducted at temperatures below the pour point. All the experiments in Figure 5.20b have the same evaporated fraction but were conducted at a different temperature. Their labels (V to IX) are the same as those in Figure 5.18a. According to Figure 5.20a those experiments made below the pour point have a low emulsion stability (at most $R_{2/1} < 0.20$) despite the high water content they have under mixing conditions ($\approx 90\%$), even the experiment IX made almost 7°C below the pour point has a low value of $R_{2/1}$.

For Vasconia Figure 5.20b, that relates $R_{2/1}$ with the evaporated fraction, gives evidence of the formation of a more stable emulsion as evaporation increases. According to Bobra [58] the surfactant behavior of asphaltenes and resins is more effective if they are presented as precipitated particles, this precipitation in the case of asphaltenes is enhanced by the evaporation of light aromatics compounds that acts as asphaltenes solvents. According to Figure 5.20b at the typical temperature of the Colombian Caribbean Sea ($25\text{--}30^\circ\text{C}$) about 15.5% of evaporation is necessary to form a stable emulsion. The fresh crude oil, however, does not form a stable emulsion.

The lower stability observed in the emulsions formed with Cusiana can be explained, according to Moldestad et al. [59], because waxy crude oils (Cusiana) form emulsions stabilized by rheological strength that exhibit a lower stability than emulsions stabilized by surfactant compounds such as asphaltenes (Vasconia).

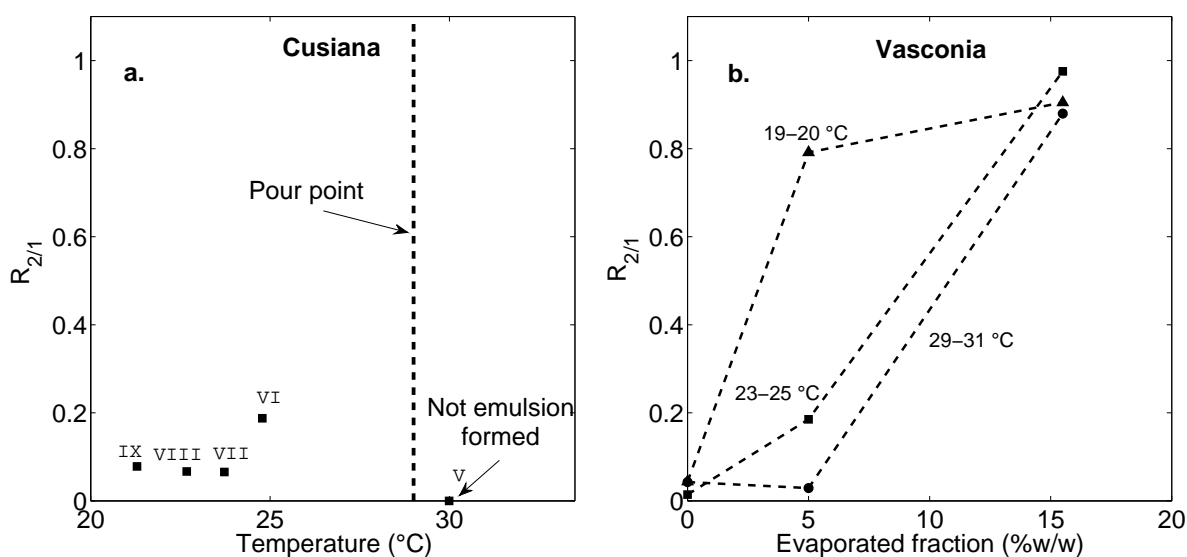


Figure 5.20: Variation of the emulsion stability parameter $R_{2/1}$ for: a. Cusiana in terms of temperature value of pour point. b. Vasconia as function of evaporated fraction with temperature as parameter.

5.2.4. Physicochemical properties

5.2.4.1. Density

The parity plot of Figure 5.21 shows the comparisons between experimental results and MEUN predictions of the density of the emulsion. The simple mixing rule initially included in MEUN and described in Section 3.2.2, estimates the change in density because of the formation of a water-in-oil emulsion with an error lower than 4% in any of the points in Figure 5.21, which is considered acceptable for the scope of this thesis.

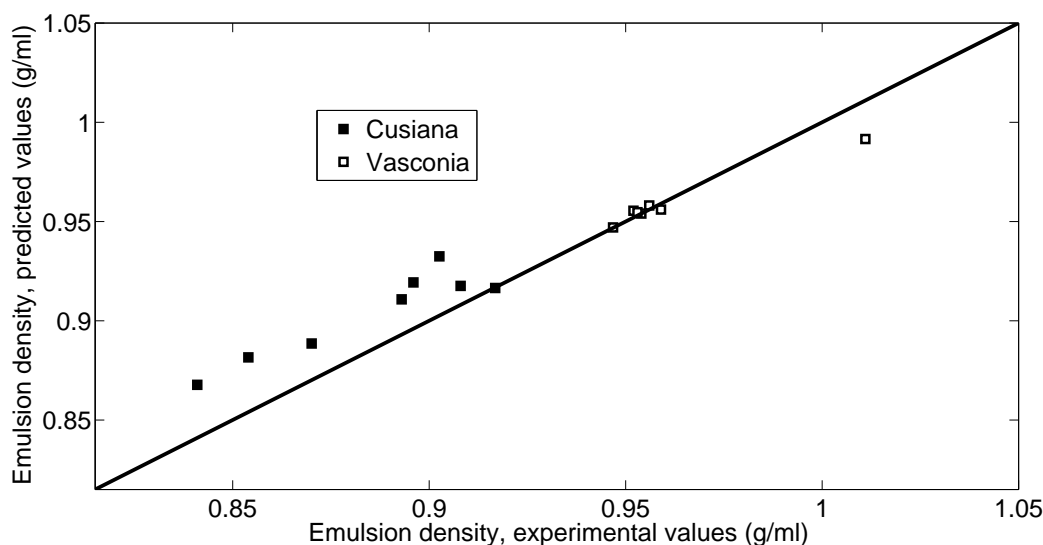


Figure 5.21: Comparison of the experimental and MEUN predictions for density of emulsions formed with Cusiana and Vasconia.

5.2.4.2. Viscosity

To model the variation of the viscosity due to emulsification MEUN uses the stability criteria proposed by Fingas [9] and explained in Table 3.1 in Section 3.2.2. Based on Fingas' definitions, emulsions formed with Vasconia crude oil after 0 to 5% of evaporated fraction (see Figure 5.20a) are meso-stable emulsions and would present an increase in viscosity of the order of 7 - 11, because the water content obtained in the mixing time is lost within hours or days. The emulsions formed with Cusiana, below the pour point would be meso-stable as well. Although Cusiana's emulsions present low values of $R_{2/1}$, they cannot be classified as unstables, because, according to Fingas, unstable emulsions are only those unable to form a water-in-oil mixture, as was the case for the experiment carried out with Cusiana at a temperature above the pour point (V in Figure 5.18a and Figure 5.20b). Stable emulsions (viscosity increase ratio = 405 - 1054) are only formed with Vasconia when the evaporated fraction is 15.5%.

Figure 5.22 compares predictions by MEUN, that take into account the stability of emulsion when predicting the viscosity increases as was described in the paragraph above, with the predictions obtained with the Mackay and coworkers' model discussed in Section 3.2.1.1 which only considers the water content of the emulsion in the correlation used to estimate the viscosity increase. The results in Figure 5.22 reveal the importance of the analysis of the stability of the emulsion when predicting changes in viscosity. In fact, Moldestad et al. [59] showed that, depending on the characteristic of the parent oil, a high-water content emulsion could have a viscosity ratio, when compared to the fresh crude, as high as 300 or as low as 0.1. This gives an idea of the complexity of modeling changes in viscosity when a water-in-oil emulsion is formed. Because the viscosity of the emulsions was not measured in this research, the model implemented in MEUN can only be understood as the best approximation to the changes in viscosity for the emulsions.

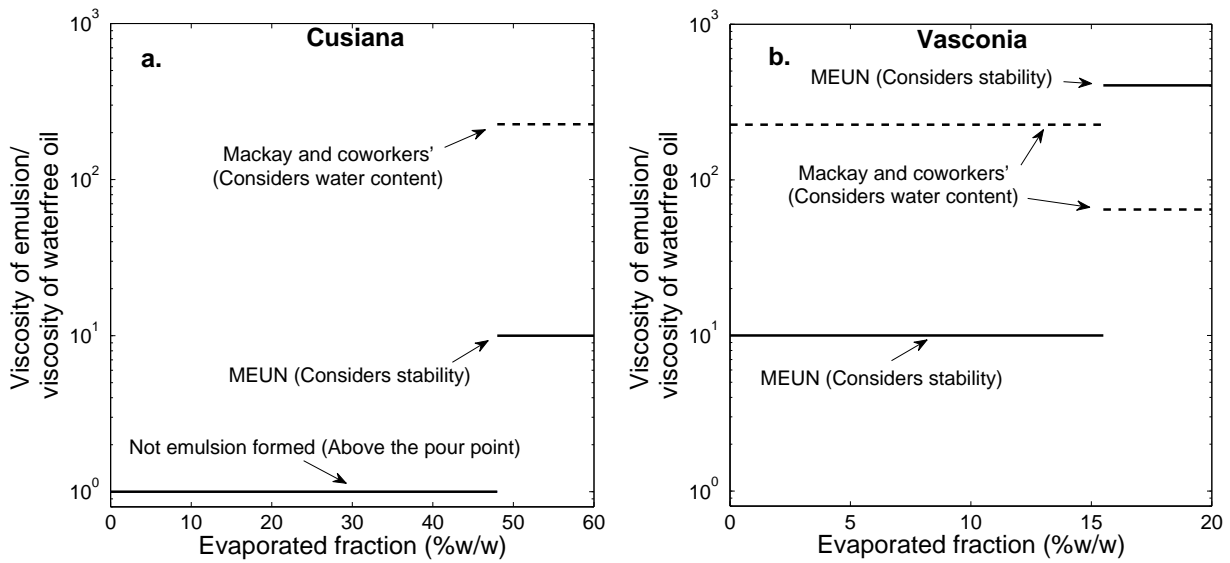


Figure 5.22: Variation of the viscosity ratio between emulsified and water-free crude oil as function of evaporated fraction. a. Cusiana, b. Vasconia. At temperature of 25°C

Combining the effects of evaporation and emulsification, the overall changes in density and viscosity are summarized in Equations 5.13 and 5.14.

$$\rho(t) = \rho_0 \underbrace{(1 + c_{eva2} F_{eva})}_I \underbrace{(1 - Y) + \rho_w Y}_{II} \quad (5.13)$$

$$\mu(t) = \mu_0 \underbrace{\exp\left[\frac{Ea}{R}\left(\frac{1}{T} - \frac{1}{T_0}\right)\right]}_{III} \underbrace{\exp(c_{eva1}F_{eva})}_{IV} \underbrace{ViscEmul(F_{eva})}_V \quad (5.14)$$

where:

Term *I*: density increase due to evaporation (see Figure 5.14)

c_{eva2} : empirical parameter, $c_{eva2} = 0.16$ for Cusiana and $c_{eva2} = 0.22$ for Vasconia (see Figure 5.14)

Term *II*: density increase due to emulsification (mixing rule)

Term *III*: viscosity increase due to temperature change (see Figure 5.16)

Ea : empirical parameter, $Ea = 41750 \text{ J/mol}$ for Cusiana and $Ea = 74826 \text{ J/mol}$ for Vasconia (see Figure 5.16)

Term *IV*: viscosity increase due to evaporation (see Figure 5.15)

c_{eva1} : empirical parameter, $c_{eva1} = 4$ for Cusiana and $c_{eva1} = 15$ for Vasconia (see Figure 5.15)

Term *V*: viscosity increase due to emulsification (see Figure 5.22)

$ViscEmul(F_{eva})$: viscosity multiplier, function of evaporated fraction and showed in Figure 5.22

Terms I and II in Equation 5.13 give acceptable predictions for both crude oils. With respect to Vasconia' viscosity, the Term V has the greater uncertainty, although experiments were carried out to establish the effect of emulsion stability, the value of viscosity increase is based on studies that considered other crude oils. For Cusiana viscosity, the uncertainty of the model depends on temperature. Above the pour point curve, terms III and IV should give good predictions and there is no uncertainty with Term V as no emulsion is formed. Below the pour point, terms III and IV are not considered as changes in viscosity due to wax precipitation are not implemented in MEUN. The predicted viscosity increase due to emulsification (7-11 times) according to Term V is based on stability analysis and requires further experimental validation. However, the most significant error predicting Cusiana's viscosity below the pour point is the lack of experimental data or theories that can be applied when wax precipitation takes place.

5.3. MEUN application to a spill incident in the Colombian Caribbean Sea

Previous sections were focused on describing general formulations for individual weathering processes as well as experimental calibration of a module, MEUN, that simulates physicochemical changes of two Colombian oils, Cusiana and Vasconia, after an oil spill. This section tests MEUN capabilities describing the general weathering behavior of Colombian crudes Cusiana and Vasconia under typical

environmental conditions of the Colombian Caribbean Sea. MEUN predictions are compared with the weathering model ADIOS v.2.0 developed by NOAA [60]. This software, of free distribution, is described by Lehr et al. [7].

In the weathering model ADIOS it is possible to introduce multiple crude oil properties in case they are known. However, only two parameters are required to perform a simulation: API gravity and viscosity at a reference temperature. In addition to these two parameters, the ADIOS simulations considered the True Boiling Point and the SARA composition of each crude as input parameters.

Four different cases, as Table 5.3 shows, were modeled to evaluate to performance of MEUN. Cases I and II consider a typical wind velocity and the upper and lower temperature limits of the Colombian Caribbean Sea (24.3°C and 30.0°C respectively) in order to test the influence of temperature difference in the overall weathering behavior for a waxy crude oils such as Cusiana. For Vasconia, Cases III and IV present typical conditions of sea surface temperature but different wind velocity. As discussed above, the wind velocity in the Caribbean Ocean varies between 3.0 and 9.9 m/s. Values of 3.0 and 6.3 m/s represent low and high velocity values in that range, respectively. Temperature variations are not studied for Vasconia because the small temperature change on the Caribbean Ocean should not have a significant impact on its weathering behavior. A value of 100 tons for the spill is characteristic of a medium-size oil spill [61] and considered appropriate for this initial study.

Table 5.3: General conditions to test MEUN predictions

Case	Crude oil	Spilled amount (tons)	Sea Surface Temperature (SST) (°C)	Wind velocity (m/s)
1	Cusiana	100	30.0	6.3
2	Cusiana	100	24.5	6.3
3	Vasconia	100	27.5	6.3
4	Vasconia	100	27.5	3.0

Figure 5.23 shows MEUN (5.23a) and ADIOS (5.23b) predictions of evaporated and dispersed fractions for Case I. Both models predict the complete removal of the spilled amount from the ocean's surface 30 hours after the start of the spill. For Cusiana, the high concentration of volatile compounds and the low viscosity favor evaporation and dispersion. While the predictions by both crudes are apparently similar, there is a difference in the dispersion rate which is higher in the predictions by

ADIOS. Although ADIOS does not give access to the code itself, one could speculate that differences in the dispersion rate are due to: (1) the fact that the viscosity predicted by MEUN is four times higher than that by ADIOS as discussed below. Given that neither MEUN, nor ADIOS predict the formation of an emulsion, the difference in viscosity should originate in the way each model estimates the change in viscosity due to evaporation. While MEUN was calibrated for Cusiana, ADIOS estimates this behavior from its crude oil database, (2) the dispersion model itself. Both models, MEUN and ADIOS, compute the dispersion rate based on the hydraulic model proposed by Delvigne and Sweeney [49]. However, this model has several empirical parameters as shown in Equation 3.21. Differences in the values of these parameters, not available for ADIOS, could explain, to some extent, the difference.

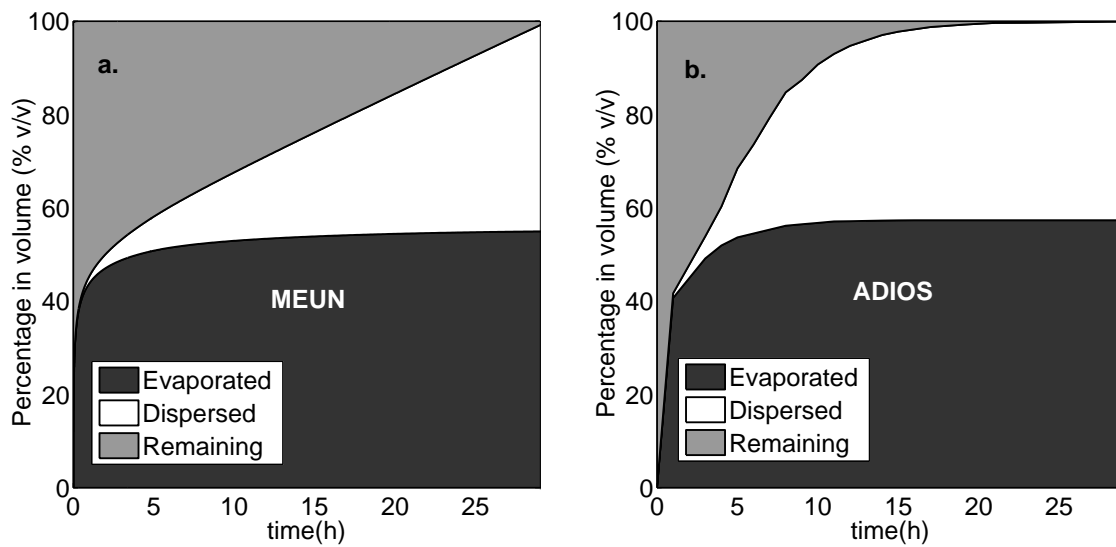


Figure 5.23: Prediction of oil spill budget for Cusiana crude oil in Case I (see Table 5.3). a. MEUN b. ADIOS.

In Case II, in an oil spill occurring at 24.5°C, 5.5°C lower than Case I, the model ADIOS calculates an evaporated fraction almost equal as in Case I (56%) while MEUN calculates an asymptotic evaporated fraction of 42%. The difference is even more significant in predictions of dispersed fraction, while MEUN predicts, after 80 hours that the dispersed fraction is close to 18%, the value predicted by ADIOS is close to 45%. To understand this difference it is important to compare the predictions of viscosity in Figure 5.25b. In this figure, ADIOS predicts almost the same viscosity for cases I and II. While MEUN predicts a considerable increase in viscosity when the evaporated fraction is higher than 42%, point B' in figures 5.24a and 5.25b.

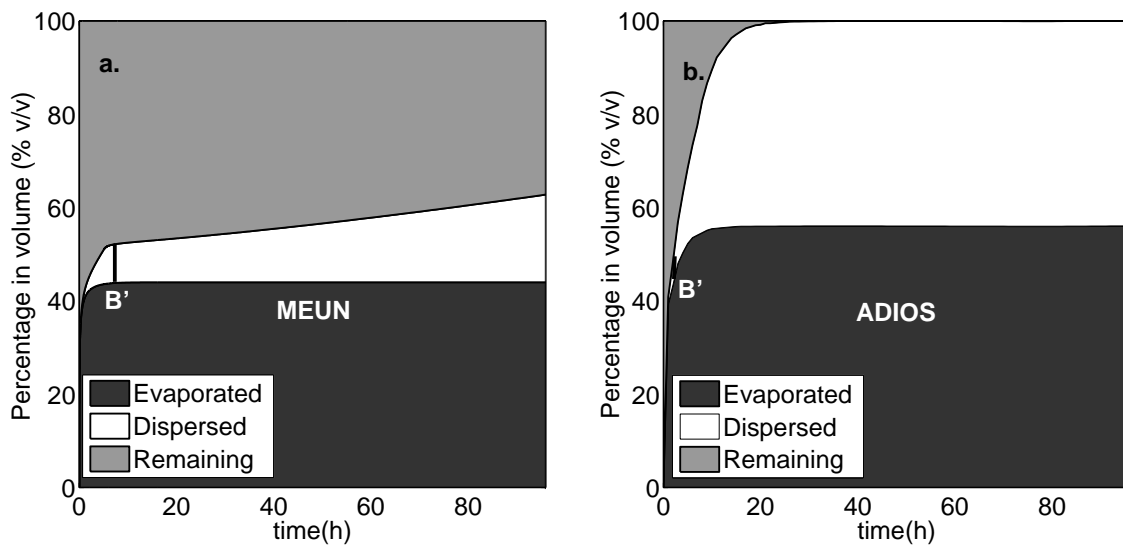


Figure 5.24: Prediction of oil spill budget for Cusiana crude oil in Case II (see Table 5.3). a. MEUN b. ADIOS.

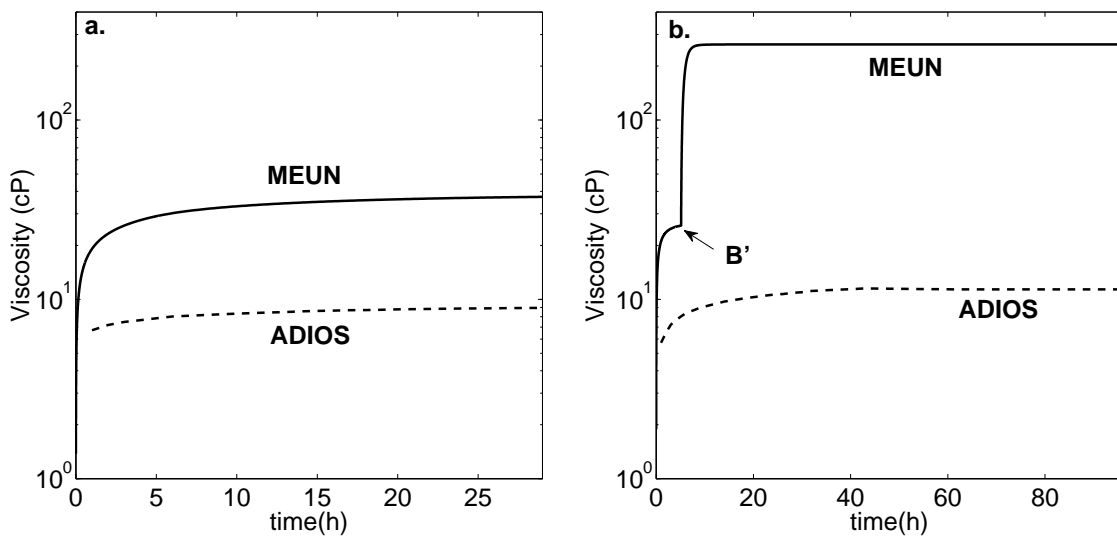


Figure 5.25: Comparison of the variation of viscosity with time as predicted with the module MEUN and the model ADIOS. a. Case I. b. Case II.

Clearly at 30°C the predictions of both models, ADIOS and MEUN, are very similar but at a temperature just 5.5°C lower, the behavior predicted by both models is significantly different for the mass balance and viscosity. To explain this, Figure 5.26 shows the pour point curve for Cusiana and the imaginary line 3°C below the pour point curve where, according to this work, the evaporation rate is virtually stopped and the emulsification process is promoted. This figure also includes, as a line, the hypothetical trajectories of the oil in cases I and II. It is important to highlight that ADIOS only

considers the pour point of fresh crude oil and not how it varies with evaporation. In fact the model ADIOS warns that simulations carried out at temperatures below the pour point may give unreliable results.

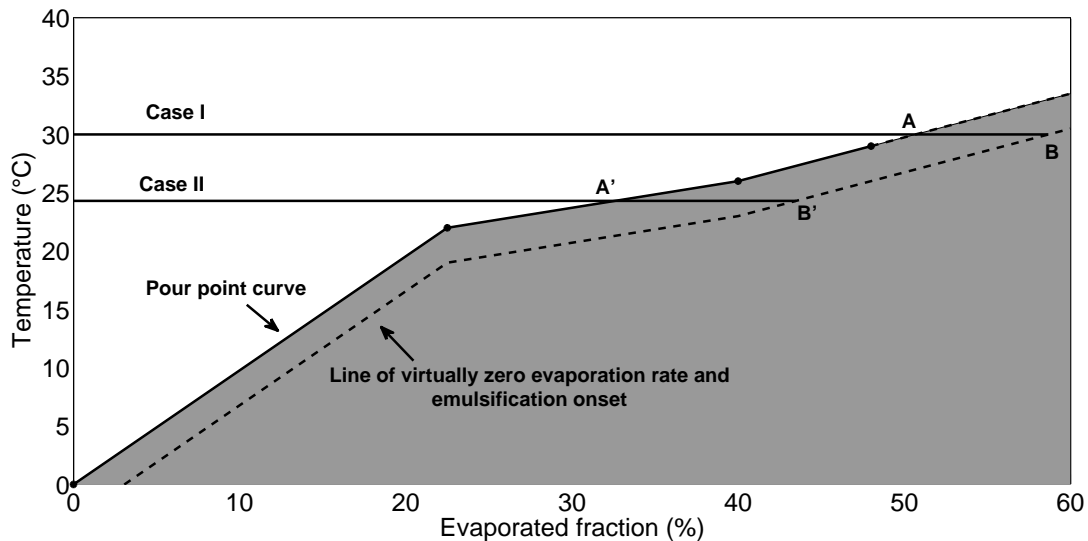


Figure 5.26: Temperature of test cases I and II with respect to pour point curve of Cusiana crude oil.

In Case I, it takes around 51% of evaporation to reach for the trajectory in Figure 5.26 to be below the pour point temperature. At this point the evaporated fraction is already asymptotic because most of the species with high volatility have already evaporated. Moreover, the crude oil on surface disappears, by the combined effect of dispersion and evaporation, before the emulsification line onset (Point B in Figure 5.26) is reached. This is the reason why the weathering behavior of Cusiana can be predicted at 30°C, even if the effect of the pour point is neglected.

Contrary, in Case II, after an oil spill occurring at 24.5°C, Cusiana reaches the pour point curve when the evaporated fraction is 33% (Point A' of Figure 5.26). At this point there is still enough oil on surface to generate a gel phase and decrease the evaporation rate as was explained in Section 5.1.2.3. ADIOS does not consider this effect, but MEUN does. The difference in the predictions of dispersed fraction is the result of reaching the emulsification onset line at the intersection point of B' (see Figure 5.26) which causes the subsequent increase in viscosity, also marked in Figure 5.25b as B'. Although the viscosity predicted by MEUN after emulsification is only 10 times higher than un-emulsified crude, it is enough to produce a significant decrease in the dispersion rate. This analysis shows the importance of a weathering model that considers the pour point curve characteristic of each crude oil, its relation to the onset of wax precipitation and its effect on the weathering processes. However, previous bench-

scale experiments revealed important characteristics of the effect of wax precipitation on oil weathering that may affect the extension of the results of this thesis when modeling the weathering of a waxy crude oil spilled in the ocean.

- According to Buist et al. [24], the pour point that is measured under static conditions with the ASTM D97-12 [22] test may not be applicable to the turbulent conditions in the ocean during an oil spill because oils under a high shear rate have a weaker semisolid structure and lower viscosity. This suggests that the conditions in the wind tunnel of this research promote gelation and may only represent the gelation process during an oil spill in a calm sea.
- Fritt-Rasmussen et al. [62] showed that the water content in wax-stabilised emulsions -as those formed with crude oil Cusiana in this research- reduces the concentration of waxes decreasing the pour point and viscosity, effects not predicted by state-of-the-art models and only handled with previous lab scale measurements. This also affects dispersion predictions as they have a strong dependence on the viscosity of the oil slick.

For Vasconia crude oil, Figure 5.27 shows respectively MEUN and ADIOS predictions of crude oil budget for Case III. Both models give very similar predictions. After 96 hours (4 days) both models predict 30.4-30.5 % of evaporated fraction and less than 1 % dispersed. The low dispersed fraction is consequence of the high viscosity predicted by both models and showed in Figure 5.28b. As discussed in section 5.2.3, Vasconia forms a stable emulsion with a significant viscosity increase once the evaporated fraction is 15.5 %. According to Figure 5.27a, that treshold is reached in one hour and that is the reason why the viscosity increases just immediately after the spill. This treshold to form an estable emulsion is one of the outputs of the model ADIOS. For this case its prediction was 16.0 % in agreement with the 15.5 % determined experimentally in this work. According to Lehr et al. [7], to estimate the emulsification onset of a new crude oil, ADIOS uses the asphaltene fraction as parameter to compare with the behavior of available information of previous oil spills and lab scale experiments with artificially weathered samples. Finally, the prediction in the variation of water content with time (Figure 5.28a) is similar in both models, being the predicted by MEUN and experimentally determined in this work 10 % lower.

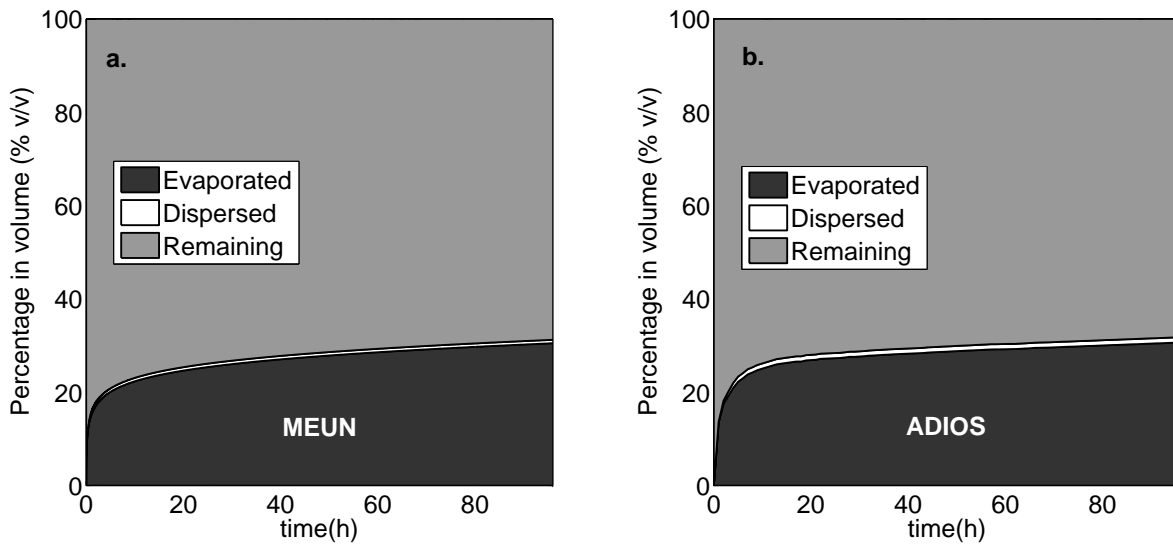


Figure 5.27: Prediction of oil spill budget for Vasconia crude oil in Case III (see Table 5.3). a. MEUN b. ADIOS.

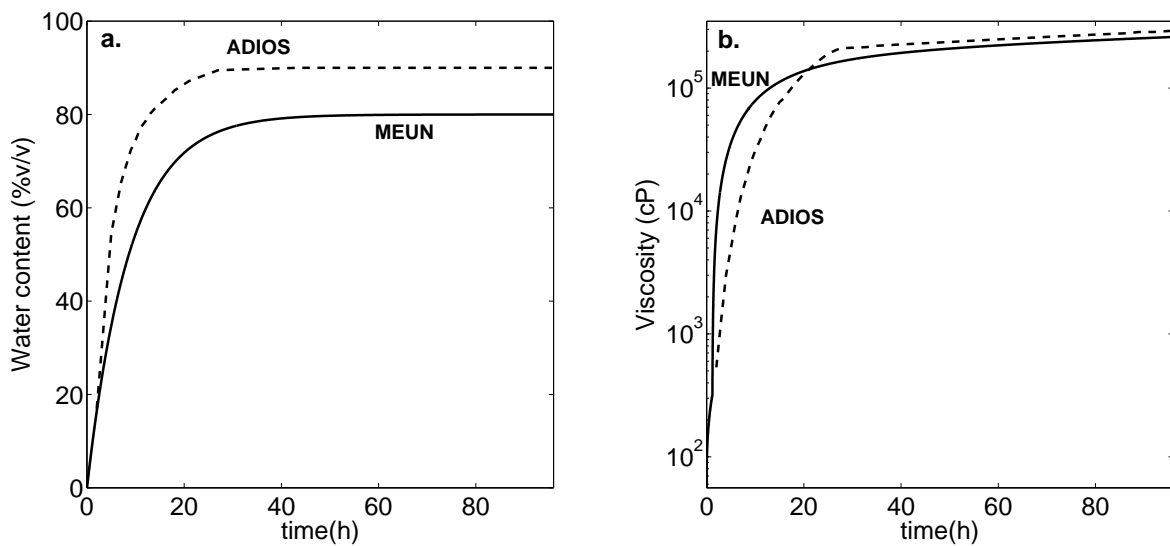


Figure 5.28: Comparison between MEUN and ADIOS predictions for Vasconia crude oil in Case III (see Table 5.3). a. Water content b. Viscosity.

Case III showed that Vasconia is very persistent on surface after an oil spill with no more than 32% of the crude lost by the combined effect of evaporation and dispersion. In Case IV, carried out at 3 m/s, MEUN and ADIOS predict 0% of dispersed fraction, this is not very different of both models predictions of Case III at 6.3 m/s. With respect to evaporation, Figures 5.29a and 5.29b compare evaporation predictions of ADIOS and MEUN for Cases III and IV respectively. Figure 5.29a of Case

III confirms the similarity between the mass balances predicted by both models and presented in Figure 5.23. Contrary, for Case IV, there are important differences between the predictions by both models with an evaporated fraction about 7% higher for ADIOS than that predicted by MEUN, which in percentage represents a difference of about 30%. As discussed in the calibration of the evaporation model, initially MEUN overestimated the evaporated fraction of Vasconia at a low wind velocity using state-of-the-art correlations for the mass transfer coefficient. These correlations have a dependence with wind velocity as $U^{0.78}$. This is the formulation implemented into ADIOS to model evaporation [7]. Given that MEUN considers an optimized correlation for the mass transfer coefficient, as discussed in Section 5.1.1.3, the difference in the predictions by both models is not surprising.

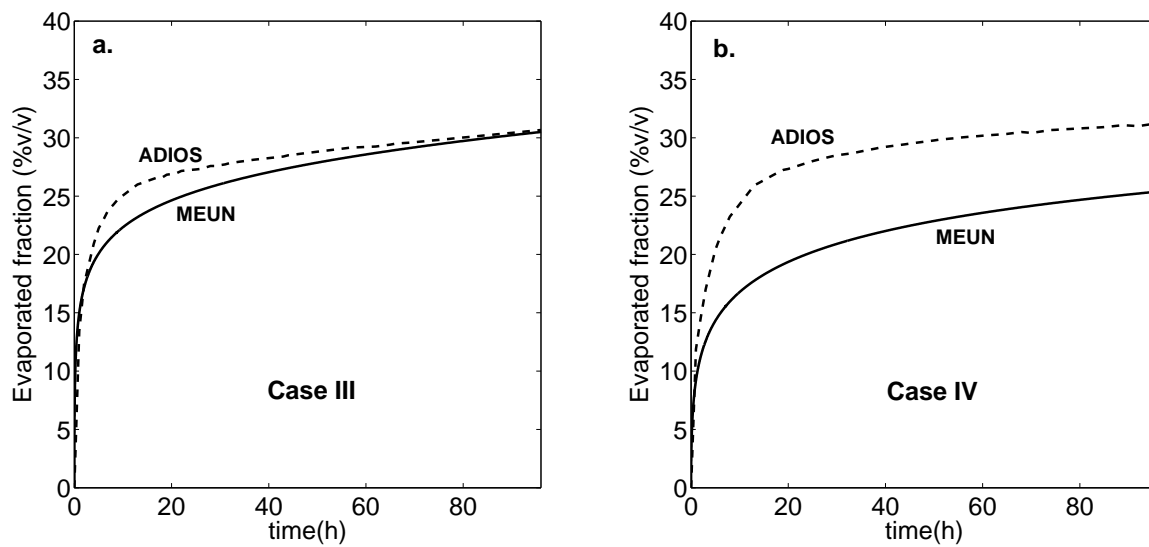


Figure 5.29: Comparison of evaporated fraction of Vasconia crude oil predicted with the module MEUN and the model ADIOS. a. Case III. b. Case IV.

Conclusions

A weathering module (MEUN, a module that can be incorporated to ocean-atmospheric models) was developed and calibrated with experimental data to predict the behavior of two Colombian crudes, Cusiana and Vasconia, during the first week after an oil spill in the Colombian Caribbean Sea.

Existing mass transfer coefficient correlations, based on water evaporation, do not correctly predict the effect of wind speed on the evaporation rate of Cusiana and Vasconia crude oils. A mass transfer coefficient that depends on the type of crude oil through API gravity and exponentially with respect to wind velocity guarantees predictions that are closer to experimental data for the evaporation of Cusiana and Vasconia crude oils in a wind tunnel. The pour point of Cusiana increases, because of evaporation, to a point that is comparable to the temperature of the Caribbean Sea and of the wind-tunnel experiments. When the oil temperature is lower than that of the pour point, a solid-like oil slick is formed, which causes a significant decrease on evaporation the rate. To model this behavior, MEUN decreases the evaporation rate from the value when the temperature is the same as the pour point to zero when the temperature is 3°C below the pour point.

Emulsification experiments carried out with the rotary cylinder method allowed to take into account crude oil specific parameters such as maximum water content, emulsification rate and the evaporative threshold to form stable emulsions. Vasconia forms an emulsion even at the beginning of the spill but to form an stable emulsion with significant increase of viscosity it demands around 15-16 % of evaporation. For Cusiana the behavior is not that simple, due to its low content of surfactant compounds, that renders as the only alternative for emulsion stabilization the precipitation of waxes when the temperature is below the pour point. According to the experiments, Cusiana needs to be 3-4 °C below the pour point to form a high water-content emulsion. This emulsion, however, is not as stable as Vasconia's emulsions.

With the calibrated model, MEUN predicts that an oil spill of Vasconia crude oil would present a

highly persistent behavior on the surface, with only about 30 % of evaporated fraction and less than 1 % of dispersion because of the high viscosity produced by the stable water-in-oil emulsion it forms. The oil remaining on surface, after an spill of Vasconia, forms an emulsion with a water content that can be higher than 80 % that represents a water to oil proportion of 1:4.

The general behavior of crude oil Cusiana in the Colombian Caribbean Sea depends significantly of the sea surface temperature. At the highest recorded temperatures in the Caribbean Sea ($\approx 30^{\circ}\text{C}$), the crude oil remains liquid as this temperature is above the pour point. At this temperature Cusiana is completely evaporated and dispersed in the first 30 hours after the spill because of its high volatility and low viscosity. Contrary, at a lower sea temperature ($\approx 25^{\circ}\text{C}$) there is a significant amount of crude oil remaining on surface by the moment it reaches the pour point and the combination of reduced evaporation and emulsion formation produces a more persistent crude oil leaving more than 40 % of crude oil remaining on surface 4 days after a possible accident.

The comparison between the predictions of MEUN and the commercial software ADIOS shows that, for the crude oil Cusiana, as ADIOS ignores the increase with evaporation of the pour point, it does not predict nor the decreases in evaporation rate nor the emulsification promotion below the pour point predicted by MEUN. For Vasconia, the differences were found predicting the evaporated fraction at low velocities, where, the prediction of ADIOS obtained from a state-of-the-art correlation, was around 30 % higher than that predicted by MEUN based on experimental calibration.

Appendix A: Expressions to calculate the thermodynamic properties of the pseudocomponents

Equations A-15- A-18 are recommended expressions by API [29] to calculate thermodynamic properties of pseudocomponents fractions of crude oil having the specific gravities (S_i) and boiling temperatures (T_{bi}) are known.

- Critical temperature

$$T_{ci} = 9.5233 \exp(-9.3145 \times 10^{-4} T_{bi} - 0.5444 S_i + 6.4791 \times 10^{-4} T_{bi} S_i) T_{bi}^{0.81067} S_i^{0.53691} \quad (\text{A-15})$$

- Critical pressure

$$P_{ci} = 31.9497 \times 10^6 \exp(-8.505 \times 10^{-3} T_{bi} - 4.8014 S_i + 5.7490 \times 10^{-3} T_{bi} S_i) T_{bi}^{-0.4844} S_i^{4.0846} \quad (\text{A-16})$$

- Molecular weight

$$M_i = 42.9654 \exp(2.097 \times 10^{-4} T_{bi} - 7.78712 S_i + 2.0848 \times 10^{-3} T_{bi} S_i) T_{bi}^{1.26007} S_i^{4.98308} \quad (\text{A-17})$$

- Acentric factor

$$w_i = \frac{\ln(101.325/P_{ci}) - 5.92714 + 6.09648/T_{rbi} + 1.28862 \ln T_{rbi} - 0.169347 T_{rbi}^6}{15.2518 - 15.6875/T_{rbi} + 13.4721 \ln T_{rbi} + 0.43577 T_{rbi}^6} \quad (\text{A-18})$$

where T_{rbi} is the reduced boiling point ($T_{rbi} = T_{bi}/T_{ci}$).

Appendix B: Deduction of emulsification rate expression

This analysis is based on the description of the rotating cylinder method discussed in Hokstad et al. [6], and similar studies that suggest the use of this methodology to predict the emulsification rate [12, 25, 41].

Considering that the emulsification rate follows a first order kinetic as follows:

$$\frac{dY}{dt} = K_{emu}(U_w) \left(1 - \frac{Y}{Y_{max}}\right) \quad (\text{B-19})$$

Integrating with the initial condition of $Y = 0$ at $t = 0$ Equation B-20 is obtained:

$$\ln \left(1 - \frac{Y}{Y_{max}}\right) = -\frac{K_{emu}t}{Y_{max}} \quad (\text{B-20})$$

The rotating cylinder method yields the half-life time of the process:

$$\text{in } t = t_{\frac{1}{2}}(U_w) \implies Y = Y_{max}/2 \quad (\text{B-21})$$

Replacing Equation B-21 and reorganizing yields Equation B-22

$$K_{emu}(U_w) = \frac{Y_{max} \ln(2)}{t_{\frac{1}{2}}(U_w)} \quad (\text{B-22})$$

Replacing Equation B-22 in the original expression proposed (Equation B-19) gives:

$$\frac{dY}{dt} = \frac{Y_{max}(t) \ln(2)}{t_{1/2}(U_w)} \left(1 - \frac{Y}{Y_{max}(t)}\right) \quad (\text{B-23})$$

However to solve the Equation B-23 it is necessary to know the half-life time as function of wind velocity ($t_{\frac{1}{2}}(U_w)$). To solve this, Equation B-24 is taken from Daling et al. [41]:

$$t_{\frac{1}{2}}(U_w)(1+U_w)^2 = t_{\frac{1}{2}}(U_{w_{ref}})(1+U_{w_{ref}})^2 \quad (\text{B-24})$$

Replacing Equation B-24 in Equation B-23 gives:

$$\frac{dY}{dt} = \frac{Y_{max} \ln(2)}{t_{\frac{1}{2}}(U_{w_{ref}})(1+U_{w_{ref}})^2} (1+U_w)^2 \left(1 - \frac{Y}{Y_{max}}\right) \quad (\text{B-25})$$

In Equation B-25 it is still missing the half-life $t_{\frac{1}{2}}|_{ref}$ at a reference wind velocity $U_{w_{ref}}$. Equation B-26 is obtained using $U_{w_{ref}} = 10$ as reference value and replacing in Equation B-25:

$$\frac{dY}{dt} = \frac{Y_{max} \ln(2)}{121 t_{\frac{1}{2}}(10 \text{ m/s})} (1+U_w)^2 \left(1 - \frac{Y}{Y_{max}}\right) \quad (\text{B-26})$$

Finally, the missing term in Equation B-26 is the half-life time at 10 m/s. According to Hokstad et al. [6], the water uptake rate in the rotating cylinder is approximately 4-6 (5 selected for this work) times faster than that observed in the field with a wind velocity of 10 m/s, this is expressed mathematically in Equation B-27:

$$t_{1/2}|_{fld} @10 \text{ m/s} = 5 t_{1/2}|_{cyl} @30 \text{ rpm} \quad (\text{B-27})$$

The final expression to simulate emulsification rate in MEUN is obtained replacing Equation B-27 in Equation B-26:

$$\frac{dY}{dt} = \frac{Y_{max}(t) \ln(2)}{605 (t_{1/2}|_{cyl} @30 \text{ rpm})} \left(1 - \frac{Y}{Y_{max}(t)}\right) \quad (\text{B-28})$$

According to Equation B-28 to simulate emulsification rate is necessary to obtain the half-life time in the rotating cylinder method at 30 rpm. In this way the weathering model considers the kinetic behavior characteristic of each crude oil.

Emulsification process can be simulated using this approach not differentially as in Equation B-23 but in discrete terms, a deduction is presented in the last part of this appendix.

Initially, replacing Equation B-22 in Equation B-20 and reorganizing it is obtained:

$$\frac{Y_{max} - Y(t)}{Y_{max}} = e^{\frac{-\ln(2)t}{t_{1/2}(U_w)}} = e^{\frac{\ln(\frac{1}{2})t}{t_{1/2}(U_w)}} \quad (\text{B-29})$$

By properties of the exponential function Equation B-29 can be written as Equation B-30

$$\frac{Y_{max} - Y(t)}{Y_{max}} = \frac{1}{2}^{\frac{t}{t_{1/2}(U_w)}} \quad (\text{B-30})$$

Evaluating in $t^* = t + \Delta t$ and $Y(t^*) = Y(t + \Delta t)$ in Equation B-30 it is obtained:

$$\frac{Y_{max} - Y(t + \Delta t)}{Y_{max}} = \frac{1}{2} \frac{t + \Delta t}{t_{1/2}(U_w)} \quad (\text{B-31})$$

Making B-31/B-30 gives:

$$Y(t + \Delta t) = Y_{max} - [Y_{max} - Y(t)] \frac{1}{2} \frac{\Delta t}{t_{1/2}(U_w)} \quad (\text{B-32})$$

Equation B-32 can be used to calculate the evolution of water content with time, in this equation is missing to express the effect of wind velocity in half-life ($t_{1/2}(U_w)$) in terms of known and/or measurable values, the reader must follow the treatment made to the analogous differential Equation B-23.

Appendix C: Expressions for the dispersion model coupled in MEUN.

The equations used in MEUN to calculate the terms of the dispersion model were taken from the description of the hydrodynamic and oil spill model MOHID [63].

- Proportionality constant (C_0)

Through this term the dispersion is affected by the increase of crude oil viscosity caused by evaporation and emulsification.

$$C_0 = \max(0, -312.25 \ln(\nu) + 2509.8) \quad (\text{C-33})$$

- Dissipated breaking wave energy per unit surface area (D_d)

$$D_d = 0.0034 \rho_w g H_{rms}^2 \text{ with : } H_{rms} = H_{sig}/\sqrt{2} \quad (\text{C-34})$$

- Fraction of sea surface hit by breaking waves (“white-caps”) per unit time (F)

To calculate this term it is usual to define a threshold of wind speed for onset of breaking waves (U_{wth}) as expressed in equations C-35 and C-36

$$\text{if } U_w \leq U_{wth} \rightarrow F = 0 \quad (\text{C-35})$$

$$\text{if } U_w > U_{wth} \rightarrow F = \frac{0.032(U_w - U_{wth})}{T_w} \quad (\text{C-36})$$

- oil particle diameter and oil particle diameter interval(d and Δd)

In this case MOHID reports typical values for these parameters

$$d = 37.5\mu m \quad \Delta d = 65\mu m \quad (\text{C-37})$$

Appendix D: Discussion of CFD simulation of the wind tunnel used in evaporation experiments.

1. Mesh description

General dimensions of the wind tunnel are presented in Figure 4.3. Because of the details of the evaporation tray, the system was represented by an unstructured mesh of about 92000 nodes using the commercial software ANSYS ICEM [64]. Figure 5.30 shows the mesh and the boundary conditions used.

2. Boundary conditions

- Inlet boundary condition: Air was introduced at constant wind velocity of 5 m/s, this velocity inlet produces in the measuring region a typical wind velocity of the Colombian Caribbean Sea.
- Outlet boundary condition: The pressure was kept constant at 85.3 kPa (atmospheric pressure) in the outlet.
- Wall boundary condition: Wind tunnel walls, blockage 1 and evaporation tray were simulated as walls with the effect of divert the flow direction.

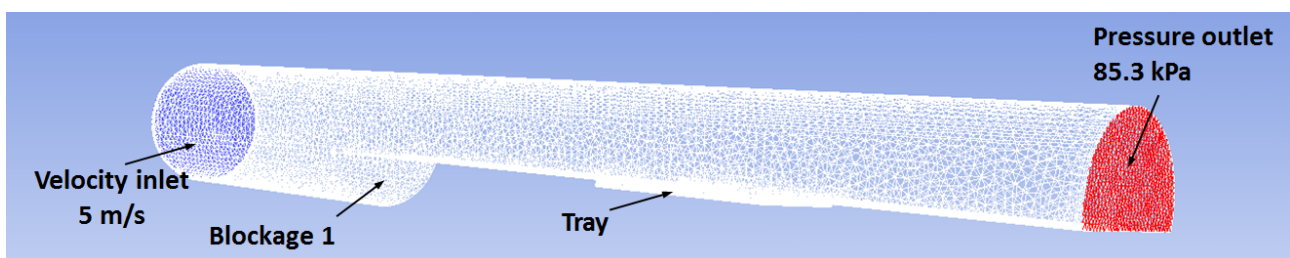


Figure 5.30: Mesh and boundary conditions of the wind tunnel simulated.

3. Models used in CFD

The main objective of this simulation is to characterize the hydrodynamics inside the wind tunnel, that way, this work considers the mass and momentum conservation equations. the highest velocities are achieved in the segment after Blockage 1 due to the reduction in the cross section. After Blockage 1, the equivalent diameter decreases from 30 cm to 22 cm, in terms of the average wind velocity, the value defined at the inlet boundary as 5 m/s increases to 7 m/s, producing a Reynolds number of 100420, this level of turbulence was represented with the k-epsilon model.

Appendix E: Sensitivity analysis to the correlation proposed for the mass transfer coefficient.

As result of an optimization procedure, this thesis proposed in Section 5.1.1.4 the Equation E-38 to compute the mass transfer coefficient for the evaporation of the Colombian crude oils Cusiana and Vasconia. This Appendix discusses the sensitivity analysis carried out to measure the uncertainty in the output of the evaporation model (in this case the evaporated fraction) due to uncertainties in the fitted parameters a , b and c of Equation E-38 referred in this analysis as the inputs parameters and represented as $\theta = [a \ b \ c]$.

$$k_w = a ({}^\circ API)^b e^{cU_w} X^{-0.11} \quad \text{with} \quad a = 3.04 \times 10^{-9} \quad b = 3.06 \quad c = 0.67 \quad (\text{E-38})$$

As example, Figure 5.31 shows with the black curve, the prediction of the evaporated fraction with the optimized values of a , b and c ($Fme_{pred}(\theta_{opt}; t_k)$) and the blue curve is the prediction obtained with one of the parameters deviated from its optimized value, both prediction for Vasconia crude oil. The deviation in the evaporated fraction with respect to that predicted with the optimized parameters is computed with Equation E-39, this equation is expressed as a relative difference because in terms of absolute difference Cusiana and Vasconia would have uncertainties not comparable.

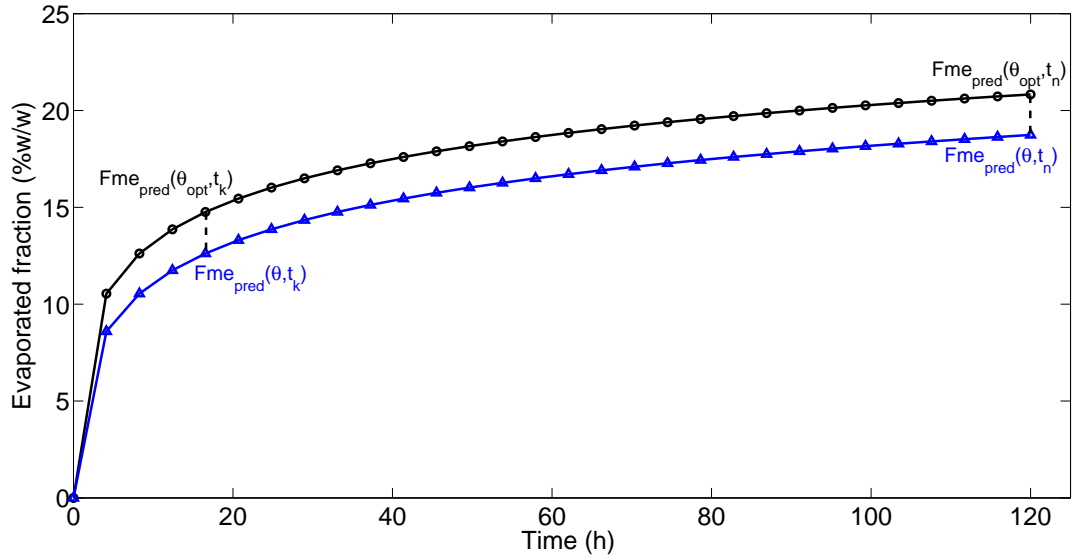


Figure 5.31: Comparison between the evaporated fraction of Vasconia predicted with the optimized parameters (θ_{opt}) and with the parameters diverted from their optimized values (θ).

$$\Delta Fme_{pred} = \frac{1}{n} \sum_{k=1}^n \frac{|Fme_{pred}(\theta_{opt}; t_k) - Fme_{pred}(\theta; t_k)|}{Fme_{pred}(\theta_{opt}; t_k)} \times 100 \quad (\text{E-39})$$

Figures 5.32a and 5.32b show for Cusiana and Vasconia, respectively, the uncertainties of the evaporated fraction as function of the inputs parameters diverted of their optimized values, expressed in terms of the resulting mass transfer coefficient. According to this figure, the predictions of evaporated fraction are more sensitive for Vasconia than for Cusiana to uncertainties in the optimized parameters. For this reason, to individualize the effect of deviations in a , b and c , the rest of the analysis is done with Vasconia crude oil.

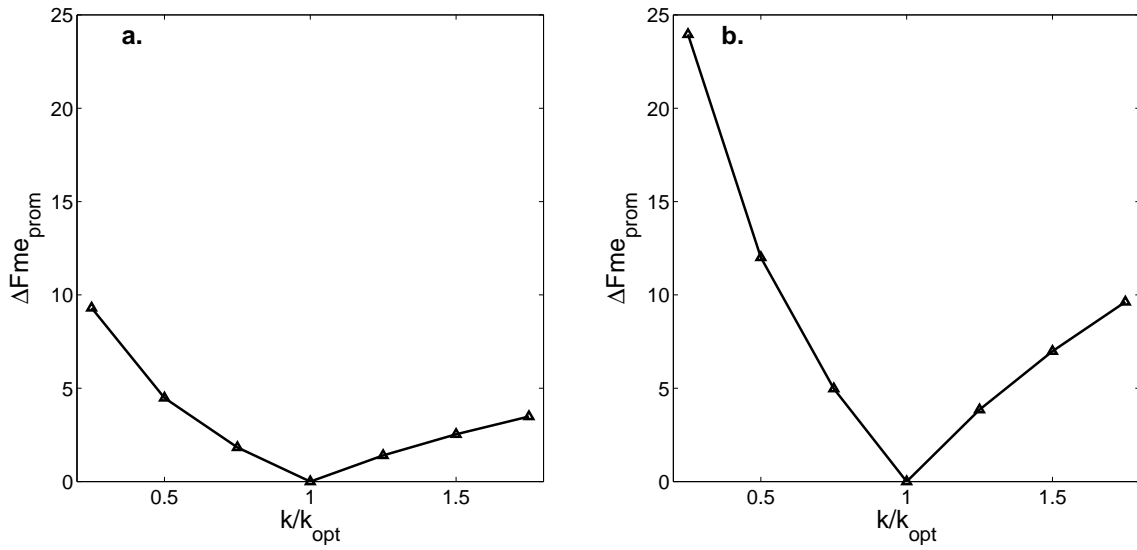


Figure 5.32: Effect of the uncertainties of the optimized parameters a , b and c (expressed in terms of the resulting mass transfer coefficient computed with Equation E-38) in the percentage error of the evaporated fraction predicted. a. Cusiana b. Vasconia.

Figures 5.33a-5.33c show the behavior of the percentage error of the evaporated fraction as function of uncertainties in the parameters a , b and c , respectively. The three figures also present the maximum uncertainty of each parameter that guaranties a percentage error equal or lower than 5% in the evaporated fraction.

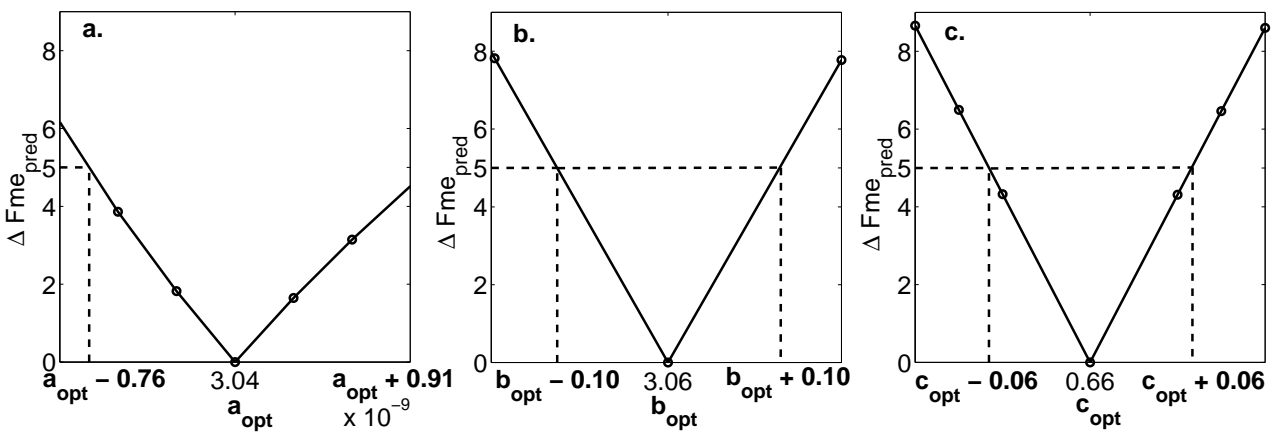


Figure 5.33: Percentage error of the evaporated fraction with respect to deviations in the optimized parameters of Equation E-38. a. parameter a . b. Parameter b . c. parameter c .

As conclusion of figures 5.33a-5.33c, equations E-40-E-42 present the evaporation model with the uncertainties in the optimized parameters a, b and c that produces a percentage error lower or equal to 5% in the predicted evaporated fraction. Term I of Equation E-40 highlights that the percentage error is with respect to the predicted value and it is not an absolute error of the evaporated fraction.

$$\underbrace{Fme_{pred} \pm 0.05Fme_{pred}}_I = 1 - \frac{1}{m_o} \sum_{i=1}^{n_{pc}} m_i \quad \text{with} \quad \frac{dm_i}{dt} = -\frac{k_w A x_i P_i^{sat} MW_i}{RT} \quad (\text{E-40})$$

$$k_w = (3.04 \times 10^{-9} \pm \Delta a) (\text{°API})^{(3.06 \pm \Delta b)} e^{(0.66 \pm \Delta c) U_w} X^{-0.11} \quad (\text{E-41})$$

$$\Delta a = 0.76 \times 10^{-9} \quad \Delta b = 0.10 \quad \Delta c = 0.06 \quad (\text{E-42})$$

References

- [1] ITOPF, “Fate of marine oil spills,” in *Technical Information Papers (TIPs)*, pp. 14–24, 2012.
- [2] T. Strøm-Kristiansen, “Weathering properties of Jordbær crude oil related to oil spill response,” tech. rep., SINTEF report, 2011.
- [3] I. Andreassen, “Weathering studies of Grosbeak crude oil,” tech. rep., available at: http://www.nofo.no/Global/Oljetyper/Forvitningsrapporter/Grosbeak_weathering_report.pdf, 2012.
- [4] P. Sebastiao and C. Guedes, “Modeling the fate of oil spills at sea,” *Spill Science Technology Bulletin*, vol. 2, no. 2-3, pp. 121–131, 1995.
- [5] Environment Canada, “Database - Oil Properties,” available at: <http://www.etc-cte.ec.gc.ca/databases/OilProperties>, 2001.
- [6] J. Hokstad, P. S. Daling, and T. Strøm Kristiansen, “Methodology for testing water-in-oil emulsions and demulsifiers. Description of laboratory procedures,” in *Formation and Breaking of W/O Emulsions*, (Alberta), pp. 239–253, 1993.
- [7] W. Lehr, R. Jones, M. Evans, D. Simecek-Beatty, and R. Overstreet, “Revisions of the ADIOS oil spill model,” *Environmental Modelling & Software*, vol. 17, pp. 189–197, Jan. 2002.
- [8] D. Mackay, I. Buist, R. Mascarenhas, and S. Patterson, “Oil Spill Processes and Models. Report No. EE/8,” in *Environment Canada*, (Ottawa, Ontario), p. 192, 1980.
- [9] M. F. Fingas, “Water-in-Oil Emulsions: Formation and Prediction,” *Journal of Petroleum Science Research*, vol. 3, no. 1, p. 38, 2014.
- [10] W. Stiver and D. Mackay, “Evaporation rate of spills of hydrocarbons and petroleum mixtures,” *Environmental Science & Technology*, vol. 18, pp. 834–840, Nov. 1984.
- [11] J. Fay, “Physical processes in the spread of oil on a water surface,” in *Proceedings of the Joint Conference on Prevention and Control of Oil Spills*, (Washington, DC.), pp. 117–125, July 1971.

- [12] P. S. Daling, M. O. v. Moldestad, O. i. Johansen, A. Lewis, and J. Rø dal, “Norwegian Testing of Emulsion Properties at Sea The Importance of Oil Type and Release Conditions,” *Spill Science & Technology Bulletin*, vol. 8, pp. 123–136, Apr. 2003.
- [13] M. F. Fingas, “A literature review of the physics and predictive modelling of oil spill evaporation,” *Journal of Hazardous Materials*, vol. 42, pp. 157–175, July 1995.
- [14] D. Mackay and C. D. McAuliffe, “Fate of hydrocarbons discharged at sea,” *Oil and Chemical Pollution*, vol. 5, pp. 1–20, Jan. 1989.
- [15] ASCE, “State-of-the-Art Review of Modeling Transport and Fate of Oil Spills,” *Journal of Hydraulic Engineering*, vol. 122, no. 11, pp. 594–609, 1996.
- [16] ITOPF, “Use of dispersants to treat oil spills,” in *Technical Information Papers (TIPs)*, pp. 38–49, 2012.
- [17] ITOPF, “Use of skimmers in oil pollution response,” in *Technical Information Papers (TIPs)*, pp. 50–65, 2012.
- [18] C. Harris, “The braer incident: Shetland islands, January 1993,” *International Oil Spill Conference Proceedings*, vol. 1995, pp. 813–819, Feb. 1995.
- [19] G. Bernal, G. Poveda, P. Roldán, and C. Andrade, “Patrones de variabilidad de las temperaturas superficiales del mar en la costa caribe colombiana,” *Ciencias de la tierra*, vol. 30, no. 115, pp. 195–208, 2006.
- [20] M. A. Ruiz and G. Bernal, “Variabilidad estacional e interanual del viento en los datos del reanálisis NCEP/NCAR en la cuenca Colombia, mar Caribe,” *Avances en Recursos Hidráulicos*, vol. 20, pp. 7–20, 2009.
- [21] Z. Huang, H. S. Lee, M. Senra, and H. Scott Fogler, “A fundamental model of wax deposition in subsea oil pipelines,” *AIChE Journal*, vol. 57, pp. 2955–2964, Nov. 2011.
- [22] . ASTM International D97, “Test method for pour point of petroleum products,” ASTM International, West Conshohocken, PA, 2012, DOI: 10.1520/D0097-12, www.astm.org.
- [23] V. Ramachandran, S. Probjot, and H. Fogler, “Delineating the Pour Point and Gelation Temperature of Waxy Crude Oils,” *SPE Journal*, vol. 7, Dec. 2002.
- [24] I. Buist, S. Potter, D. Mackay, and M. Charles, “Laboratory studies on the behavior and cleanup of waxy crude oil spills,” *International Oil Spill Conference Proceedings*, vol. 1989, pp. 105–113, Feb. 1989.

- [25] P. S. Daling and T. StrØ m, “Weathering of Oils at Sea: Model/Field Data Comparisons,” *Spill Science & Technology Bulletin*, vol. 5, pp. 63–74, Apr. 1999.
- [26] M. Reed, O. i. Johansen, P. J. Brandvik, P. Daling, A. Lewis, R. Fiocco, D. Mackay, and R. Prentki, “Oil Spill Modeling towards the Close of the 20th Century: Overview of the State of the Art,” *Spill Science & Technology Bulletin*, vol. 5, pp. 3–16, Apr. 1999.
- [27] M. Fingas, “Chapter 9 - Evaporation Modeling,” in *Oil spill science and technology*, pp. 201–242, Boston: Gulf Professional Publishing, 2011.
- [28] J. Payne, B. Kirstein, G. McNabb, J. Lambach, Redding, R., R. Jordan, W. Hom, C. Oliveira, G. Smith, and D. M. Baxter, “Final report, multivariate analysis of petroleum weathering in the marine environment-Sub Arctic, Vol. 1 - technical results,” tech. rep., 1984.
- [29] T. Daubert and R. Danner, *API Technical Data Book - Petroleum Refining, 5th ed.*, American Petroleum Institute. american p ed., 1989.
- [30] W. J. Lehr, “Review of modeling procedures for oil spill weathering behavior,” pp. 51–90, UK: WIT Press, Southampton, 2001.
- [31] X. Chao, N. Shankar, and H. F. Cheong, “Two- and three-dimensional oil spill model for coastal waters,” *Ocean Engineering*, vol. 28, pp. 1557–1573, Dec. 2001.
- [32] D. P. French-McCay, “Oil spill impact modeling: development and validation,” *Environmental Toxicology and Chemistry*, vol. 23, no. 10, p. 2441, 2004.
- [33] M. Nagheeby; M. Kolahdoozan, “Numerical modeling of two-phase fluid flow and oil slick transport in estuarine water,” *International Journal of Engineering Science and Technology*, vol. 7, no. 4, pp. 771–784, 2010.
- [34] A. Berry, T. Dabrowski, and K. Lyons, “The oil spill model OILTRANS and its application to the Celtic Sea.,” *Marine pollution bulletin*, vol. 64, pp. 2489–501, Nov. 2012.
- [35] W. C. Yang and H. Wang, “Modeling of oil evaporation in aqueous environment,” *Water Research*, vol. 11, pp. 879–887, Jan. 1977.
- [36] M. R. Riazi and G. A. Al-Enezi, “Modelling of the rate of oil spill disappearance from seawater for Kuwaiti crude and its products,” *Chemical Engineering Journal*, vol. 73, pp. 161–172, May 1999.

- [37] M. Hamoda, S. Hamam, and H. Shaban, "Volatilization of crude oil from saline water," *Oil and Chemical Pollution*, vol. 5, pp. 321–331, Jan. 1989.
- [38] M. F. Fingas, "Modeling evaporation using models that are not boundary-layer regulated," *Journal of Hazardous Materials*, vol. 107, pp. 27–36, Feb. 2004.
- [39] Aspen Technology Inc., "Getting Started Modeling Petroleum Processes," 2004.
- [40] NOAA, "ADIOS (Automated Data Inquiry for Oil Spills) User's Manual," tech. rep., Hazardous Materials Response and Assessment Division, NOAA, Seattle, 1993.
- [41] P. S. Daling, P. J. Brandvik, D. Mackay, and O. Johansen, "Characterization of crude oils for environmental purposes," *Oil and Chemical Pollution*, vol. 7, pp. 199–224, Jan. 1990.
- [42] M. Fingas and B. Fieldhouse, "Formation of water-in-oil emulsions and application to oil spill modelling," *Journal of hazardous materials*, vol. 107, pp. 37–50, Mar. 2004.
- [43] M. Fingas, B. Fieldhouse, and J. Mullin, "Water-in-oil Emulsions Results of Formation Studies and Applicability to Oil Spill Modelling," *Spill Science & Technology Bulletin*, vol. 5, pp. 81–91, Apr. 1999.
- [44] M. Nazir, F. Khan, P. Amyotte, and R. Sadiq, "Multimedia fate of oil spills in a marine environment An integrated modelling approach," *Process Safety and Environmental Protection*, vol. 86, pp. 141–148, Mar. 2008.
- [45] F. You and S. Leyffer, "Mixed-integer dynamic optimization for oil-spill response planning with integration of a dynamic oil weathering model," *AIChE Journal*, vol. 57, no. 12, pp. 3555–3564, 2011.
- [46] I. Buchanan and N. Hurford, "Methods for predicting the physical changes in oil spilt at sea," *Oil and Chemical Pollution*, vol. 4, no. 4, pp. 311–328, 1988.
- [47] M. Fingas and B. Fieldhouse, "How to model water-in-oil emulsion formation," *International Oil Spill Conference Proceedings*, vol. 2005, pp. 647–654, May 2005.
- [48] M. Reed, P. Daling, M. O. v. Moldestad, P. J. Brandvik, J. Resby, F. Leirvik, O. i. Johansen, K. Skognes, B. Hetland, and T. Schrader, "Revision of the OCS Oil-Weathering Model: Phases II and III," tech. rep., 2004.
- [49] G. A. L. Delvigne and C. E. Sweeney, "Natural dispersion of oil," *Oil and Chemical Pollution*, vol. 4, no. 4, pp. 281–310, 1988.

- [50] J. Fay, "The Spread of Oil Slicks on a Calm Sea," *Massachusetts Institute of Technology. Fluid Mechanics Laboratory*, pp. 53–63, 1969.
- [51] Ecopetrol, "Actualidad," available at: [http://www.ecopetrol.com.co/especiales/Carta Petrolera 110/rev_actualidad.htm](http://www.ecopetrol.com.co/especiales/Carta_Petrolera_110/rev_actualidad.htm), 2004.
- [52] ANSYS, "FLUENT, Academic Research, Release 13.0, ANSYS. Inc."
- [53] J. Abulencia and L. Theodore, "Turbulent flow in pipes," in *Fluid Flow for the Practicing Chemical Engineer*, ch. 14, pp. 147–166, Hoboken, New Jersey: John Wiley & Sons, Inc, 2009.
- [54] O. G. Sutton, "Wind Structure and Evaporation in a Turbulent Atmosphere," *Proceedings of the Royal Society A: Mathematical, Physical and Engineering Sciences*, vol. 146, pp. 701–722, Oct. 1934.
- [55] D. Mackay and R. S. Matsugu, "Evaporation rates of liquid hydrocarbon spills on land and water," *The Canadian Journal of Chemical Engineering*, vol. 51, pp. 434–439, Aug. 1973.
- [56] R. F. Visintin, T. P. Lockhart, R. Lapasin, and P. D'Antona, "Structure of waxy crude oil emulsion gels," *Journal of Non-Newtonian Fluid Mechanics*, vol. 149, pp. 34–39, Feb. 2008.
- [57] T. Strøm Kristiansen, A. Lewis, P. S. Daling, J. N. Hokstad, and I. Singasaas, "Weathering and dispersion of naphthenic, asphaltenic and waxy crude oils," *International Oil Spill Conference Proceedings*, vol. 1997, pp. 631–636, Apr. 1997.
- [58] M. Bobra, "Water-In-Oil Emulsification: A Physicochemical Study," *International Oil Spill Conference Proceedings*, vol. 1991, pp. 483–488, Mar. 1991.
- [59] M. Moldestad, F. Leirvik, O. Johansen, P. Daling, and A. Lewis, "Environmental Emulsions: A Practical Approach," in *Emulsions and Emulsion Stability* (J. Sjøblom, ed.), ch. 10, pp. 355–381, Taylor & Francis, second ed., 2005.
- [60] NOAA - Office of Response and Restoration, "ADIOS2," available at: archive.orr.noaa.gov/adios, 2011.
- [61] ITOPF, "Oil Tanker Spill Statistics 2013," tech. rep., available at: http://www.itopf.com/fileadmin/data/Documents/Company_Lit/OilSpillstats_2013.pdf, 2014.
- [62] J. Fritt-Rasmussen, P. J. Brandvik, A. Villumsen, and E. H. Stenby, "Comparing ignitability for in situ burning of oil spills for an asphaltenic, a waxy and a light crude oil as a function of

weathering conditions under arctic conditions,” *Cold Regions Science and Technology*, vol. 72, pp. 1–6, Mar. 2012.

[63] MOHID, “MOHID, Modelling Water Resources,” available at: <http://www.mohid.com>, 2009.

[64] ANSYS, “ICEM, Academic Research, Release 13.0, ANSYS. Inc.”